HfC STRUCTURAL FOAMS SYNTHESIZED FROM POLYMER PRECURSORS

Except where reference is made to the work of others, the work described in this dissertation is my own or was done in collaboration with my advisory committee. This dissertation does not include proprietary or classified information.

_____

Haibo Fan

Certificate of Approval:

ZhongYang Cheng Assistant Professor Materials Engineering	Bryan A. Chin, Chair Professor Materials Engineering
Dong-Joo Kim Assistant Professor Materials Engineering	William C. Neely Professor Chemistry and Biochemistry

Stephen L. McFarland
Dean
Graduate School

HfC STRUCTURAL FOAMS SYNTHESIZED FROM POLYMER PRECURSORS

Haibo Fan

A Dissertation

Submitted to

the Graduate Faculty of

Auburn University

in Partial Fulfillment of the

Requirements for the

Degree of

Doctor of Philosophy

Auburn, Alabama
December 16, 2005

HfC STRUCTURAL FOAMS SYNTHESIZED FROM POLYMER PRECURSORS

Haibo Fan

Permission is granted to Auburn University to make copies of this dissertation at its discretion, upon request of individuals or institutions and at their expense.
The author reserves all publication rights.

_____
Signature of Author

_____
Date

VITA

Haibo Fan, son of Chaoying Fan and Yulan Shi, was born on November 18, 1976, in Ugrat Front Banner, Inner-Mongolia, the People's Republic of China. He graduated from Ugrat Front Banner No.1 High School in 1994. He studied at Tianjin University for four years and graduated with a Bachelor of Engineering degree in Mechanical Engineering in July 1998. He entered Auburn University in August 2000 to pursue his M.S. and Ph.D. degrees in Materials Engineering. He received his M.S. degree in May 2003.

In April 2005, he married Min Ding.

DISSERTATION ABSTRACT

HfC STRUCTURAL FOAMS SYNTHESIZED FROM POLYMER PRECURSORS

Haibo Fan

Doctor of Philosophy, Dec. 16, 2005
(M.S., Auburn University, 2003)
(B.S., Tianjin University, 1998)

153 Typed Pages

Directed by Bryan A. Chin

A study was conducted to investigate a new low cost approach to produce Hafnium Carbide (HfC) structural foams through the thermolysis and pyrolysis of polymer precursors. Hafnium carbide has a melting point of over 3900°C, the highest melting point of any known binary alloy. HfC structural foams can be fabricated into high temperature components or used as a thermal insulation material. Current available methods for creating HfC structural foams are time consuming, expensive or the material produced lacks mechanical strength.

The objectives of this research were to produce HfC foam through the thermolysis and pyrolysis of Hf containing polymer mixture, optimize the properties of the HfC foam, and develop a knowledge base of acceptable process parameters.

With the proposed method, HfC foam was produced by mixing a hafnium containing Macromolecular Metal Complex (MMC) and carbon source polymers, followed by heat treating the mixture under vacuum. XRD analysis showed that the produced foam was largely composed of HfC, with small amounts of hafnium oxide. The foam total porosity was measured to be over 85%. The HfC lattice parameter was found to range from 0.4613 nm to 0.4647 nm. The HfC conversion mechanism was investigated using Residual Gas Analysis, where it was observed that polymer decomposition occurred from 80 through 550 $^{\circ}$C and HfC conversion started around 1100 $^{\circ}$C.

The HfC foam mechanical properties and microstructure were improved by optimizing the process methods and parameters. The initial research yielded an HfC foam with a compression strength of 15.16 ± 4.66 MPa and evenly distributed foam cells with diameter sizes up to 50 μm. Continued research showed that HfC foams with total porosity of about 85% (density 1.9g/cm^3), and a foam compression strength of 212 ± 25MPa were achievable.

The proposed methodology for synthesizing HfC foam was found to be simple, inexpensive and require less production time. The process can be controlled to produce HfC foams with a desirable microstructure and good mechanical strength.

ACKNOWLEDGMENTS

The author would like to thank Dr. Bryan A. Chin for providing the opportunity to undertake this research project and for his advice, mentorship and guidance during the entire course of this research. Sincere appreciation is expressed to Dr. Clyde H. Wikle, III for his important suggestions and constant support on both technical and documentary aspects of the project. The author would also like to thank Dr. William Gale for his help with the metallography techniques, vacuum equipment and other experimental methods. He would like to thank Dr. Jeffrey Fergus for his help with the XRD data analysis and Dr. Bart Prorok for assistance with the nanoindentation hardness measurements. Sincere appreciation is expressed to his graduate committee members, Dr. Zhongyang Cheng, Dr Dong-Joo Kim, and Dr. William C. Neely, for their guidance and support. The author would like to thank Kirk Williams for his help with the experimental techniques at the start-up of the project, Nanda K. Ravala for his significant support of the project, and Bobby Hicks for combustion boat manufacturing. Appreciation is expressed to Rui Shao for her help in particle size analysis. Assistance also came from Roy Howard, David Lindahl and Keith Krome with experimental materials and techniques.

The author would like to thank his wife Min Ding, his parents, and his brother Linbo Fan for their most important encouragement and support.

Style manual or journal used: Journal of the American Ceramic Society

Computer Software used: Microsoft Word 2000, Microsoft Excel 2000

TABLE OF CONTENTS

LIST OF FIGURES xi

LIST OF TABLES xv

1 INTRODUCTION 1

1.1 HfC Properties Overview 1

1.2 HfC for Aerospace Applications 5

1.3 HfC Oxidation Resistance Studies 7

1.4 Advantages of HfC Foam for Space Applications 10

2 REVIEW OF HfC SYNTHESIS TECHNOLOGY 12

2.1 HfC Particles Synthesis Methods 12

2.2 Other Manufacturing Methods for HfC Components 12

2.2.1 Reaction Forming 13

2.2.2 CVD 14

2.2.3 Vacuum Plasma Spray 17

2.2.4 HIP, Sintering and Other Methods 18

2.2.5 Synthesizing HfC Foam from Polymer Precursors 20

3 OBJECTIVES 22

4 MATERIALS AND METHODS 24

4.1 Polymer Precursors 24

4.1.1 Hafnium Containing MMC 24

4.1.2 Carbon Source Polymers 26

4.2 Mixing of Polymers 29

4.2.1 Sieving and Storage of Hafnium Containing MMC 29

4.2.2 Polymer Mix Ratios 31

4.2.3 Mixing Methods 32

4.3 Thermolysis and Pyrolysis 40

4.4 Polymer Powder Compaction 43

4.5 HfC Foam Characterization 48
4.5.1 XRD, SEM, Compression Tests, and Density Measurements 48

4.6 Thermolysis and Pyrolysis Chemistry Study 48
4.6.1 Residual Gas Analysis (RGA) 49
4.6.2 RGA Analysis System Setup 51

4.7 Summary of Experimental Procedures 51

5 RESULTS AND DISCUSSION 55

5.1 Thermolysis and Pyrolysis Chemistry Study 56
5.1.1 Vacuum Pressure vs. Furnace Temperature Change During Heat Treatment 56
5.1.2 RGA and XRD Analysis 59

5.2 Hand Mixing 74
5.2.1 Effect of Mixing Ratio on HfC Foam Density 79
5.2.2 Mixture Ratio Extremes 83
5.2.3 Effect of Thermolysis Parameters on HfC Foam Density 83
5.2.4 HfC Foam Characterization 84

5.3 Vacuum Mixing 96
5.3.1 Polymer Preform Sample 97
5.3.2 HfC Foam Characterization 99

5.4 Polymer Powder Compaction 105
5.4.1 Polymer Powder and Polymer Cylinders 106
5.4.2 HfC Foam Sample Characterization 115

6 CONCLUSIONS 130

7 FUTURE WORK 133

7.1 Thermolysis and Pyrolysis Chemistry 133

8 REFERENCES 134

LIST OF FIGURES

Figure 1 HfC structure with FCC Bravais Lattice 3

Figure 2 C--Hf Phase diagram 4

Figure 3 A schematic of the Vacuum Plasma Spray (VPS) forming process..... 19

Figure 4 Hafnium trifluoroacetylacetonate (Formula: $C_{20}H_{16}F_{12}HfO_8$) 25

Figure 5 Devcon 2 Ton/Clear Weld Epoxy System..... 27

Figure 6 Resin *Component 1* formula: $C_{15}H_{16}O_2$..... 28

Figure 7 Resin *Component 2* formula: C_3H_5ClO..... 28

Figure 8 Aminoethylpiperazine formula: $C_6H_{15}N_3$..... 30

Figure 9 Nonylphenol formula: $C_{15}H_{24}O$..... 30

Figure 10 Aluminum mold for hand mixing..... 34

Figure 11 Vacuum mixer and pump system connections 36

Figure 12 Polymer loading in the syringe for vacuum mixing 38

Figure 13 Typical temperature profile for HfC foam processing 42

Figure 14 Glen Mills, Labtechnics dish and puck crusher..... 46

Figure 15 Microtrac S3500 particle size analyzer 47

Figure 16 LEYBOLD INFICON H200M RGA 50

Figure 17 RGA analysis system diagram..... 52

Figure 18 RGA analysis system set-up..... 53

Figure 19 Experimental procedure flow diagram for HfC foam fabrication..... 54

Figure 20 Ellingham diagram showing HfC conversion from HfO_2 58

Figure 21 Changes in vacuum pressure when polymer preform samples were continuously heated from room temperature to 1410 ^{o}C 59

Figure 22 RGA mass spectrum at 22°C 64

Figure 23 RGA mass spectrum at 179 ^{o}C 65

Figure 24 RGA mass spectrum at 315°C 66

Figure 25 RGA mass spectrum at 550 ^{o}C 67

Figure 26 RGA mass spectrum at 1010 ^{o}C 68

Figure 27 RGA mass spectrum at 1161 ^{o}C 69

Figure 28 RGA mass spectrum at 1250 ^{o}C 70

Figure 29 RGA mass spectrum at 1410 ^{o}C 71

Figure 30 28amu ion concentration profile with increasing temperature 72

Figure 31 XRD spectra for polymer samples heat treated at different temperatures for 4 hours 73

Figure 32 Photograph of preform (mixing ratio: 2:1) before heat treatment 76

Figure 33 HfC foam (mixing ratio: 3:1) after processing 77

Figure 34 Three different specimens after halting processing at each of the three major steps (from left to right: preform, after thermolysis, after pyrolysis). 78

Figure 35 Effect of mixing ratio on HfC foam density 81

Figure 36 Effect of mixing ratio on HfC foam total porosity 82

Figure 37 Remains of an epoxy-only specimen exposed to the HfC foam process heat treatment. (Note that the specimen boat was completely filled with hardened epoxy before the heat treatment.) 85

Figure 38 Density of foams produced at different thermolysis times and temperatures .. 86

Figure 39 X-Ray diffraction spectrum for an HfC foam (hand mixed with a 3:1 ratio)... 87

Figure 40 XRD Spectra of HfC-HfO_2 powder mixtures with different HfO_2 weight percentages 89

Figure 41 HfO_2 weight percentage vs. HfO_2/(HfC+HfO_2) XRD peak height ratio relationship 90

Figure 42 Lattice parameter a_0 determination approach for a specimen mixed with 1:1 ratio. 92

Figure 43 SEM micrographs of a 4:1 ratio HfC foam at 20X (upper) and 80X (lower) magnification..... 94

Figure 44 Hand mixed preform sample broken surface (1:1 Mixing ratio). Upper Figure shows entrained air pockets. Lower Figure shows Hf containing agglomerated particles. 95

Figure 45 Cross-sectional surface of a vacuum mixed polymer preform sample..... 98

Figure 46 Vacuum mixed HfC foam sample after heat treatment 100

Figure 47 SEM photos of the broken surface of a vacuum mixed HfC foam sample. Upper picture is a general view and lower picture is a magnified view, which show uniform cell sizes in the range of 20 ~ 200μm. 101

Figure 48 XRD spectrum for a vacuum mixed HfC foam sample 103

Figure 49 Polymer particles on a copper tape..... 108

Figure 50 Magnified view of polymer particles 109

Figure 51 Particle size distribution of powder made by mortar & pestle 110

Figure 52 Polymer pellet (cylinder) made from cold pressing of polymer powder..... 112

Figure 53 Broken surface of the sample in Figure 52..... 113

Figure 54 Magnified view of Figure 53 114

Figure 55 HfC foam created from polymer cylinders 117

Figure 56 Broken surface of HfC foam sample made from Polymer Powder Compaction 118

Figure 57 Cell structure of HfC foam sample in Figure 56 119

Figure 58 Connected particles and cells of HfC foam sample in Figure 56 120

Figure 59 XRD spectrum for HfC foam sample made using Polymer Powder Compaction 121

Figure 60 Particle size distribution of powder pulverized for 5min using Labtechnics pulverizer 126

Figure 61 Particle size distribution of powder pulverized for 15 min using Labtechnics pulverizer 127

Figure 62 Particle size distribution of powder pulverized for 30 min using Labtechnics pulverizer 128

Figure 63 Effect of powder processing methods on foam density and compression strength 129

LIST OF TABLES

Table 1 Selected properties of hafnium carbide. 2

Table 2 Potentially suitable structural materials for use at ultra high temperatures 6

Table 3 Epoxy resin constituent..... 26

Table 4 Epoxy hardener constituent 29

Table 5 Densities of the polymer preforms and HfC foam specimens. 79

Table 6 Lattice parameter measurements for HfC foam specimens. 92

Table 7 Compression strength of Hand Mixed HfC foam samples 96

Table 8 Compression strength of Vacuum Mixed HfC foam samples 104

Table 9 Compression strength of HfC foam samples made using Polymer Powder Compaction (mortar and pestle) 122

Table 10 Summary of particles size analysis for polymer powder made with different methods and processing times. 124

1 INTRODUCTION

Hafnium Carbide (HfC) has been of interest for various applications due to its desirable physical and chemical properties. HfC has the highest melting point of any known binary alloy, at about 3900°C, and offers desirable high specific strength, and a stable oxide at high temperatures. These properties make HfC an appealing candidate for space and aerospace ultra high temperature applications that involve temperatures above 1600°C. With its high hardness and high current capacity at high temperatures, HfC also finds applications in coatings for cutting tools [1,2] and coatings for field emitter tips and arrays [3-8].

1.1 HfC Properties Overview

HfC, like several other transition metal mono-carbides, has a B1 (NaCl) lattice structure, which is FCC Hf metal with carbon occupying the octahedral interstitial sites (as shown in **Figure 1**). C atoms are able to nest in the interstices of the Hf lattice due to the large difference in size between the C atom and the Hf atom. Hf-C bonding is mostly metallic, though it also has some covalent and ionic nature. Thus, HfC has physical properties close to those of metals, such as high electrical and thermal conductivities. HfC can be formed over a wide range of composition, from $HfC_{0.60}$ to $HfC_{0.99}$, due to the incomplete occupation of Hf lattice interstitial sites by C atoms.

The sub-stoichiometric HfC formation results in various amounts of distortion of the Hf lattice by carbon interstitials, which in turn produce an indeterminate HfC lattice parameter. [9]

The C-Hf binary phase diagram is shown in **Figure 2**. The simplicity of single carbide formation shown in the phase diagram leads to a single phase microstructure of this material. Other properties of hafnium carbide are summarized in **Table 1**.

Table 1 Selected properties of hafnium carbide. [9]
Note: Test temperature is 20°C unless otherwise stated.

Structure	Cubic close packed (FCC B1, NaCl) structure
Lattice Parameter	0.4636 nm
Space Group	Fm3m
Composition	$HfC_{0.60}$ to $HfC_{0.99}$
Molecular Weight	190.50 g/mol
Color	Silver gray
X-ray Density	12.67 g/cm^3
Melting Point	3928°C (melts without decomposition)
Heat of Formation, at 298 K	209.6151 (KJ/g-atom metal)
Entropy at 298.15 K (S^o)	39.48 KJ/mol
Thermal Conductivity	20.0 W/m.^{o}C
Thermal Expansion	6.6 (x 10^{-6}/ ^{o}C)
Electrical Resistivity	37-45 μΩ·cm
Vickers Hardness	26.1 GPa
Modulus of Elasticity	350 - 510 GPa
Shear Modulus	193 GPa
Bulk Modulus	241 GPa

Variations in the amount of dissolved carbon and oxygen have led to a wide range of values being reported for the mechanical properties, lattice parameter, and electromagnetic data for HfC. Removal of carbon from the lattice results in reductions in hardness and other mechanical properties, as was reported in Opeka *et al.*'s study [10] of the mechanical properties of Hf-based ceramics, in which they found that the transition

temperature of HfC exhibited strong stoichiometric dependence, decreasing from 2200°C for $HfC_{0.98}$ to 1100°C for $HfC_{0.67}$ ceramics.

The effect of dissolved oxygen on HfC's mechanical properties is not clear. However HfC is one of the most difficult carbides to produce with a low oxide content. For sub-stoichiometric HfC, which has unoccupied octahedral interstitial sites present in the lattice, oxygen atoms tend to fill the empty interstitial sites and form oxycarbide, which can be considered to be a solid solution of HfO and HfC. Removal of the oxycarbide phases depends on the partial pressure of CO surrounding the samples during processing.[11]

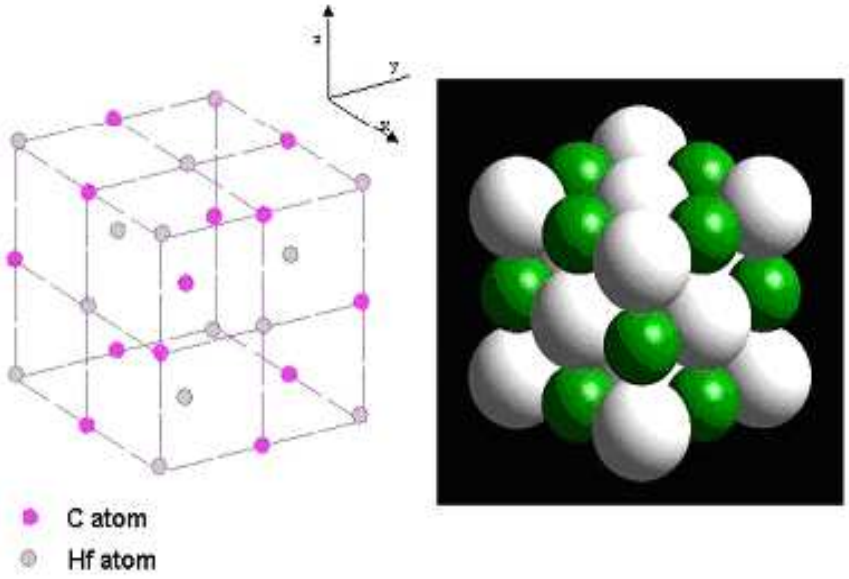

Figure 1 HfC structure with FCC Bravais Lattice

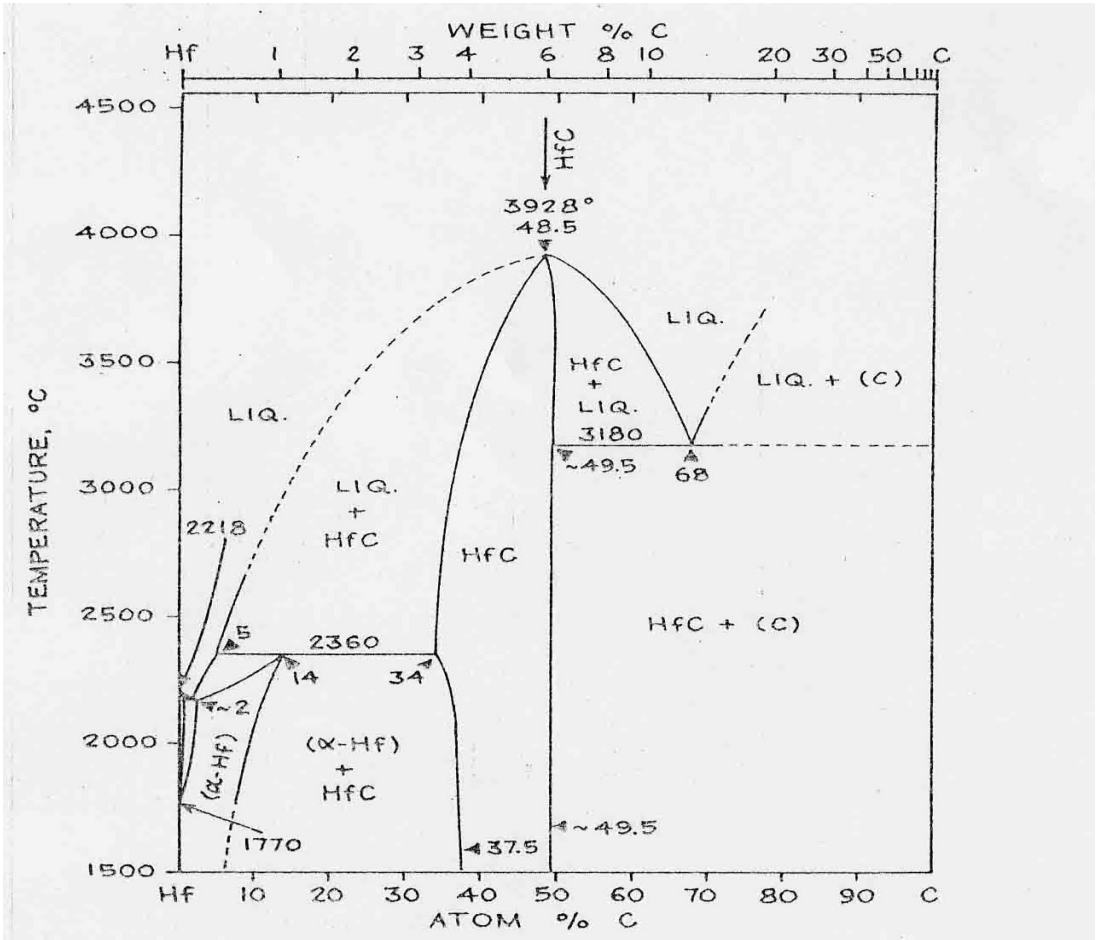

Figure 2 C--Hf Phase diagram [12]

1.2 HfC for Aerospace Applications

HfC has been intensively studied for decades as a structural material for aerospace and space applications at ultra high temperatures.

A common aerospace material used in aircraft brakes, rockets and reentry systems is carbon-carbon (CFC or RCC), which is comprised of carbon-fiber reinforcement in a carbon matrix. CFC has the highest specific strength (strength normalized with density) of any material above 1000°C, but this material's oxidation resistance is limited. Like its other carbon counterparts, CFC oxidizes rapidly above 500°C. Oxidation protection is provided by a silicon carbide coating that is normally applied by pack cementation or Chemical Vapor Deposition (CVD), usually in combination with other materials such as boron to promote self-healing characteristics. When oxidized, the SiC coating is transformed into a layer of glassy silicon dioxide (SiO_2), which is capable of providing good oxidation protection up to 1500°C. However above 1500°C, the viscosity of the SiO_2 decreases rapidly and the carbon matrix is endangered by exposure to an oxidative atmosphere. At temperatures above 1600°C and low oxygen partial pressures, SiC offers little oxidation protection resistance, as it reacts to form the volatile suboxide SiO. SiO forms rapidly by simple gasification. [13]

To address the difficulties experienced by CFC at ultra high temperatures, various other materials have been investigated. A recent report by Sayir [14] discussed in detail the selection of potentially suitable structural materials for use at ultra high temperatures for aerospace and space applications. These potential materials are summarized in **Table 2**. It was suggested that materials for these applications must meet several requirements simultaneously, such as a high melting temperature, high specific

strength, good oxidation resistance, and ease of fabrication. The most basic requirement is that a material should not undergo any significant surface degradation in ultra high temperature, highly corrosive environments. This requirement eliminates from consideration all the materials that react with oxygen to form volatile products. Refractory metals like W, Mo, Os, and Ta are unsatisfactory due to their low specific strength, in addition to their poor oxidation resistance. Ir and its alloys are costly and difficult to fabricate into components.

Table 2 Potentially suitable structural materials for use at ultra high temperatures[14]

Candidate Materials	Requirements			
	Melting Temperature	Specific Strength	Oxidation Resistance	Ease of fabrication
ZrB_2 and HfB_2, and their composites	Moderately high temperatures	--	Moderate	Moderate
W, Mo, Os, Ta	High ~ ultra high temperatures	Low	Poor	--
Ir and Ir alloys	Ultra high temperatures	Low	--	Difficult
HfC, TaC, NbC, ZrC, WC, W_2C, VC,MoC	Ultra high temperatures	High	Moderate	Difficult

HfB_2-SiC materials have been considered the best oxidation resistant material over the entire range from room temperature up to 2000°C. Studies [15,16] shown that the addition of SiC to HfB_2 can improve the oxidation resistance of HfB_2 due to the formation of a two-phase borosisilicate glass/HfO_2 scale. However, for temperatures

above 2000°C and applications involving low oxygen partial pressure or water vapor environments, the degradation of HfB_2-SiC materials is still significant.

For temperatures above 2000°C, due to HfO_2's stability at high temperatures, pure HfO_2 forming material, HfC, is a promising alternative to HfB_2-SiC. This is because: (1) HfC has a high melting temperature of about 3900°C; (2) HfC's oxidation product, HfO_2, has a high melting point of 2774°C; and (3) without hydroxide phase formation, HfO_2 is chemically stable at high temperatures.

1.3 HfC Oxidation Resistance Studies

Although not a major problem for short term high temperature applications, HfC's oxidation product HfO_2's porous nature has hindered HfC's use in long term applications. Numerous studies have been conducted on HfC's oxidation resistance properties.

Bargeron and Benson's discovery[17] of the formation of an "oxycarbide" layer during HfC oxidation increased interest in studying the oxidation behavior of HfC as part of the search for a protective oxide layer. During the examination of an oxidized hafnium carbide film Bargeron and Benson found a new layer which they identified as the hafnium "oxycarbide". The new layer was dense in appearance and formed between the inner residual unoxidized hafnium carbide and the outer oxide. The layer consisted of hafnium, carbon and oxygen and had a well-defined composition over its entire thickness. This discovery was important because it provided alternate oxidation reaction paths and different oxidation rate limiting steps, namely diffusion through the oxycarbide and forming an oxide by oxidation of the oxycarbide, instead of diffusion through the oxide and forming an oxide by oxidation of the carbide.

Bargeron *et al.*'s later work [18] reported that HfC exhibited superior oxidation resistance to HfB_2 when they studied the oxidation of hafnium carbide at temperatures in the range of 1400°C to 2060°C. The three layers were again observed and the middle dense oxycarbide interlayer's oxygen diffusion characteristics were studied. Their results indicated that the oxide interlayer was actually a better diffusion barrier for oxygen than either of the other layers. Based on x-ray microanalysis, x-ray diffraction, and resistance measurements, the interlayer was identified as an "oxygen-deficient oxide of hafnium with a carbon impurity".

Wuchina and co-works [10,19,20] studied the oxidizing behavior of HfC, together with HfN and HfB2, under furnace (1500°C, 1 atm.), arc jet (2000~2400°C, 0.01 atm) and rocket motor chamber (2000°C, 5~34 atm) conditions. A change in the oxidation mechanism was found between oxidation tests at low temperatures and higher temperatures. In the lower temperature (<1500°C) furnace tests, the thickness of the oxide scale was found to be controlled by grain boundary processes; while in higher temperature (>2000°C) arc jet tests, bulk diffusion overwhelmed the grain boundary processes. The investigators suggested that the better low-temperature oxidation performance of substoichiometric carbides and nitrides was due to the larger grain size of these materials, which reduced grain boundary area and thus provided fewer diffusion paths. A denser HfO_2 scale, suggesting better oxidation protection, was observed from substoichiometric HfC than stoichiometric HfC. Under normal oxidation conditions, HfC produces a porous oxide scale with pore channels that allow CO to diffuse through the scale to the outer surface. The denser HfO_2 scale was believed to be caused by a smaller CO gas volume generated at the interface by substoichiometric HfC, which in

turn reduced the pore channels in both number and size and allowed the scale to sinter and fill. It was suggested that this discovery could be used to reduce oxidation rates by forcing solid-state diffusion control.

Wuchina and co-workers also discovered an interlayer at the oxide/carbide interface, both in the low-temperature furnace test and the higher temperature arc jet test. The interlayer in the lower temperature samples was identified as carbon, and the interlayer in arc-jet tested samples was tentatively identified as hafnium oxycarbide.

Shimada and co-workers [21-27] made important contributions to understanding of the oxidation mechanism of hafnium carbide by studying the oxidation of hafnium carbide single crystals. Their initial study [21] of the oxidation of HfC single crystals with the (100) orientation was carried out at temperatures of 600°C to 900°C, where they found that the HfO_2 scale consisted of two regions, a compact layer and a porous layer. Both layers showed the presence of carbon.

Studies [22,23] of oxidation of single crystal HfC with the (200) orientation showed that the compact, pore-free layer's thickness remained constant after a prolonged time, while the porous, cracked layer thickness grew linearly. The compact layer was separated from the HfC crystal in the form of carbon-containing films [24]. It was found that the residual carbon in the films obtained at 700~1300°C were amorphous, but in the films at 1500°C, graphite formation was observed.

Oxidation of HfC powder [25-27] was also conducted by Shimada *et al.*. Results showed that at temperatures of 380 to 600°C, the oxidation of Hf in HfC occurred and yielded free carbon. At temperatures above 600°C, the free carbon was oxidized forming CO_2. Two exothermic Differential Thermal Analysis (DTA) peaks were observed during

HfC oxidation. The lower temperature DTA peak appeared at about 400°C, but the higher temperature DTA peak changed with oxygen partial pressure, shifting to higher temperatures with decreasing oxygen partial pressure. It was suggested that the lower temperature peak was due to the oxidation of Hf in HfC, with formation of carbon and HfO_2, and the higher temperature DTA peak was due to CO_2 formation from free carbon.

1.4 Advantages of HfC Foam for Space Applications

Lightweight and High Melting Temperature

The current trends towards aerospace development include the need for lightweight materials for heat insulation. Cellular materials, such as HfC foam, offer an attractive combination of properties of low overall weight, strength, stiffness, and thermal conductivity. There are many potential applications for HfC foam in space propulsion systems. Thrust chambers and rocket nozzles for small chemical rockets are a relatively low-risk application that may benefit from the material's durability and weight advantages. For large chemical rockets, the possible application for HfC foam is the expansion of the turbopump operating temperature envelope. The large temperature gain that may be possible by using HfC materials could translate into enormous savings in dollars per pound of payload-to-orbit. [28]

Ease of Fabrication

Since HfC is hard and brittle and has a high melting point, HfC foams offer many advantages when fabrication costs are considered in order to provide monolithic, near-net-shape components with complex shapes.

Machining of HfC has been difficult due to HfC's high hardness and brittle nature. Arc melting has been used for synthesizing limited, simple shapes of HfC components. Vacuum Plasma Spray, which has also been used to produce HfC components with simple shapes, uses a high electrical current passing through HfC powder, and spray melted HfC droplets. The VPS system is, however, complicated and the process is costly. Chemical Vapor Deposition is another technique being used to produce refractory metal carbides, but CVD is an intrinsically slow process, requiring hours to produce micrometers of material.[29]

Thermal Stress Relief

HfC foam can provide more effective thermal stress relief in applications for thermal insulation and oxidation protection at ultra high temperatures. In environments that experience large temperature gradients and cyclic thermal stress, HfC foam is a promising candidate for use where other solid monolithic materials can't survive.

In the present investigation, a low cost, simple approach that requires less production time was studied to produce HfC structural foams through thermolysis and pyrolysis of polymer precursors. It was found that the proposed methodology of synthesizing HfC foam can be controlled to produce HfC foams with the desired microstructure and mechanical strength.

2 REVIEW OF HfC SYNTHESIS TECHNOLOGY

2.1 HfC Particles Synthesis Methods

The traditional method of preparing HfC particles is the direct reaction of Hf metal or Hf hydride powders with carbon. Hafnium carbide powder can be prepared by the carburization of hafnium sponge (**Equation 1**) or by the carburization of hafnium hydride at 1600~1700°C (**Equation 2**). Hafnium carbide powder can also be prepared by the reaction of HfO_2 with carbon at 1800~2200°C in hydrogen.

$$\mathbf{Hf + C = HfC} \quad (1)$$

$$\mathbf{HfH + C = HfC + H_2} \quad (2)$$

Pure HfC particles with a homogenous composition are difficult to achieve. High-purity gases or a good vacuum, in combination with very high temperatures, are required to process pure HfC.

2.2 Other Manufacturing Methods for HfC Components

HfC foam, which is a high temperature structural material, falls into the category of inorganic ceramic foam material. By definition, ceramic foams are a specific class of porous material that consists of a three-dimensional array of polyhedral cells, with an average linear dimension ranging from 10 μm to 7 mm, packed to fill space and possessing a geometry that, when isotropic, can be approximated to that of a

tetrakaidecahedron.[30] Cells can be surrounded by ceramic walls or the solid may be contained only in the cell edges (struts).

In 1963, Schwartzwalder and Somers carried out one of the first investigations into ceramic foams. [31] Since then the number of papers and patents about ceramic foams has increased dramatically, indicating a growing scientific and industrial interest in these materials. However, most research efforts have focused on foam material such as alumina, zirconia, mullite, cordierite, silicon carbide and silica. Very little attention has been paid to HfC for ceramic foam applications, and little work has been reported on producing *pure* HfC foams. The reaction forming method has been used by other investigators to produce *pure*, high density HfC foams. If a more general definition of "HfC" foam is used, then the other methods by which HfC foam can be produced are: 1) CVD to create a *Graphite foam-HfC coated* composite foam; 2) VPS (vacuum plasma spray) to fabricate near solid HfC components; and 3) reactive sintering and hot isostatic pressing (HIP ing) of HfC particles to create a near solid HfC structure.

2.2.1 Reaction Forming

The Reaction Forming method was reported by Palmisiano *et al.* [29] to produce porous HfC material. This method involved placing a glassy carbon preform on a bed of molten Hf metal or Hf metal-silicon alloy. The molten metal wicks inside the porous carbon preform and reacts, forming an HfC foam structure.

The carbon preform was produced by initially mixing a resin and a curing catalyst together, then heat treating the mixture in two steps (a low-temperature phase and a high-temperature phase). The low-temperature heat treatment (323 K to 473 K) cured

the resin, and then the high-temperature treatment (773 K to 1473 K) decomposed the resin to create a porous carbon preform.

This glassy carbon preform was then placed on a bed of Hf and heated above the melting point of the Hf metal. The molten Hf metal wicked inside the porous carbon preform and reacted, forming refractory metal carbide foam. Since pure Hf metal has a very high melting point, 2473 K, 12.0 wt.% Si can be added to the Hf metal for infiltration at a lower temperature of 2103 K.

The researcher suggested that by varying the density and the pore structure of the carbon preform, the final structure porosity (from 5% to 50%) could be controlled. The geometry of the HfC component could be modified by adjusting the shape of the initial casting mold for the resin-based mixtures.

There are several drawbacks of the reaction forming approach for creating HfC foam: 1) the method involves creating carbon foam; 2) high temperatures above 2400K are required for the Hf infiltration; and 3) Si contamination is an inherent problem, although Si can help reduce the infiltration temperature to 2103 K. Other concerns are oxygen contamination during the high temperature infiltration of pure Hf, and the high cost of the whole process.

2.2.2 CVD

Numerous studies have been conducted to use CVD to develop HfC protective coatings on different substrates. In 1993, Emig et al. [32] studied high-temperature hafnium carbide and hafnium nitride coatings for carbon fiber reinforced carbon (CFC) and carbon fiber reinforced silicon carbide (C/SiC). A thermal CVD reactor and hafnium

tetrachloride, methane and hydrogen gases were used. A carbon-free hafnium carbide deposit was possible according to predictions based on thermodynamic modeling of the CVD reactions involved. Ache *et al.* [33] used secondary-neutral mass spectrometry to measure the carbon content in the hafnium carbide layers obtained this way. The deposited layer carbon-to-hafnium ratio was reported to closely agree with the thermodynamic model predictions.

Sourdiaucourt *et al.* [34-37] studied the deposition of hafnium carbide onto a carbon foam substrate. Glassy carbon foam with a low density was prepared and used for their CVD process. The carbon foam was synthesized in three steps: impregnation of a polyurethane polymeric foam by phenolic resin, curing of the resin, and pyrolysis of the mixture. After pyrolysis the polyurethane skeleton totally decomposed into gaseous products, while the phenolic resin formed a solid carbon foam structure. The carbon foam porosity was 65 pores per inch, with a high open porosity of 98%. The CVD precursors used were an Hf-C-Cl-H system. Based on their theoretical analysis, [34] methane (CH_4) and hafnium chloride [$HfCl_x$ (x = 2, 3, 4)] were used as the carrier gases. For the CVD processes typically used by this group, [35] the substrate temperature was set to 1673K, and the carrier gas temperature was 1473K. A maximum HfC film thickness of 75 μm was reported, at a growth rate of 37.5 $\mu m/h^{-1}$. Stoichiometric HfC was produced under standard conditions, while a mixed HfC + C deposit was obtained when a high methane molar fraction was used. The HfC coating reinforcement effect was observed when a coated and an uncoated carbon foam sample were heated to 2773K and compression tested. It was also observed that after the test, the adhesion between the Hf coating and carbon substrate was lost. [36]

Wunder and co-workers [38-42] conducted a series studies on HfC coatings on carbon fiber-reinforced carbon composite (CFC) materials. Their initial study [38] investigated hafnium chloride ($HfCl_4$) and methane (CH_4) in an excess of hydrogen (H_2) as coating precursors. Their later work [39-42] attempted to deposit multilayer coatings on CFC composites, which consisted of pyrolytic carbon as a ground layer, hafnium carbide as a diffusion barrier, and silicon carbide as a oxidation protection layer. They reported that HfC, which has a high affinity towards O_2, functioned well as a diffusion barrier, as did the SiC as the top layer at temperatures up to 1450°C.

Recent work by Sayir [14] investigated the use of the CVD technique to produce monolithic hafnium carbide (HfC) and tantalum carbide (TaC). Carbon fiber reinforcement was used to improve the toughness and strength of monolithic HfC, TaC, and HfC/TaC. The addition of tantalum carbide (TaC) in the HfC matrix was studied in order to improve the microstructure.

Toughness improvement was shown in the strain-to-failure values for the $C_{fiber}/PG_{interface}/HfC_{matrix}$ composites, that were larger than 1% and, in many cases, reached as high as 2%. This strain capability exceeds that of most ceramic matrix composites. However the reported tensile strength of the $C_{fiber}/PG_{interface}/HfC_{matrix}$ composite was low, about 26MPa.

Other related work on CVD deposition of HfC was done by Healy *et al.* [43] who investigated the organometallic chemical vapor deposition (OMCVD) of transition metal carbides (M = Ti, Zr, Hf, and Cr) from tetraneopentyl-metal precursors. Metal carbides were deposited on Si, Al_2O_3, and stainless steel substrates from $M[CH_2C(CH_3)_3]_4$ at 300 ~ 750°C and at a pressure of 10^{-2} ~10^{-4} torr. Spatenka *et al.* [44] deposited HfC film by

plasma-enhanced CVD using bis(h-cyclopentadienyl)dimethylhafnium, Cp_2HfMe_2, as precursor.

A major drawback associated with the CVD method is the slowness of the deposition process, which requires hours of operation to produce layers of materials in the order of micrometers thickness. Another concern is the possible cracking and delamination of the HfC layer due to CTE (coefficient of thermal expansion) mismatches between the HfC layer and the substrate material when the structure is under cyclic thermal stress or in a steep temperature gradient.

2.2.3 Vacuum Plasma Spray

Agarwal *et al.* [45] studied near net forming of hafnium-based ceramic components using the vacuum plasma spray (VPS) technique. A schematic of their VPS forming process is shown in **Figure 3**. With Agarwal's system, Hf based ceramic powders (HfB_2, HfC, HfN) were fed into the plasma flame region and melted by a plasma arc. High velocity molten particles were deposited on a rotating graphite or metallic mandrel, which was removed chemically or mechanically after the deposition. High current and low voltage was used to generate the plasma.

The near net HfC components shown in their work were thin-walled cylinders with a wall thickness of 0.5 or 1 mm and a diameter of 12 mm and 50 mm. The HfC deposit was very dense, with a micro porosity less than 2%. Micro-cracks of the order of 0.4μm in width and 15~20μm long were observed throughout the deposited structure, which was attributed to the rapid solidification and corresponding shrinkage experienced during spray forming. The composition of the deposit was determined to be mainly HfC,

with traces of HfO_2. The reason for the presence of HfO_2 in the deposit was not fully understood.

The VPS (Vacuum Plasma Spray) process is complicated and requires very high electrical currents for operation. The HfC deposit created is a highly dense material with a simple shape, which is undesirable for space applications.

2.2.4 HIP, Sintering and Other Methods

Grant and Robinson [46,47] reported using Hot Isostatic Pressing (HIP) to form a new group of cobalt-based alloys containing 3-18% hafnium carbide. HIP is a forming process that combines simultaneous heat and pressure to consolidate metal or ceramic powders. The process uses elevated temperatures and a very high vacuum to remove air and moisture from the powder, followed by high inert gas pressures and elevated temperatures to remove internal voids and create a strong metallurgical bond in the material. The HIP product is a clean homogeneous material with a uniformly fine grain size and a near 100% density. Drawbacks for this method are the expensive equipment and required special handling of materials. Also, HIP is limited as to the size and shape of the part produced, and typically involves low process productivities and high manufacturing costs. It is difficult to apply the method to the production of a porous HfC structure.

The sintering method was used by Panasyuk [48] and Ordan'yan *et al.,* [49] and pulsed electric current sintering was used by Suganuma and Kitagawa [50] to created dense HfC carbide parts. An explosive-consolidation method was used by Kecskes *et al.* [51] to produce a moderately dense HfC product.

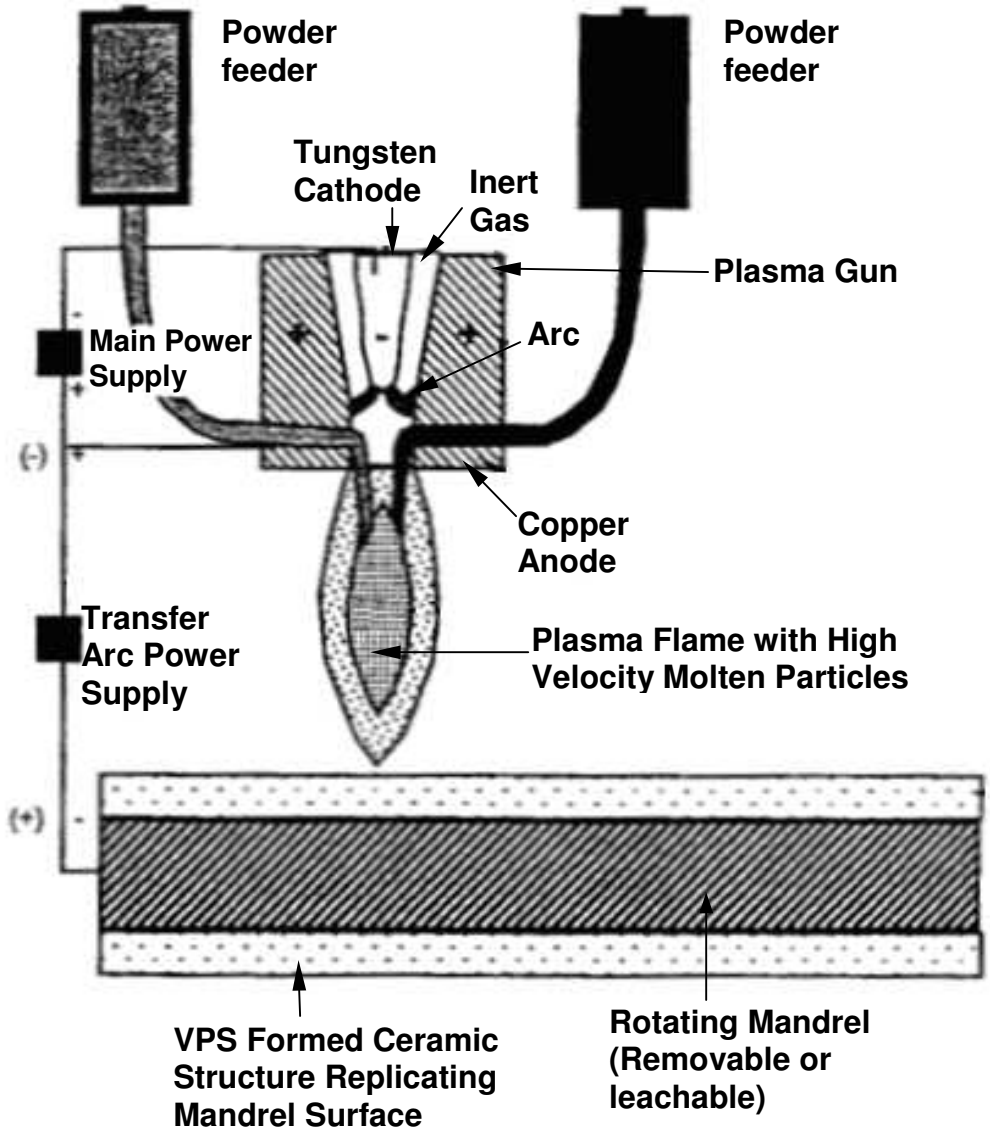

Figure 3 A schematic of the Vacuum Plasma Spray (VPS) forming process

2.2.5 Synthesizing HfC Foam from Polymer Precursors

Current research into hafnium carbide foam largely stems from the Institute of Chemical Physics in Chernogolovka (ICP-C)'s effort to produce hafnium carbide coatings on graphite. The scientific team at the ICP-C in Russia, led by Professors Lemenovskii and Pomogailo, has developed a low temperature polymeric based process to fabricate HfC of high purity and yield. They have developed a series of processes to synthesize the necessary monomers and the subsequent polymerization and pyrolysis procedures to fabricate HfC. [52,53]

In ICP-C's research, an approach was utilized to produce a hafnium carbide coating on graphite substrates, in which a Carbon Source Polymer and a hafnium containing Macromolecular Metal Complex (MMC) were mixed together and subjected to thermolysis and pyrolysis. During the heat treatment the polymers burned off, and the hafnium and carbon remaining reacted, forming hafnium carbide. The hafnium carbide *foam* was discovered while testing different polymers to find out their effect on HfC coatings. It was found that when thermosetting epoxy resins were used, the polymer foamed before HfC conversion, creating hafnium carbide *foams* instead of a solid HfC structure.

Further investigation of these findings resulted in a one-step procedure for creating hafnium carbide open-cell foam. Using this method, the polymer mixture starts out solid, but begins to foam during heat treatment under vacuum. This occurs because as the polymers decompose, the gasses produced cause the material to foam. All gaseous products are removed by the vacuum system, leaving behind an open celled cellular matrix.

This method shows promise as a low cost, reliable method for producing low-density HfC foams. The HfC foam created can be easily machined into shape, thus reducing fabrication costs. By incorporating high-temperature materials, such as fibers or other structures in the polymer preform, the HfC foam properties can be engineered to suit particular applications, such as heating insulation and/or load bearing materials in space applications.

3 OBJECTIVES

The overall goal of this research is to develop a simple, low cost method to produce low-density HfC foam with a desired HfC composition, uniform microstructure, and good mechanical properties. The foam will be produced through thermolysis and pyrolysis of a hafnium containing Macromolecular Metal Complex (MMC) and carbon source polymers. These polymers should be cast to shape at room temperature, without any special precautions. A group of acceptable preparation process parameters will be developed to assist in the commercialization of the product.

Specific objectives are:

a) **Produce HfC foam from polymer precursors**

   Synthesize HfC foam by heat treatment of the polymer precursors under vacuum.

   1) Determine the effect of different polymer ratios on foam density
   2) Determine the effect of a range of thermolysis parameters on foam density

b) **Determine the mechanism of HfC conversion from polymer precursors**

   1) Determine the temperature ranges at which the HfC conversion occur
   2) Determine the overall reactions that take place during high temperature pyrolysis.

c) HfC Foam Processing

1) Determine the factors that affect the HfC foam structure during polymer mixture sample preparation.
2) Optimize the preparation techniques to produce a uniform foam structure and the desired mechanical properties.

d) HfC Foam Characterizaion

1) Determine the composition of HfC foams.
2) Measure the compression strength of HfC foams.
3) Examine the microstructure of HfC foams.

4 MATERIALS AND METHODS

4.1 Polymer Precursors

The HfC foam was synthesized using the hafnium containing Macromolecular Metal Complex (MMC) hafnium trifluoroacetylacetonate ($Hf(F_3\text{-}AcAc)_4$), and carbon source polymers bisphenol-A (DGEBPA) epoxy resin and hardener. Hafnium trifluoroacetylacetonate was studied in the ICP-C's research to produce HfC coatings.[52,53] However, the combination of carbon source polymers together with hafnium trifluoroacetylacetonate to produce HfC foams was first used for the research reported here.

4.1.1 Hafnium Containing MMC

The hafnium containing MMC hafnium trifluoroacetylacetonate was purchased from Alfa Aesar (Stock number: 19275). The formula and structure of the polymer are shown in **Figure 4**. The as received chemical was a white powder packed under argon, with a chemical purity of over 97.5%. The impurities were zirconium compound and H_2O. The presence of the zirconium compound impurities resulted from the low levels of zirconium that are found with Hf naturally; the separation of the two elements is difficult. H_2O impurities are introduced by the easy absorption of moisture by hafnium trifluoroacetylacetonate under normal atmospheric conditions. Hafnium trifluoroacetylacetonate has a melting point range of 128~129°C.

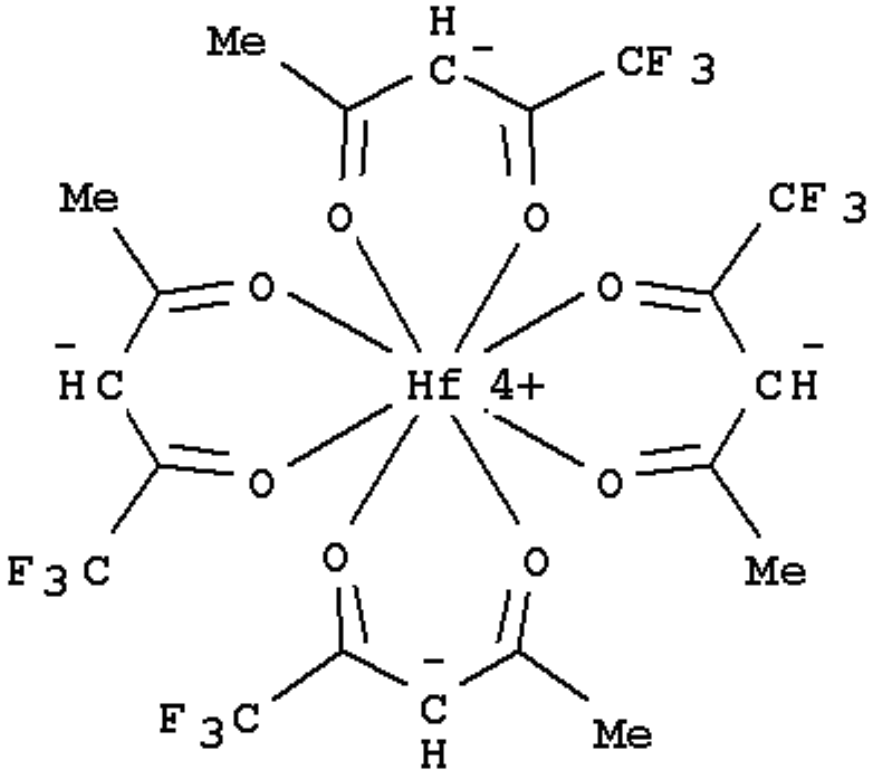

Figure 4 Hafnium trifluoroacetylacetonate (Formula: $C_{20}H_{16}F_{12}HfO_8$)

4.1.2 Carbon Source Polymers

The Bisphenol A diglycidyl ether resin & harder used were the Devcon 2 Ton/Clear Weld Epoxy System. This epoxy system has a nominal curing time of 30 minutes at room temperature. The epoxy resin is a colorless, transparent liquid, and the hardener is a light yellow, transparent liquid. The packaging system for the Devcon 2-Ton epoxy, shown in **Figure 5,** was specifically designed for the resin and hardener to be mixed at a volume ratio of 1:1.

4.1.2.1 Epoxy Resin

The constituents of the epoxy resin are given in **Table 3**. The epoxy resin's chemical formula and structure are shown in **Figure 6** and **Figure 7**.

Epoxy Resin Formula**:** $(\underbrace{C_{15}H_{16}O_2}_{\text{Component 1}}\cdot\underbrace{C_3H_5ClO}_{\text{Component 2}})_x$

Table 3 Epoxy resin constituent

Constituent	Abbreviation	Weight percent (%)
Bisphenol A diglycidyl ether resin	DGEBPA	>60

Figure 5 Devcon 2 Ton/Clear Weld Epoxy System

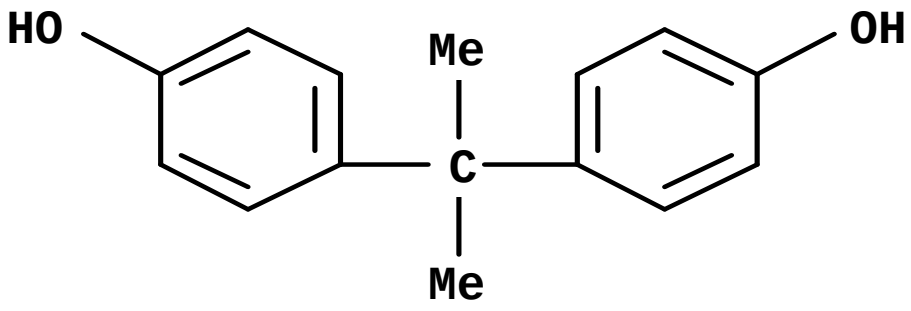

Figure 6 Resin *Component 1* formula: $C_{15}H_{16}O_2$

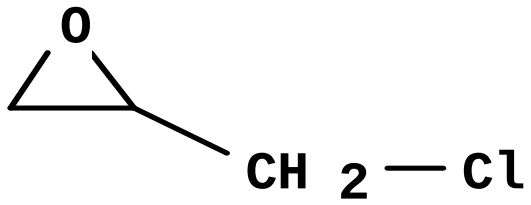

Figure 7 Resin *Component 2* formula: C_3H_5ClO

4.1.2.2 Epoxy Hardener

The constituents of the epoxy hardener are listed in **Table 4**. **Figure 8** and **Figure 9** show the formula and structure of the constituents of the epoxy hardener.

Table 4 Epoxy hardener constituent

Constituent	Abbreviation	Weight percent (%)
Aminoethylpiperazine	AEP	15-25
Nonylphenol	--	75-85

4.2 Mixing of Polymers

4.2.1 Sieving and Storage of Hafnium Containing MMC

The hafnium containing MMC, hafnium trifluoroacetylacetonate, was purchased from Alfa Aesar and received as a white powder. Visual inspection of the as received chemical generally revealed yellow-colored hard particles in the powder, with sizes up to 1mm in diameter. The manufacturer claimed that these particles were composed of hafnium trifluoroacetylacetonate that had agglomerated due to moisture absorption.

Experiments showed that these particles during tended to degrade the mechanical properties of the HfC foams. The particles were hard and did not break up or dissolve during the polymer mixing operation, thus tending to produce a locally hafnium-trifluoroacetylacetonate-rich region in the polymer mixture and resulting in large cells in the HfC foam during thermolysis and pyrolysis. These large cells created variability of foam structure and reduced the mechanical properties of the HfC foam.

In order to remove these particles, the hafnium trifluoroacetylacetonate powder was sieved twice before use, first a 200μm mesh then a 150μm mesh sieve

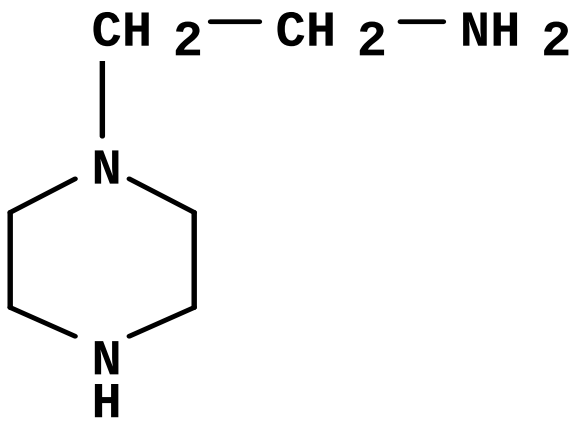

Figure 8 Aminoethylpiperazine formula: $C_6H_{15}N_3$

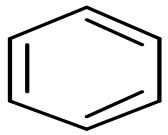

D1 — OH

D1 — (CH 2) 8 — Me

Figure 9 Nonylphenol formula: $C_{15}H_{24}O$

(Fisher Scientific Standard Testing Sieve). After sieving, the powder was free of hard particles and was stored in a SANPLA Dry Keeper. The cover of the powder storage bottle was sealed to prevent further contamination by moisture.

4.2.2 Polymer Mix Ratios

hafnium trifluoroacetylacetonate was hand mixed with the epoxy resin & hardener to different ratios to investigate the effect of mix ratio on HfC foam properties. To mix these polymers, the resin and hardener were combined and hand stirred to reach a uniform epoxy mixture, after which the hafnium trifluoroacetylacetonate was added and stirred until a uniform mixture was achieved.

The mixing ratio of hafnium trifluoroacetylacetonate with the epoxy mixture was varied in weight ratios from 1:1 to 4:1 (hafnium trifluoroacetylacetonate : epoxy mixture). Increasing the proportion of the hafnium trifluoroacetylacetonate was attempted in order to promote HfC conversion during the subsequent heat treatment processes.

A high viscosity polymer paste was produced for all the mixing ratios studied. Increasing the proportion of the hafnium trifluoroacetylacetonate in the mixture tended to accelerate the epoxy curing speed, which was normally around 30 minutes at room temperature. Mixing with a ratio of 1:1 was relatively easy and yielded a paste with a viscosity low enough that a uniform mixture was easily achieved. Higher ratios up to 4:1 were more difficult to handle, requiring quicker mixing (30s ~ 50s) since the paste viscosity increased rapidly due to epoxy curing. For ratios higher than 4:1, the polymer mixture hardened so quickly that in most cases it became unmixable before sufficient hafnium trifluoroacetylacetonate powder could be added.

As a result, the present study was limited to an examination of mixtures with ratios of 1:1 ~ 4:1 due to the difficulties involved. The effect of these polymer mixing ratios on the final HfC foam properties was investigated.

4.2.3 Mixing Methods

Different methods of mixing the polymer precursor were investigated. Two methods: hand mixing and vacuum mixing were studied. Procedures and equipment for both methods are introduced in the following sections.

4.2.3.1 Hand mixing

Hand mixing offered a simpler approach to mixing the polymers. The polymer precursor mixing and preform sample molding processes utilized a digital weighing scale (model Denver Instrument M-310, with an accuracy of $\pm$ 0.1 mg), disposable plastic mixing trays, a glass stirring rod, and a custom made aluminum mold. To accelerate polymer curing, a Delta 9039 open air box furnace was employed to store the polymer preform samples.

Initially, a specific amount of hafnium trifluoroacetylacetonate powder and epoxy (resin + hardener) were measured with the digital weighing scale according to the predetermined weight ratios and placed into two separate plastic mixing trays. The epoxy resin and hardener were then mixed with the glass rod to reach a uniform epoxy mixture, after which the measured hafnium trifluoroacetylacetonate powder was gradually added while the mixture was stirred with the glass rod until a uniform polymer paste was achieved. Depending on the mixing ratios, the final pastes had different viscosities, all with a yellowish color. The total mixing time varied for the different ratios and sample

amounts; for a typical 2 to 5 gram hafnium trifluoroacetylacetonate sample and a 1:1 mixing ratio, the total mixing time was less than 2 minutes.

The polymer paste was then transferred to a pre-designed mold in order to produce cylinder-shaped polymer preform samples. The mold, shown in **Figure 10**, was made from aluminum alloy 6061 T6. The aluminum plate thickness was 15mm. Ten through holes, each with a diameter of 13mm, were drilled and used as molding chambers for the polymer paste. Since the polymer paste had a high viscosity, preventing leakage during the polymer filling process was relatively easy and the use of a layer of aluminum foil as backing material at the bottom of the mold was sufficient for the purpose. It was found that the mold surfaces that come into contact with the polymer paste during processing had to be polished to a surface finish of better than √64. A surface finish rougher than this led to the cracking of preform samples during ejection from the mold, even with the use of mold release compounds.

After filling the mold holes with polymer paste, the mold with the polymer preform samples was transferred to a Delta 9039 open air box furnace and baked at 50°C for 36 ~ 48 hours to promote polymer curing. Higher temperatures were not used in order to prevent possible polymer decomposition reactions.

When the sample was completely cured, the backing aluminum foil was removed, and an aluminum rod with a diameter of 13mm was used to eject the polymer preform samples from the bottom side of the mold. Care was taken during this process to avoid sample cracking.

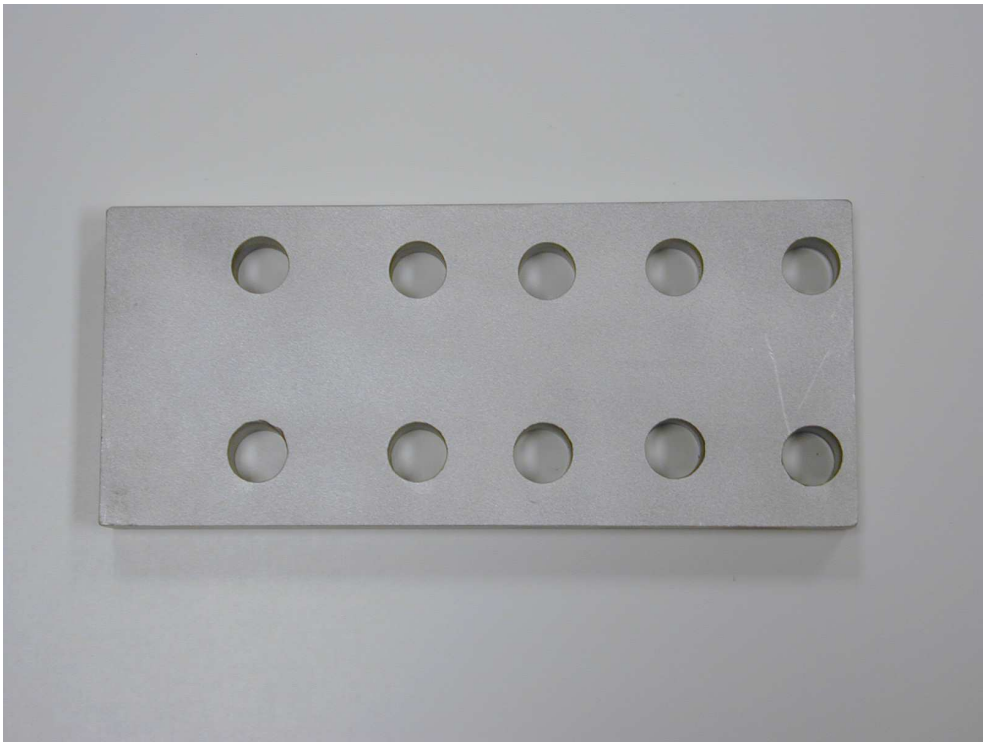

Figure 10 Aluminum mold for hand mixing

4.2.3.2 Vacuum mixing

To optimize the foam microstructure and improve the HfC foam mechanical properties, vacuum mixing of the polymers was also tested to determine whether vacuum mixing would improve mixing uniformity and reduce air pockets trapped inside the mixture during the mixing process.

A vacuum mixer was built to facilitate the vacuum mixing process. As shown in **Figure 11,** the vacuum mixer consisted of four parts: a hand drill that acted as a mixing motor, a pull-push rotary motion vacuum feed-through purchased from Vacuum Research Corporation, a NW-16 Tee that allows the air to be pumped out, and a disposable plastic 20cc syringe that served as a mixing chamber.

The vacuum feed-through enabled both linear and rotary motion of the mixing shaft. This allowed the mixing paddle to move up and down, reaching the entire depth of the polymer paste while rotating. Since a steel paddle tends to scrape off pieces of plastic from the syringe and contaminate the polymer preform sample, Teflon paddles were designed and used for this process. Two paddles were used simultaneously. The upper paddle mixed liquid and forced it downward, while lower paddle mixed the liquid and forced it upward. During mixing, the mixing paddles were moved up and down manually to achieve uniform mixing.

The syringe functioned both as a mixing chamber and a mold to produce cylindrical polymer preform samples. After the preform samples had cured completely, the disposable syringes were broken open to eject the samples.

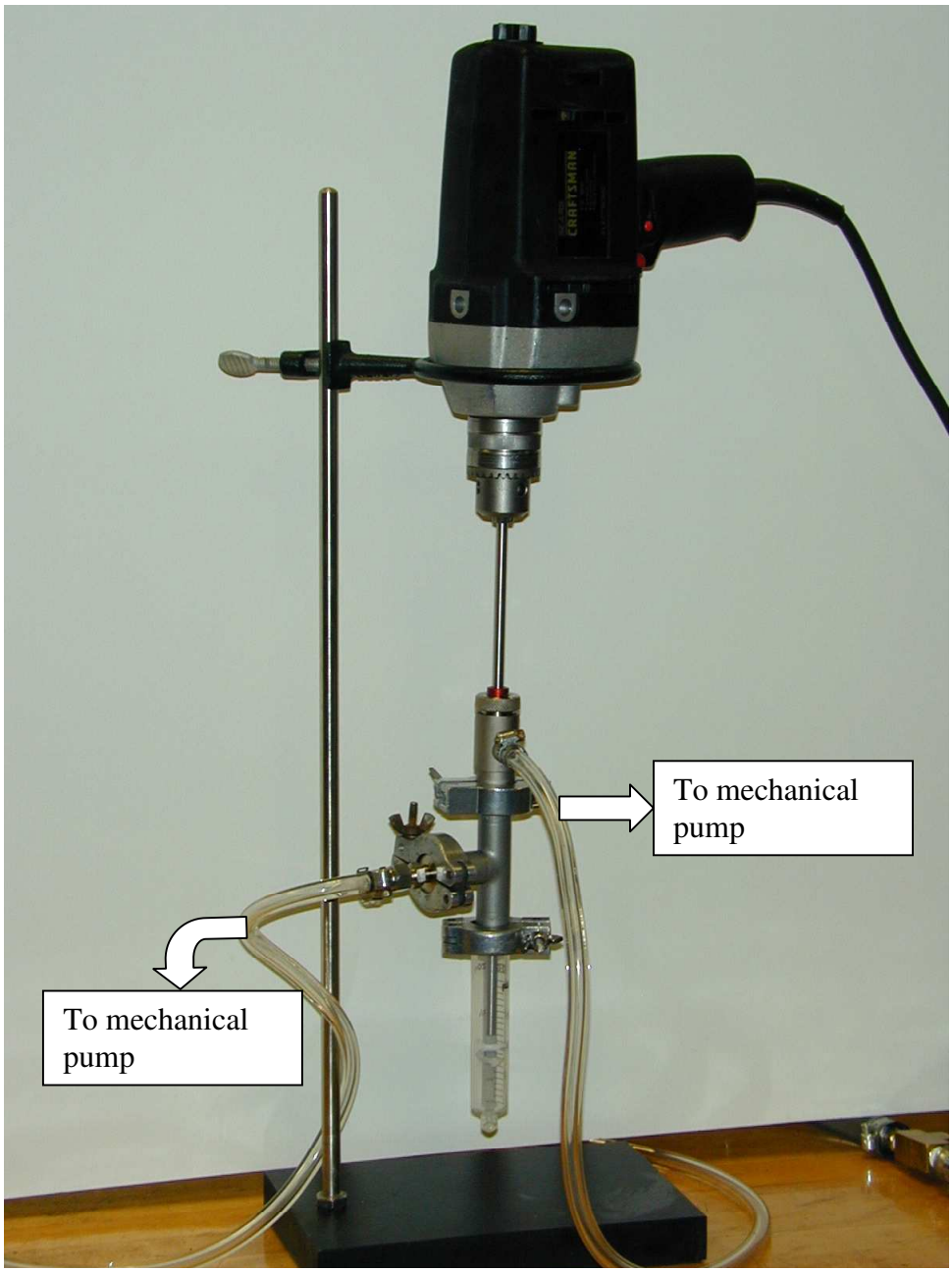

Figure 11 Vacuum mixer and pump system connections

Different polymer ratios (1:1 ~ 4:1) were again tested with the vacuum mixer, but only the ratio 1:1 yielded a uniform mixture. Higher ratios were unsatisfactory due to high viscosity and rapid curing of the polymer paste during the mixing process. For ratios higher than 1:1, polymer pastes adhered quickly to the mixing paddle and shaft, and rotated together with the paddle as a bulk piece in the syringe. Since no forced paste flow was possible once this had occurred, the pastes at these ratios did not reach an acceptable uniformity.

As with the hand mixing process, the vacuum mixing procedure started with weighing out the polymer. Specific amounts of hafnium trifluoroacetylacetonate powder were measured with the digital weighing scale according to the predetermined weight ratios and then each sample was divided into two roughly equal portions and placed into two separate plastic mixing trays.

Loading of the polymers into the syringe involved two steps in order to create the loading layout shown in **Figure 12**. First, one tray of powder was added into the syringe and then the same weight of epoxy resin & hardener was added on top of it. This process was then repeated. Predetermined amounts of epoxy resin & hardener were squeezed into the syringe directly, without premixing. It was important to use epoxy resin & hardener as the upper layer because when the vacuum pumps started to evacuate the syringe, this layer acted as a seal, preventing the powder underneath from being sucked into the vacuum pump. The polymer loading layout also helped produce a roughly uniform mixture to start the mixing with, thus improving the final mixing result.

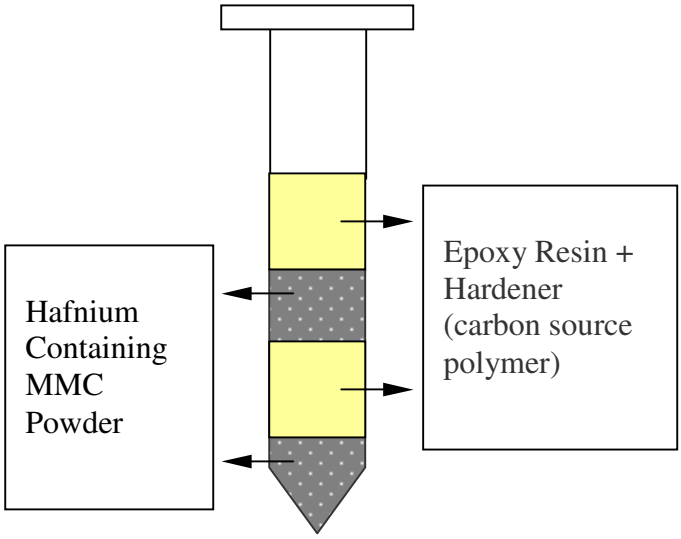

Figure 12 Polymer loading in the syringe for vacuum mixing

The syringe, loaded with polymers, was then connected to the vacuum mixer's NW-16 Tee port, as shown in **Figure 11,** and pumping was started. Two mechanical pumps were connected to the vacuum mixer. The pump connected to the lower outlet pumped down the syringe chamber, while the pump connected to the upper outlet pumped down the vacuum feed-through chamber. The vacuum was monitored with vacuum gauges for both chambers. Once pumping started, the syringe chamber and feed-through chamber achieved a vacuum of 29 inHg in less than 10 seconds. Pumping was extended for about 30 to 60s to completely remove the air bubbles trapped inside the viscous epoxy resin and hardener.

Once an adequate vacuum had been achieved in both chambers, the mixing motor was started. The mixing shaft rotation speed was set at about 600 rpm. The syringe was pushed upward slowly to immerse the rotating mixing paddles into the polymers. Once the mixing paddle had reached the bottom of the syringe, the syringe was moved downward to allow the paddle to mix the top layer of the polymer mixture. Four to five cycles of up-and-down motion were repeated before a satisfactory mixture uniformity was reached. The total mixing time was controlled to be less than 2 minutes in order to finish mixing before the polymer curing.

Once mixing had been completed, the paddle was removed from the polymer paste, but paddle rotation was continued for another 1 minute to spin off residual paste on the paddle. Then the mixing motor was stopped.

Vacuum pumping was extended for a further 5 minutes to remove residual bubbles in the polymer mixture. Then both pumps were turned off and the syringe was uninstalled. The syringe was transferred to an open air box furnace and stored for 36 to

48 hours to promote polymer curing. The furnace temperature was set at 50°C; higher temperatures were not used to prevent possible polymer decomposition reactions.

To clean the apparatus, the paddle and shaft were removed from the vacuum mixer, immersed in a beaker of denatured alcohol and cleaned in an ultrasonic bath for 30 minutes.

The disposable syringe was used as a mold to produce the cylindrical polymer preform samples. Once the polymer sample had cured completely, the syringe was cut open to eject the polymer preform sample.

4.3 Thermolysis and Pyrolysis

Polymer preform samples were subjected to a heat treatment process under a vacuum atmosphere to produce the final HfC foam. A LINDBERG 54553 tube furnace, which is capable of a maximum temperature of 1500°C, was used for the heat treatment. A Brew furnace, which was made by Thermal Electronics Inc. that can reach a maximum temperature of 2100°C was also used for some samples due to its larger chamber for producing larger size samples. For both furnaces, a vacuum of 5×10^{-5} torr was maintained during the heat treatment.

The heat treatment operation was a two-phase procedure: thermolysis and followed by pyrolysis. The thermolysis phase, at lower temperatures, produced the preliminary foam structure by allowing gas generation and removal during polymer decomposition. The pyrolysis phase, at higher temperatures, finished the HfC foam formation by removing completely the gaseous products and completing the HfC conversion.

The ICP-C team determined that under a dynamic vacuum, the polymer decomposition gaseous products were completely removed within the first 5 hours at 1300°C. However, most of the gas was evolved during the first five minutes of the pyrolysis. Their results also indicated that a pyrolysis temperature of 1300°C for 3 hours was sufficient to convert a significant fraction of the HfC (approximately 90%).

Preliminary results in the current research showed that a thermolysis temperature of 200°C with a dwell time of 30 minutes was sufficient to obtain a relatively good HfC foam structure. A higher pyrolysis temperature (1400°C) and longer dwell time (4 hours) than that of the ICP-C team were used for pyrolysis in order to ensure complete conversion of HfC. **Figure 13** shows a typical temperature profile used in this research, consisting of a thirty-minute burn-off at 200°C (thermolysis), followed by a slow ramp up to 1410°C and a dwell time of 4 hours (pyrolysis).

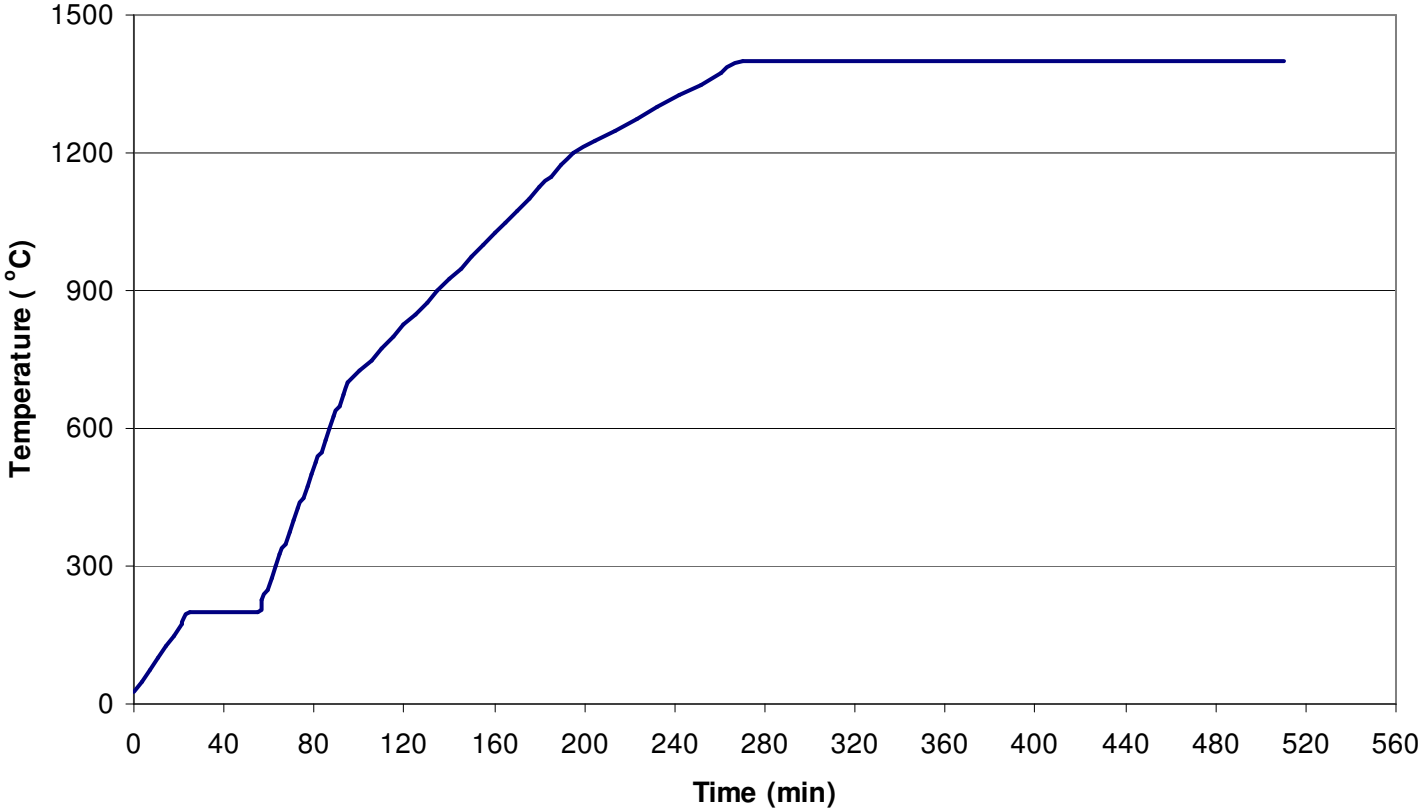

Figure 13 Typical temperature profile for HfC foam processing

4.4 Polymer Powder Compaction

In the processes described so far the cured polymer preform samples (either hand-mixed or vacuum-mixed) were moved to a vacuum furnace and subjected to a low temperature thermolysis and then high temperature pyrolysis. There were no stoppages during the heat treatment. HfC foam produced in this way has a "naturally" formed foam structure and the foam cell sizes are determined solely by the gases generated during the thermolysis step.

To reduce the variability in the final HfC foam properties that is introduced by the natural cell growth process, an additional step was added after thermolysis. The heat treatment was stopped after thermolysis, the furnace was cooled to room temperature, and the polymer preform samples were removed from the vacuum furnace. At this stage, the samples were still polymeric in nature, and had experienced a marked expansion in sample size due to the foaming effect during thermolysis. These samples were then pulverized using a porcelain mortar and pestle (Coors 60317-60319) and the polymer powder produced was then sieved with a Fisher Scientific No.100 Stand Testing Sieve with a mesh size of 150 μm in order to control particle size.

To optimize the polymer particle size and expedite the pulverizing process, a second approach using a Glen Mills, Labtechnics Model LM 1/P dish and puck crusher (**Figure 14**) for the pulverizing process. This crusher requires a 3-phase 235V power supply and a pneumatic pressure supply of 85 Psi, and is capable of pulverizing materials to particle sizes of 75 μm in about 5 minutes.

In order to pulverize the polymer samples, they were first broken into blocks of about 5 mm in length. Thirty grams of the material were then placed into the pulverizing bowl, the bowl placed into the cabinet under the pressurized air clamp, and the lid was closed. The timer was set to 5 minutes and the START button depressed until the mill cycle engaged. Once the chamber ceased to vibrate, the powder was removed from the pulverizing bowl and sieved with a Fisher Scientific No.100 Stand Testing Sieve with a mesh size of 150 μm to control particle size.

To analyze the particle size distribution of the polymer powder produced, a SEM was initially used to take pictures of the particles and image analysis software applied to estimate the particle size. The final analyses used a Microtrac S3500 Particle Size Analyzer (**Figure 15**) for particle size analysis. The Microtrac S3500 analyzer employs laser diffraction techniques and can measure particle sizes from 0.024 to 2800 microns. Both dry and wet powder samples can be used with this machine. To prepare a wet sample, 0.3g of polymer powder was mixed into 15 ~ 20 ml of water. The suspension was placed in an ultrasonic bath for 15 minutes to break up agglomerated particles and then loaded into the sample chamber. The analyzer performed measurements automatically. To analyze a dry sample, 0.7 to 1.4g of dry powder was needed. Here, dry powder samples were directly sucked into the analyzer via a stainless steel tube for measurements. For both wet and dry samples, a processing time of only 10~20 seconds was needed. A report was generated by the analyzer's software, with information about particle size distribution, and average particle sizes based upon different calculation methods.

The sieved powder, produced either by mortar & pestle or by the Labtechnics crusher, was then cold pressed to produce polymer pellets (or polymer cylinders). For the cold pressing step, a die set (Spex Certiprep Pellet Die 3613) with a mold inner diameter of 13 mm was used. The sieved powder was poured into the die set mold chamber and compressed with a manual hydraulic compressing unit. The compressing pressure was 38 ksi, and the hold time was 5 minutes.

The polymer cylinders produced by cold compaction were solid and the outer surfaces were smooth. These cylindrical samples were then heat treated with a second thermolysis and final pyrolysis to produce HfC foams. HfC foam produced using this polymer powder compaction method had a different microstructure from the samples made using the previous natural cell growth approach. The compaction foams consisted of connected HfC particles and very few closed cells were observed. These HfC foams had a more uniform foam cell structure and were mechanically stronger than foams produced using the previous approaches.

Figure 14 Glen Mills, Labtechnics dish and puck crusher

Figure 15 Microtrac S3500 particle size analyzer

4.5 HfC Foam Characterization

After the HfC foam had been produced via the thermolysis and pyrolysis of the polymer precursors, further study was conducted to characterize the composition, microstructure and mechanical properties of the HfC foam. A range of techniques were used for these efforts.

4.5.1 XRD, SEM, Compression Tests, and Density Measurements

XRD was used to confirm the conversion of HfC, analyze the foam composition and measure the lattice parameters of the HfC foam materials. A Rigaku Geigerflex XRD machine and a Cu target were used.

A JEOL 840 Scanning Electron Microscope (SEM) was used to investigate the microstructure of the HfC foam and polymer cylinder samples. Prior to SEM inspection of polymer samples, a Pelco SC-6 Sputter Coater was used to gold coat the samples.

A QTest Tension-Compression Test Machine and a 100KN MTS load cell were used to determine the mechanical strength of the HfC foams.

Simple geometrical measurements using calipers, combined with weight measurement, were conducted to determine the foam bulk density and total porosity. A more accurate density measurement of the HfC foam was performed using gas displacement and mercury porosimetry, conducted by an outside laboratory (Micromeritics Instrument Corporation).

4.6 Thermolysis and Pyrolysis Chemistry Study

The reaction chemistry involved in the thermolysis and pyrolysis of polymer samples is very complicated. The ICP-C team's research[52,53] indicated that HfC

conversion reactions commence at approximately 1200°C. However they did not report any attempts to clarify the mechanisms of the polymer decomposition process or the HfC conversion process. In the present work, the thermolysis and pyrolysis were investigated in order to provide insight into polymer reactions at lower temperatures and HfC conversion at higher temperatures.

A study of changes in vacuum pressure and furnace temperature during the heat treatments was conducted. Residual Gas Analysis (RGA), combined with XRD analysis, was used to characterize the chemical reactions. Volatile species were analyzed in-line by RGA and solid phase samples were examined with XRD to study composition changes at different processing temperatures.

4.6.1 Residual Gas Analysis (RGA)

A residual gas analyzer, which is a mass spectrometry device, can be used under vacuum to identify individual gases and their concentrations in a gas mixture. A LEYBOLD INFICON H200M (**Figure 16**) RGA system was used for the present work. Pressure reduction measures had to be taken to maintain the RGA sensor at a sufficiently level of vacuum because the analyzer has an upper operation pressure limit of 10^{-4} Torr. The RGA sensor's molecular mass detection range is 1 ~ 200 amu (atomic mass unit).

The LEYBOLD INFICON H200M RGA system (**Figure 16**) includes an RGA sensor, which operates under vacuum, an electronics module, which operates the sensor, and TWare 32 software, which works in conjunction with an external computer to display data and control the electronics.

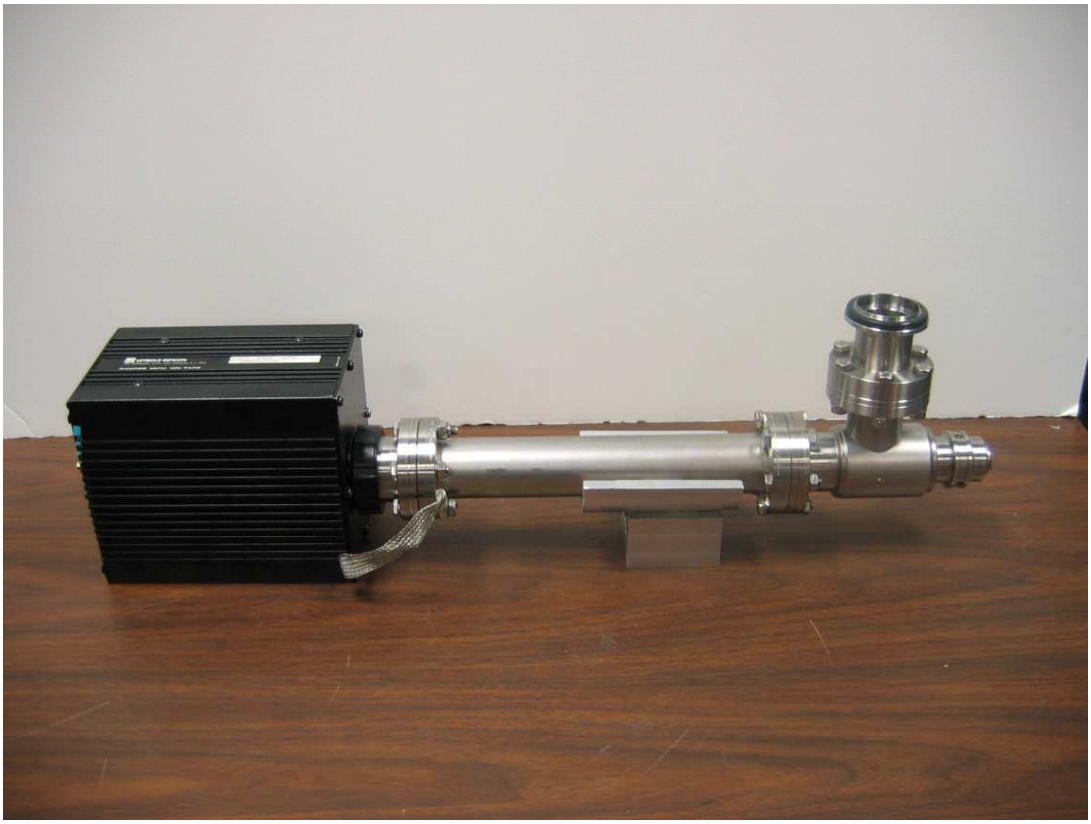

Figure 16 LEYBOLD INFICON H200M RGA

The RGA sensor consists of three parts: an ion source, a quadrupole mass filter, and an ion detector. The ion source contains a heated filament that emits electrons. These electrons collide with and charge the target gas molecules in the system. Ions produced from charged gas molecules move into the quadrupole mass filter and are separated according to their mass-to-charge ratio. Ions that pass through the quadrupole mass filter strike the ion detector, become neutralized, and draw a signal current that is proportional to the ion concentration.

The RGA electronics module interprets the output of the sensor and works with the system software TWare 32 to display sensor signal on an external computer. TWare 32 is a Windows-based software package and the computer is connected to the RGA via an RS232 interface.

4.6.2 RGA Analysis System Setup

The complete RGA analysis system diagram is shown in **Figure 17** and the system set-up is shown in **Figure 18**. Since the RGA could only operate at pressures lower than 10^{-4} Torr, several pressure reduction measures were taken to keep the RGA sensor at a sufficient level of vacuum. One method was a simple conductance limiting technique, which drew the sample gas through a side path to the RGA sensor rather than placing the sensor directly in the major gas line.

4.7 Summary of Experimental Procedures

The experimental procedures described in the previous sections are summarized in **Figure 19.** A detailed discussion of the experimental results obtained is given in **Chapter 5**.

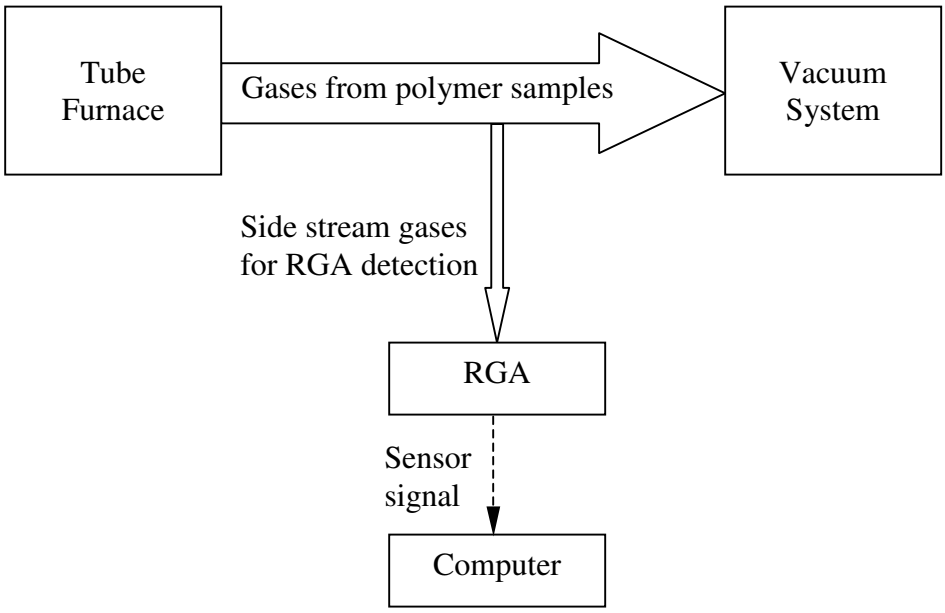

Figure 17 RGA analysis system diagram

Figure 18 RGA analysis system set-up

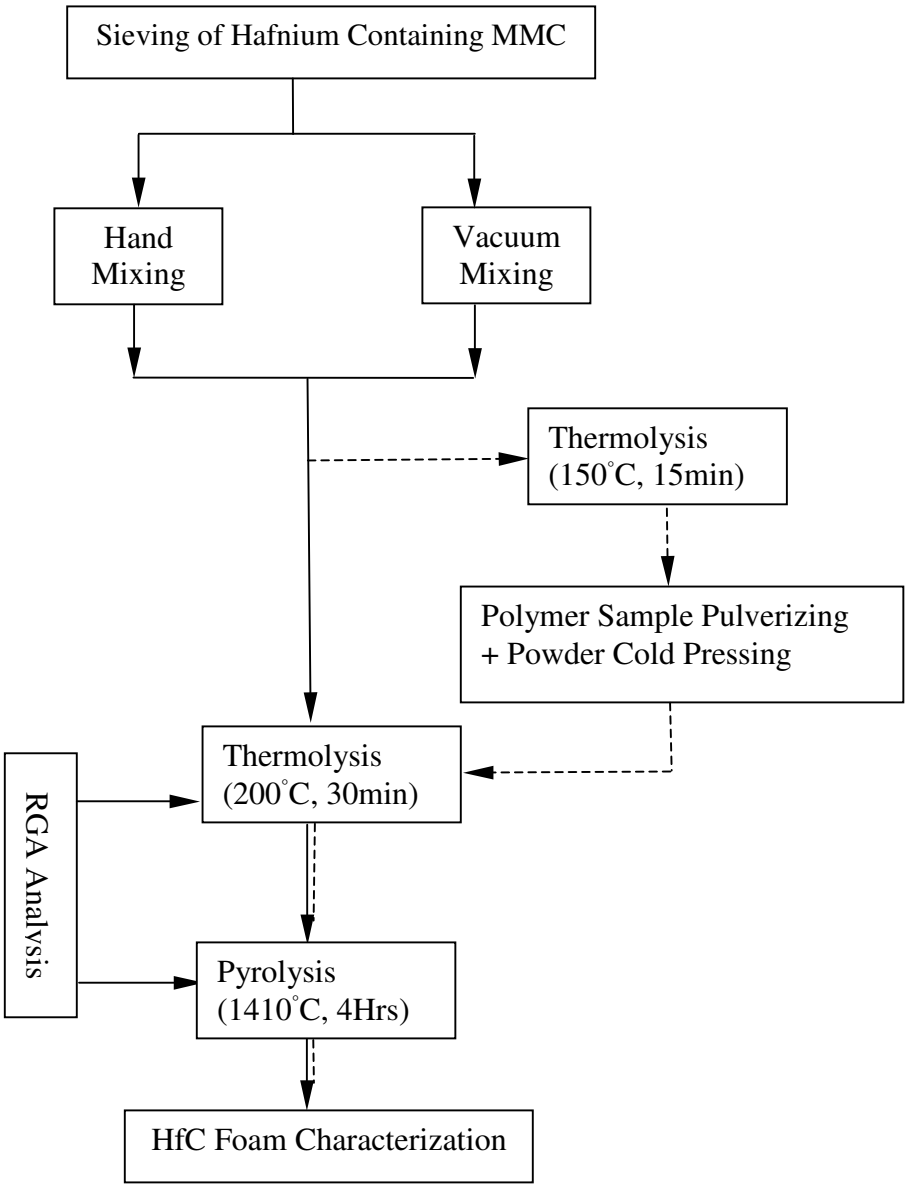

Figure 19 Experimental procedure flow diagram for HfC foam fabrication

5 RESULTS AND DISCUSSION

Figure 19 shows the experimental procedures and relationship between the two major series of experiments conducted for the present study. These experiments comprised:

(1) Investigation of the mechanism of HfC conversion from polymer precursors:

- Thermolysis and pyrolysis chemistry studies.

(2) Optimization of the HfC foam properties: experiments to investigate the factors affecting HfC foam structure, and varying the preparation techniques accordingly to optimize the foam properties:

- Hand mixing
- Vacuum mixing
- Polymer powder compaction

Specifically, the thermolysis and pyrolysis chemistry were investigated to determine the temperature ranges at which HfC conversion occurs and identify the overall reactions that occur during high temperature pyrolysis. For HfC foam properties optimization, three techniques, Hand Mixing, Vacuum Mixing, and Polymer Powder Compaction were investigated and the foam structure and mechanical properties obtained using each method were compared.

5.1 Thermolysis and Pyrolysis Chemistry Study

Vacuum Pressure vs. Furnace Temperature change during the heat treatment process was investigated. A Residual Gas Analyzer (RGA), combined with XRD analysis, was used to characterize the chemical reactions. Volatile species were analyzed in-line by RGA and solid phase products were examined with XRD to study the composition changes at different processing temperatures.

Figure 20 is the Ellingham diagram of HfC conversion from HfO_2. As indicated in the diagram, the pyrolysis heat treatment condition was below the equilibrium line, where HfC and CO are more stable. Based upon this diagram, HfC conversion should occur if there were HfO_2 and C in the foam material at the pyrolysis condition.

5.1.1 Vacuum Pressure vs. Furnace Temperature Change During Heat Treatment

Vacuum Pressure vs. Furnace Temperature change was studied to provide a qualitative picture of the polymer decomposition and HfC conversion reactions.

A small piece of vacuum mixed polymer preform sample weighing 6.7mg was placed into a graphite combustion boat and heat treated under vacuum in the tube furnace. A constant heating rate of 2.88°C/min, and a heating time of 465 minutes were used for a non-stop heating of the sample from 75°C to 1410°C. A quicker heating rate of 7.2°C /min was used to heat the sample from room temperature to 75°C. Volatile species that evolved during this heating were analyzed in-line by RGA using the set-up shown in **Figure 17**.

The sample weight and the heating rate from 75°C to 1410°C were carefully selected through experiments. These parameters ensured that the maximum vacuum

pressure would not exceed 10^{-4} Torr, the upper operation limit of the RGA sensor. The heating rate from room temperature to 75°C was not as critical because no polymer decomposition reactions were observed in this range.

Figure 21 shows the vacuum pressure gauge readings when the sample was continuously heated from room temperature to 1410°C. The vacuum pressure variations correspond to gas generation from the polymer sample during polymer decomposition and HfC conversion. Each pressure reading on the curve corresponds quantitatively with the real time overall gas generation at a particular temperature.

As shown in **Figure 21,** three temperature regimes showed significant pressure changes. The first regime started at about 80°C and ended at about 550°C. The second regime started at about 1010°C and ended at about 1250°C. There is a final regime that showed a minor pressure variation starting at about 1390°C that did not end until 1410°C was exceeded.

The first pressure peak regime (80 ~ 550°C) is thought to be linked with the decomposition of polymers, while the second and third regimes (1010 ~ 1410°C) appear to be associated with the HfC conversion reaction. RGA and XRD results have further corroborated these hypotheses.

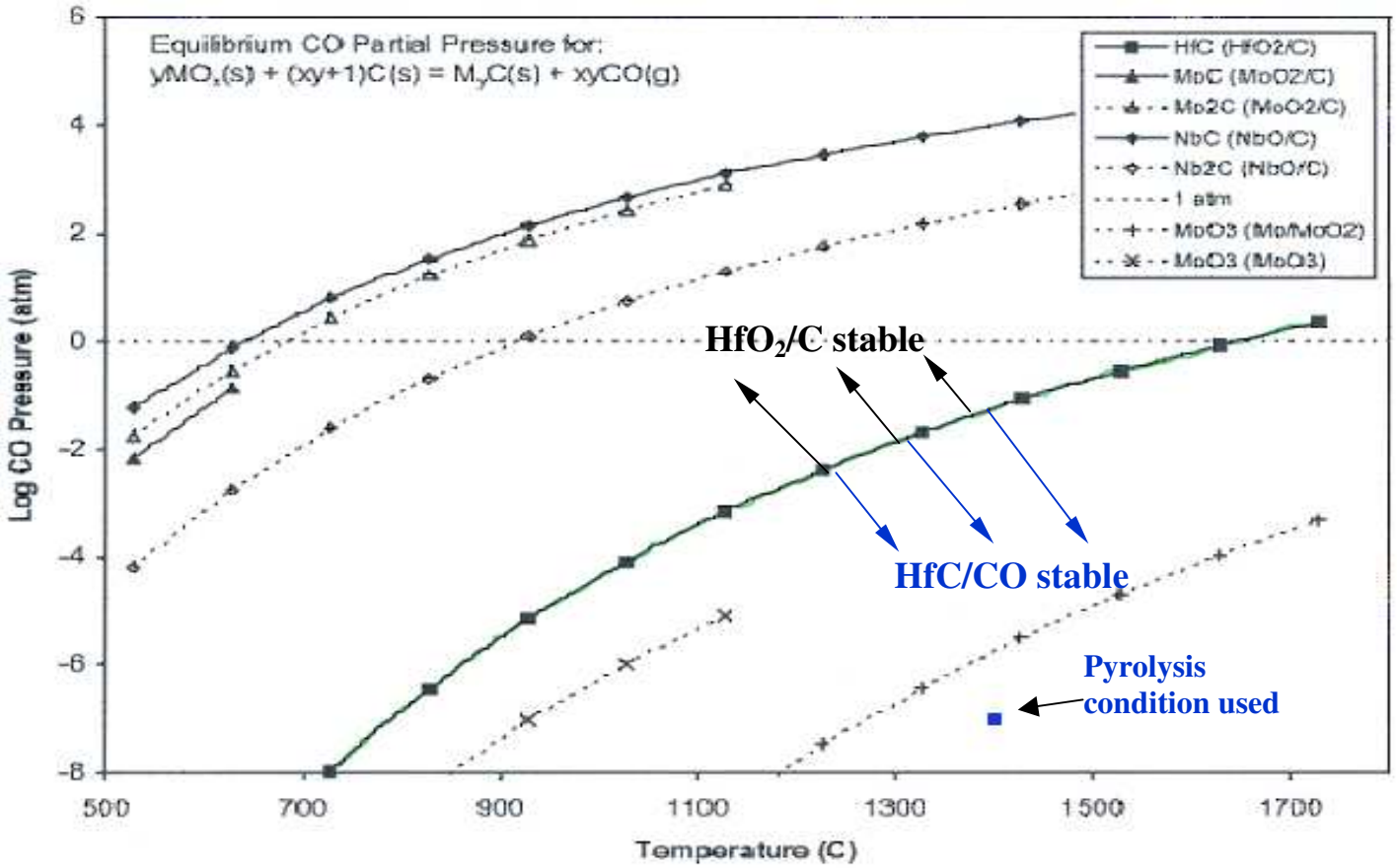

Figure 20 Ellingham diagram showing HfC conversion from HfO_2

HfO_2+ 3C = HfC + 2CO

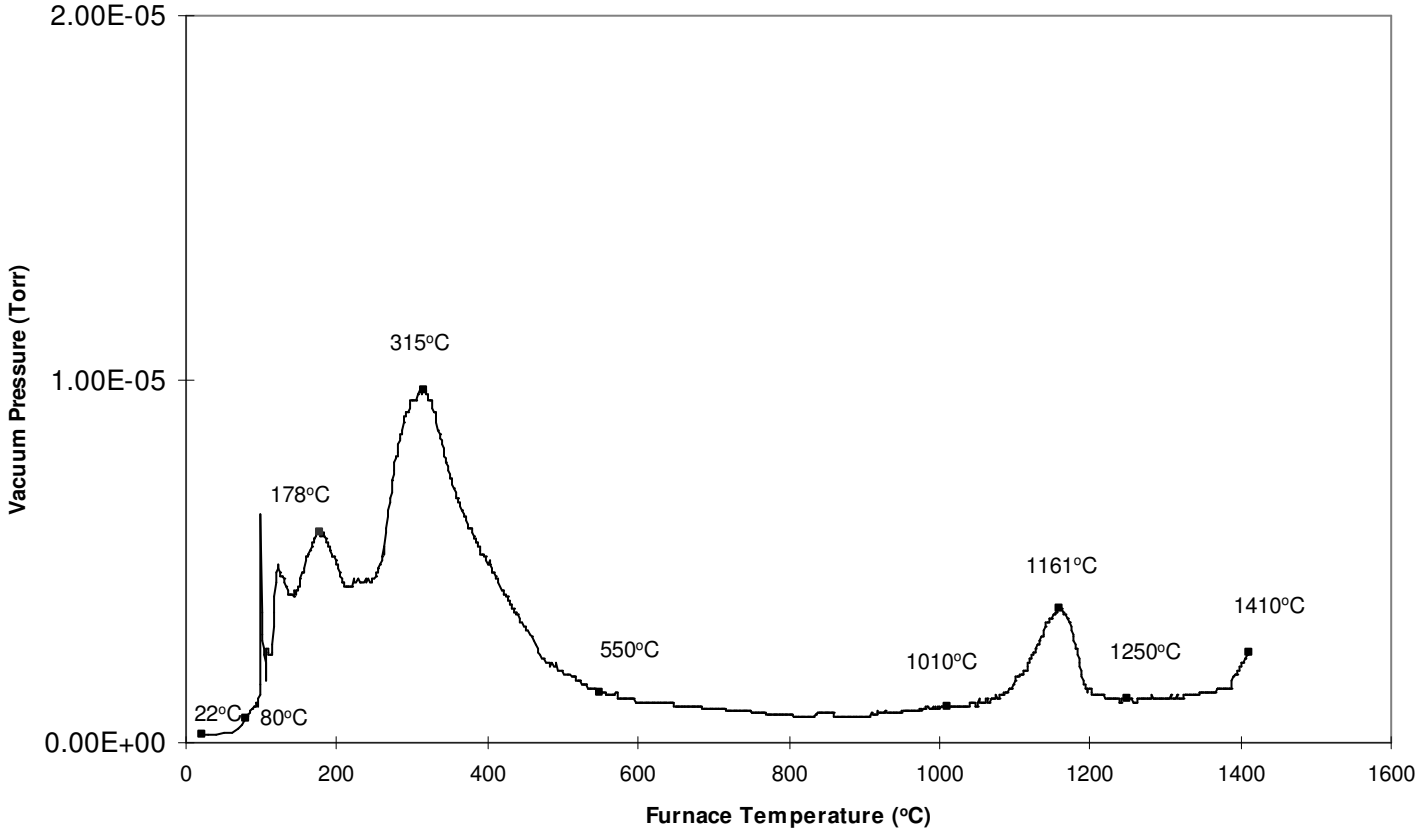

Figure 21 Changes in vacuum pressure when polymer preform samples were continuously heated from room temperature to 1410 °C

5.1.2 RGA and XRD Analysis

RGA analysis was performed simultaneously during the above mentioned heat treatment in order to analyze the composition of the gas evolved. RGA analysis procedure was discussed in section **4.6.2**. RGA measurement involves the ionization of detected gases and measurement of the gas ion current as an indication of gas concentration, the higher the detected ion current, the higher the specific gas ion concentration. In this work, in order to ensure gas concentrations between different spectra comparable, detected ion current was used as an absolute measurement of ion concentration, although other measures such as gas partial pressure were also available.

During measurements, the RGA ionizes the gases to be detected, which may cause the decomposition of gas molecules during the detection process and result in the appearance of "fragment" ions in the spectra. The fragmentation process is complicated, especially in the case of large polymer molecules, where chain scission occurs forming multiple fragment ions with different masses. Complete identification of these fragment ions from non-fragment ions with the same mass is a complicated task, which calls for other chemical analysis techniques to be used. The RGA sensor used in this work was capable of detecting of a maximum detection molecular mass of 200amu, which was limited compared to the large masses of the polymer molecules to be detected. Due to the above considerations and the scope of the present research, only three molecular masses: 18amu, 28amu, and 44amu were examined in detail in the RGA spectra (**Figure 22** through **Figure 29**) in order to formulate a qualitative picture of the chemical reactions occurring during the heat treatment.

Figure 22 through **Figure 29** show the RGA mass spectra at the different heat treatment temperatures indicated in **Figure 21**.

Figure 22 shows the gas spectrum at 22°C before the heat treatment was started. Peaks at 18amu (H_2O) and 28amu (N_2, CO) were detected, together with a smaller peak at 44amu (CO_2). These mass peaks probably arose due to the residual air and pump oil molecules in the vacuum system.

Figure 23 and **Figure 24** are the gas spectra at 179°C and 315°C, respectively. Compared to **Figure 22**, there is a significant increase in the mass peak heights at 18amu (H_2O), 28amu (CO, C_2H_4) and 44amu (CO_2, C_3H_6). A significant number of mass peaks that correspond to different organic vapors were present, which is consistent with intense polymer decomposition. A comparison of **Figure 23** and **Figure 24** shows mass peaks with larger amu values in **Figure 24**, which arose probably due to the larger-mass groups produced by chain scission at higher temperatures.

Figure 25 is the gas spectrum at 550°C. In this figure, all the large-amu mass peaks shown in **Figure 24** have disappeared, suggesting a significant reduction in the amount of organic vapors being released. A significant decease in the mass peak heights of 18amu (H_2O), 28amu (CO, C_2H_4) and 44amu (CO_2, C_3H_6) were also observed. Both these phenomena indicate that the polymer decomposition is complete at around 550°C.

Figure 26 through **Figure 29** show the gas spectra at temperatures over 1000°C. Compared with the spectra in **Figure 22** through **Figure 25,** only a few mass peaks at lower amu were observed. The absence of large aum mass peaks suggests that no organic vapor was present at these temperatures.

Figure 30 shows the concentration change for 28amu ions. Here, the peak height for 28amu (CO) started to increase at about 1010°C, reached its first maximum at about 1161°C, then decreased to a minimum at about 1250°C, and finally recovered to reach a secondary maximum at 1410°C. At these temperatures, the CO concentration changes can be attributed to HfC conversion. According to the above observations, CO is the oxidation product of following reactions:

At lower temperatures:

HfO_2 + C (amorphous carbon) HfC + HfC_xO_y + HfO (dissolved in HfC) + CO(g) (3)

At higher temperatures:

HfC_xO_y + Hf (dissolved in HfC) HfC + HfO (dissolved in HfC) (4)

HfO (dissolved in HfC) + C (dissolved in HfC) HfC + CO(g) (5)

All three reactions should occur at temperatures from 1010°C to 1410°C. However in **Figure 21** and **Figure 30,** the peak at 1161°C should be the result of the dominance of the lower temperature reaction (**Equation 3**), while the peak at 1410°C most likely results from the dominance of the higher temperature reactions (**Equation 4, 5**).

Figure 31 shows XRD spectra for samples heat treated at 550°C, 1010°C, 1250°C and 1410°C for 4 hours. **Figure 31** indicates that the sample at 550°C was composed mainly of HfO_2, and no HfC peaks were present. This result indicates that polymer decomposition occurred without HfC conversion up to 550°C. The XRD spectrum for samples at 1010°C showed that the samples were composed mainly of HfO_2, with no HfC present. This suggests that the HfC conversion had not yet started at this

temperature. HfC peaks were more significant than HfO_2 peaks in the spectrum at 1250°C, indicating that the HfC conversion commenced in the temperature range of 1010°C ~ 1250°C. In the XRD spectrum for samples at 1410°C, HfC peaks became dominant although HfO_2 peaks were present, indicating that the HfC conversion was substantially complete at this point.

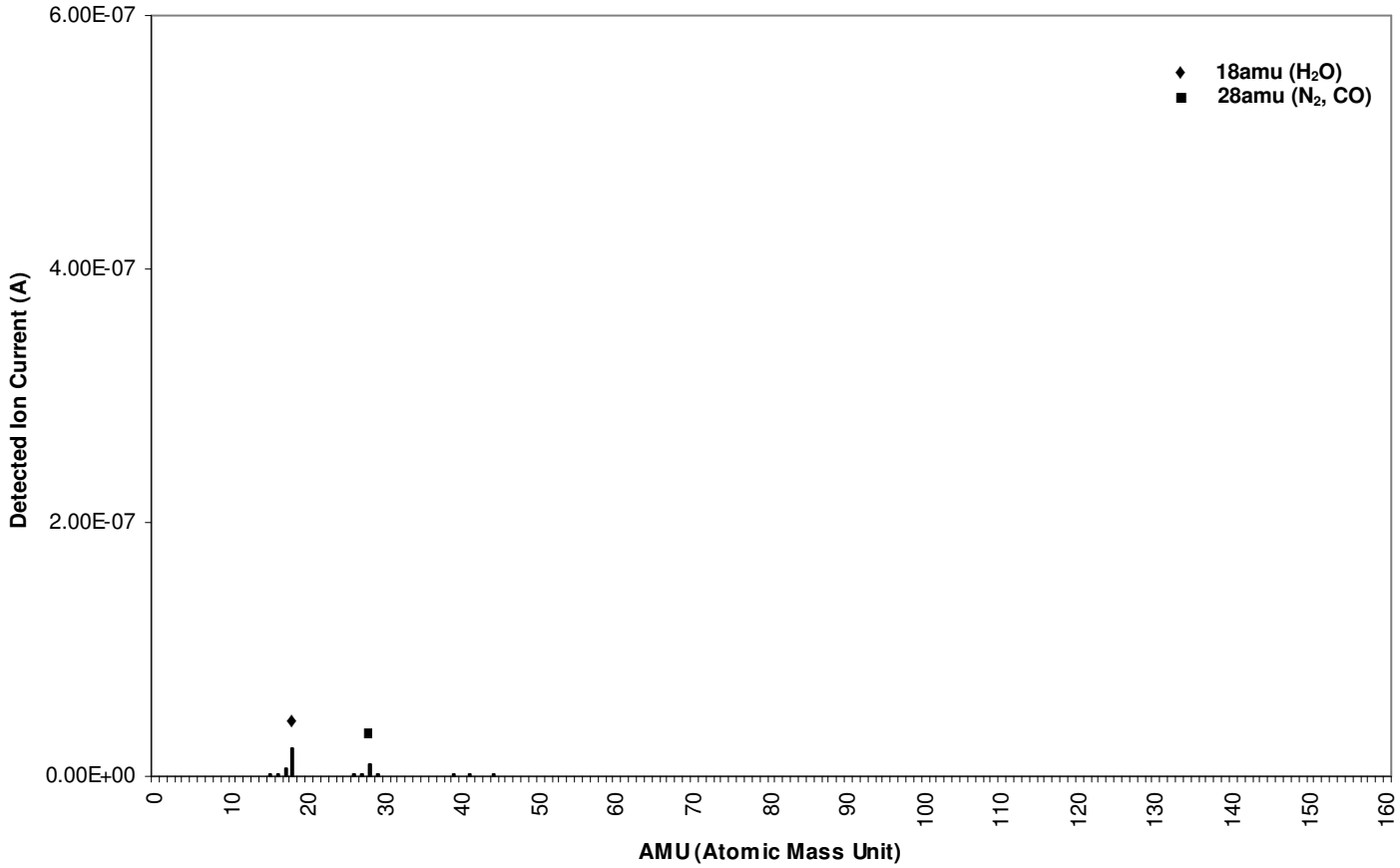

Figure 22 RGA mass spectrum at 22°C

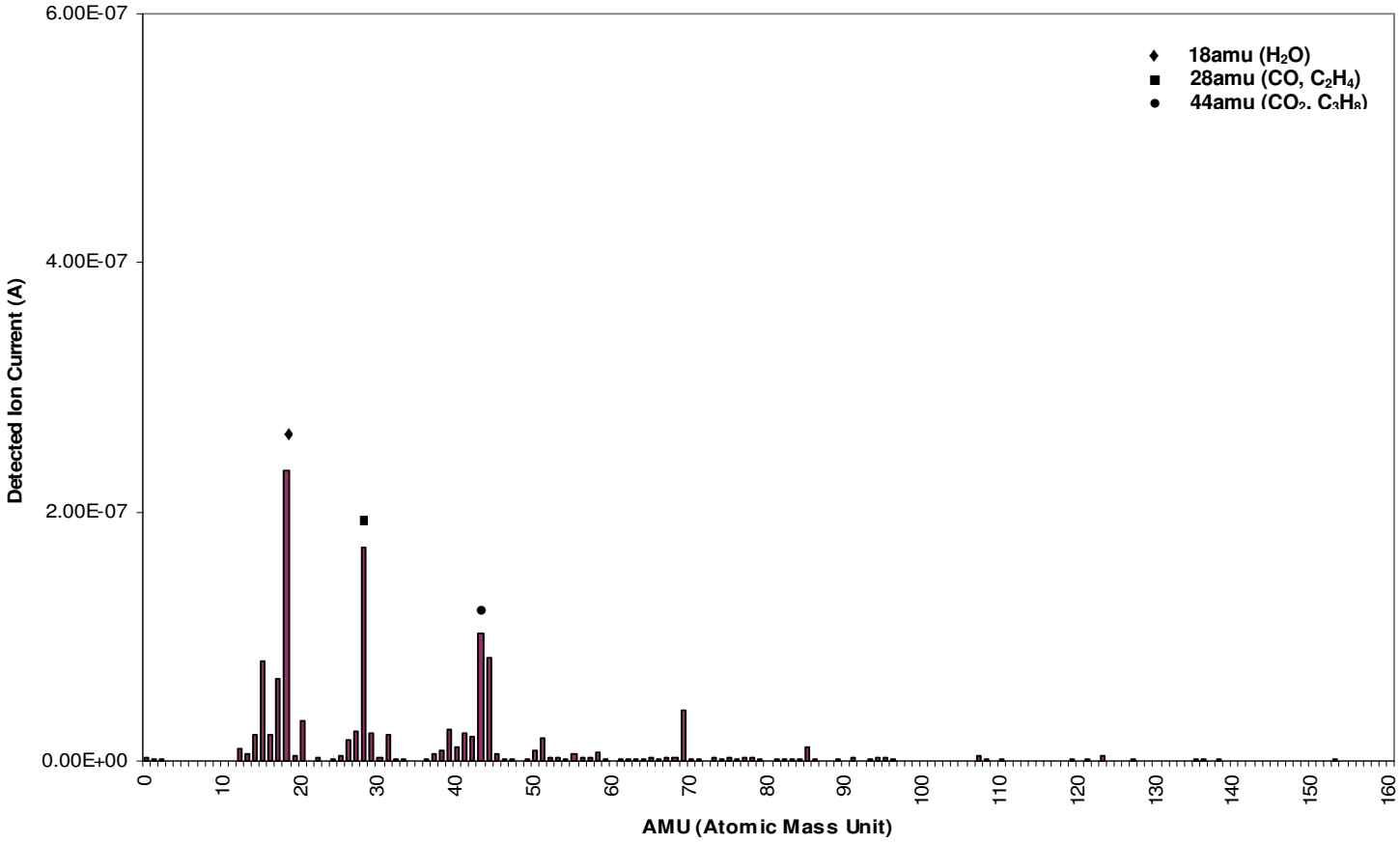

Figure 23 RGA mass spectrum at 179 ^{o}C

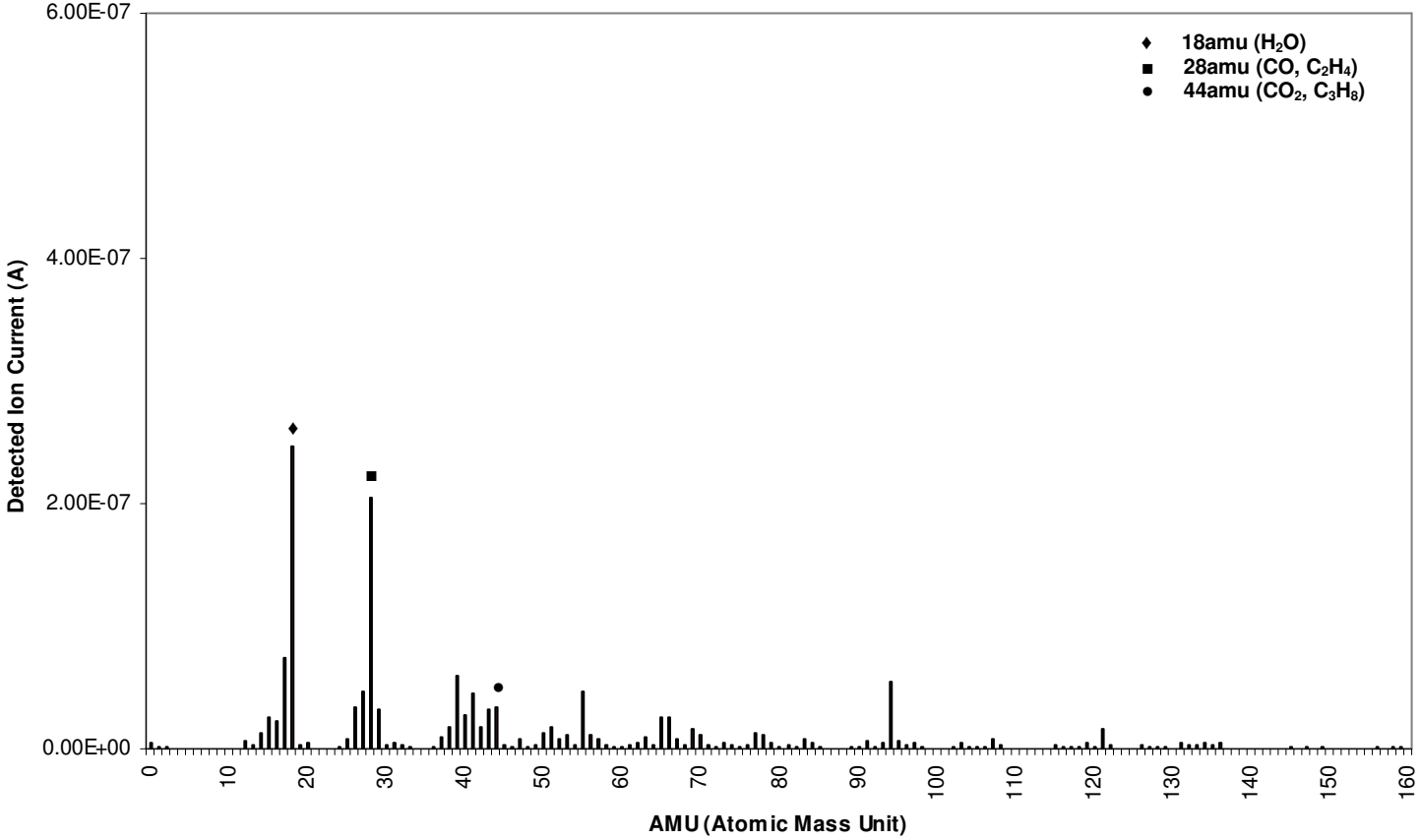

Figure 24 RGA mass spectrum at 315°C

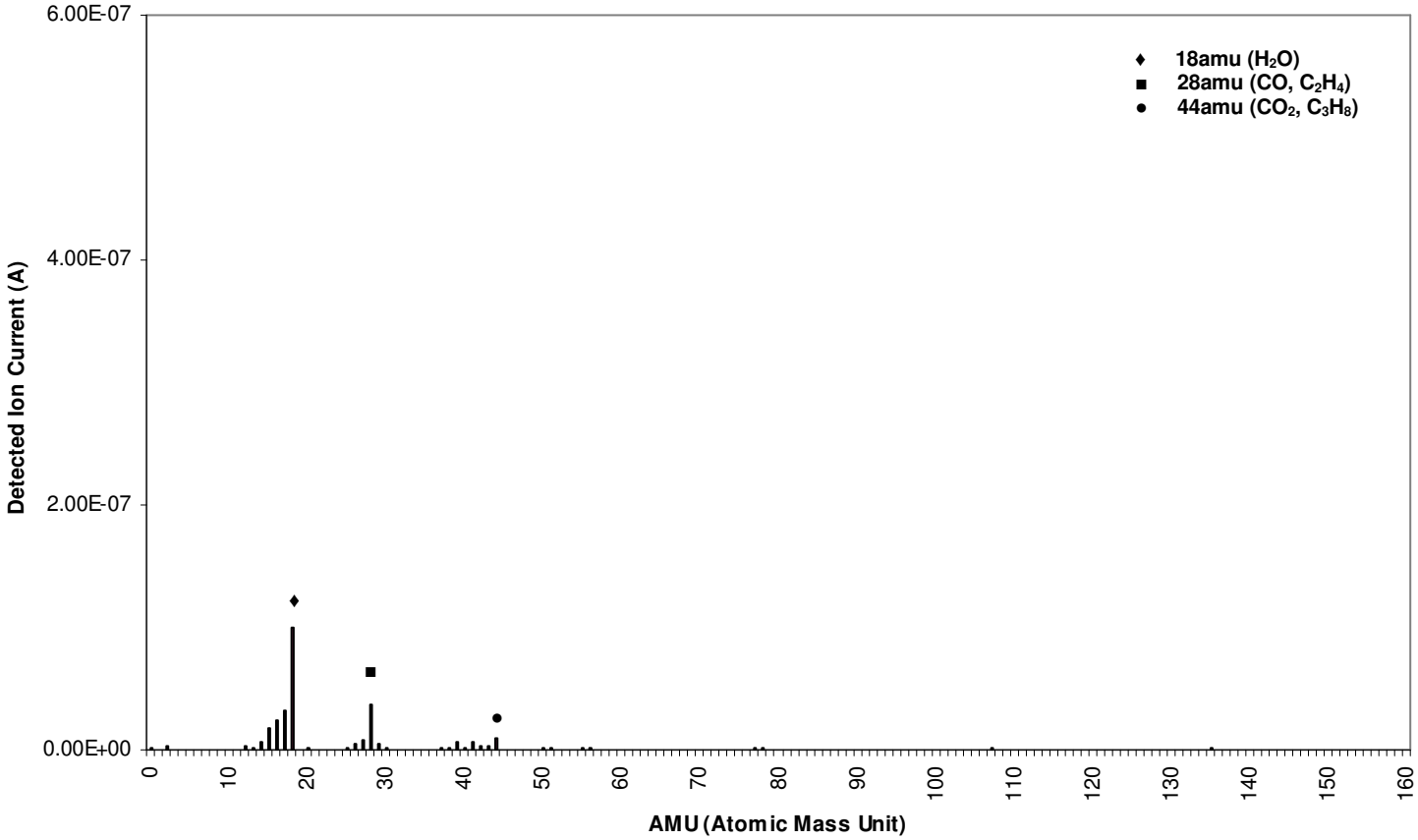

Figure 25 RGA mass spectrum at 550 ^{o}C

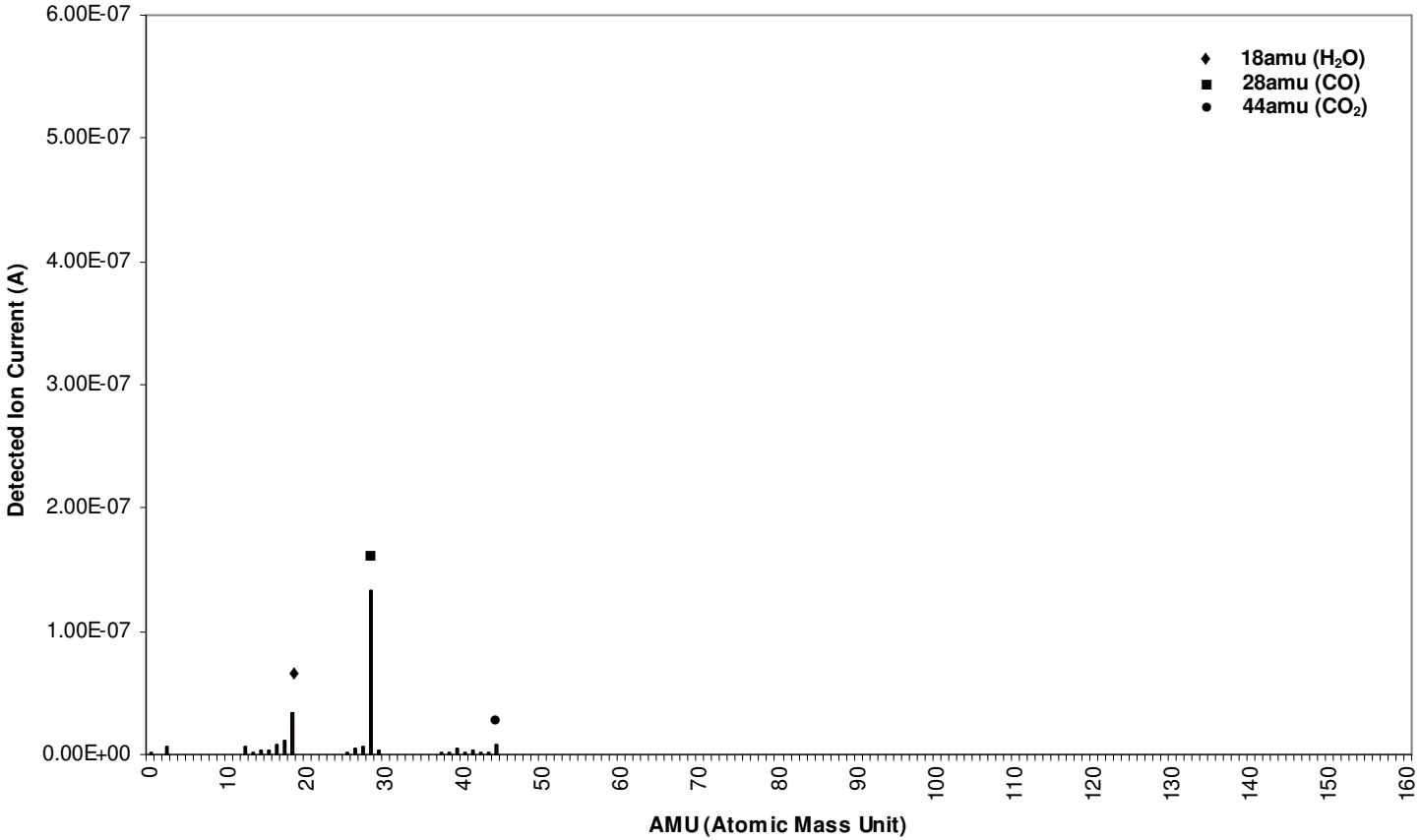

Figure 26 RGA mass spectrum at 1010 °C

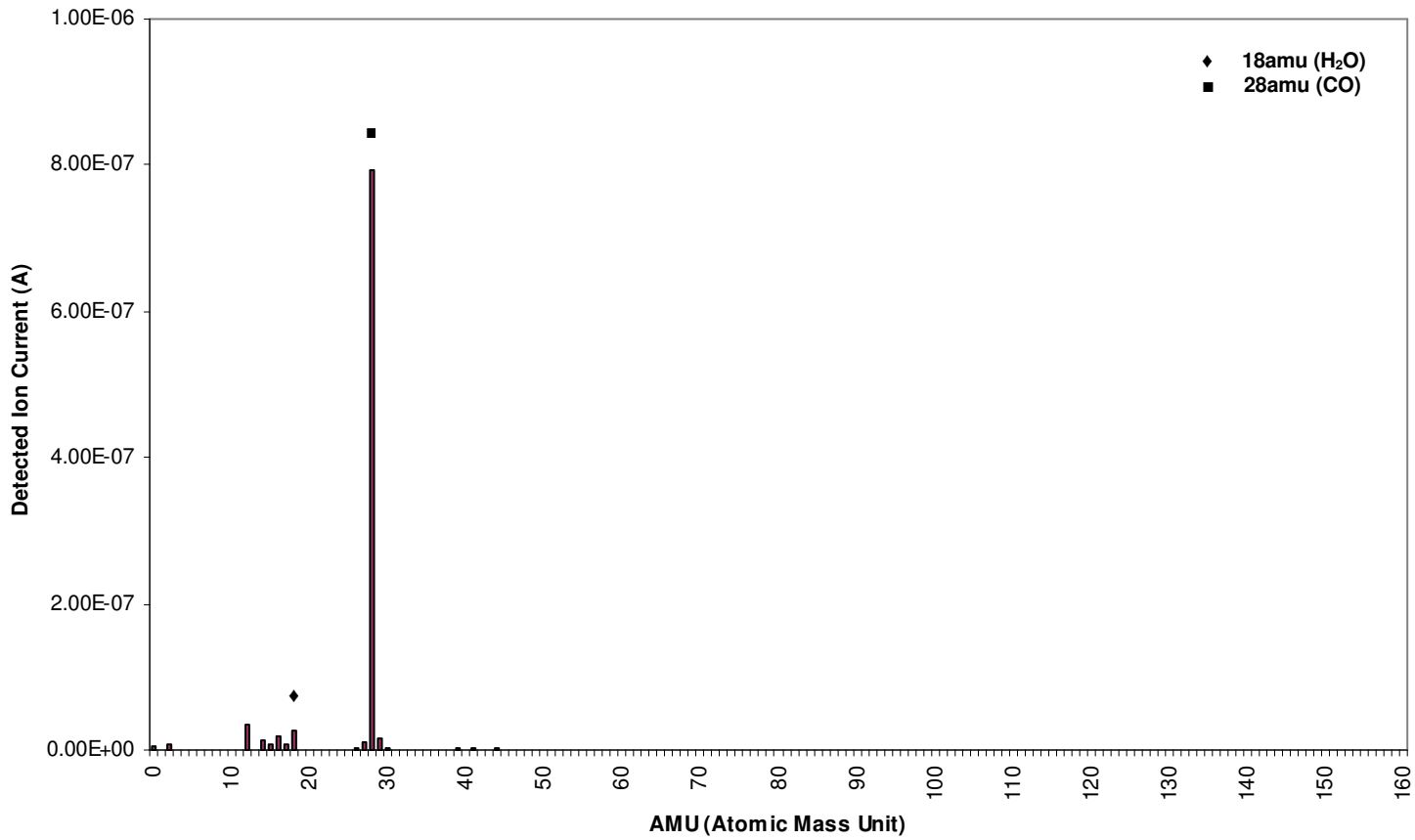

Figure 27 RGA mass spectrum at 1161 ^{o}C

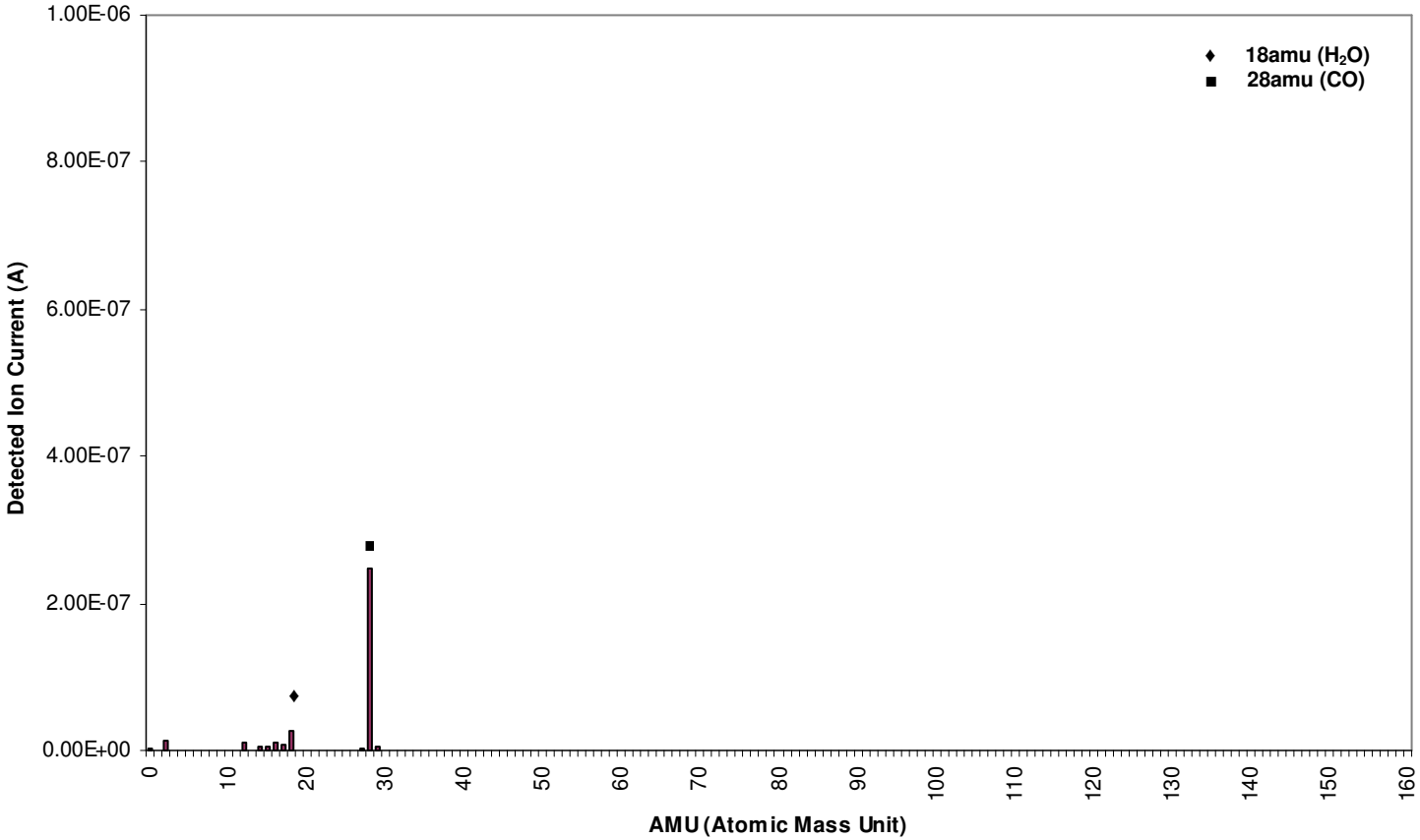

Figure 28 RGA mass spectrum at 1250 °C

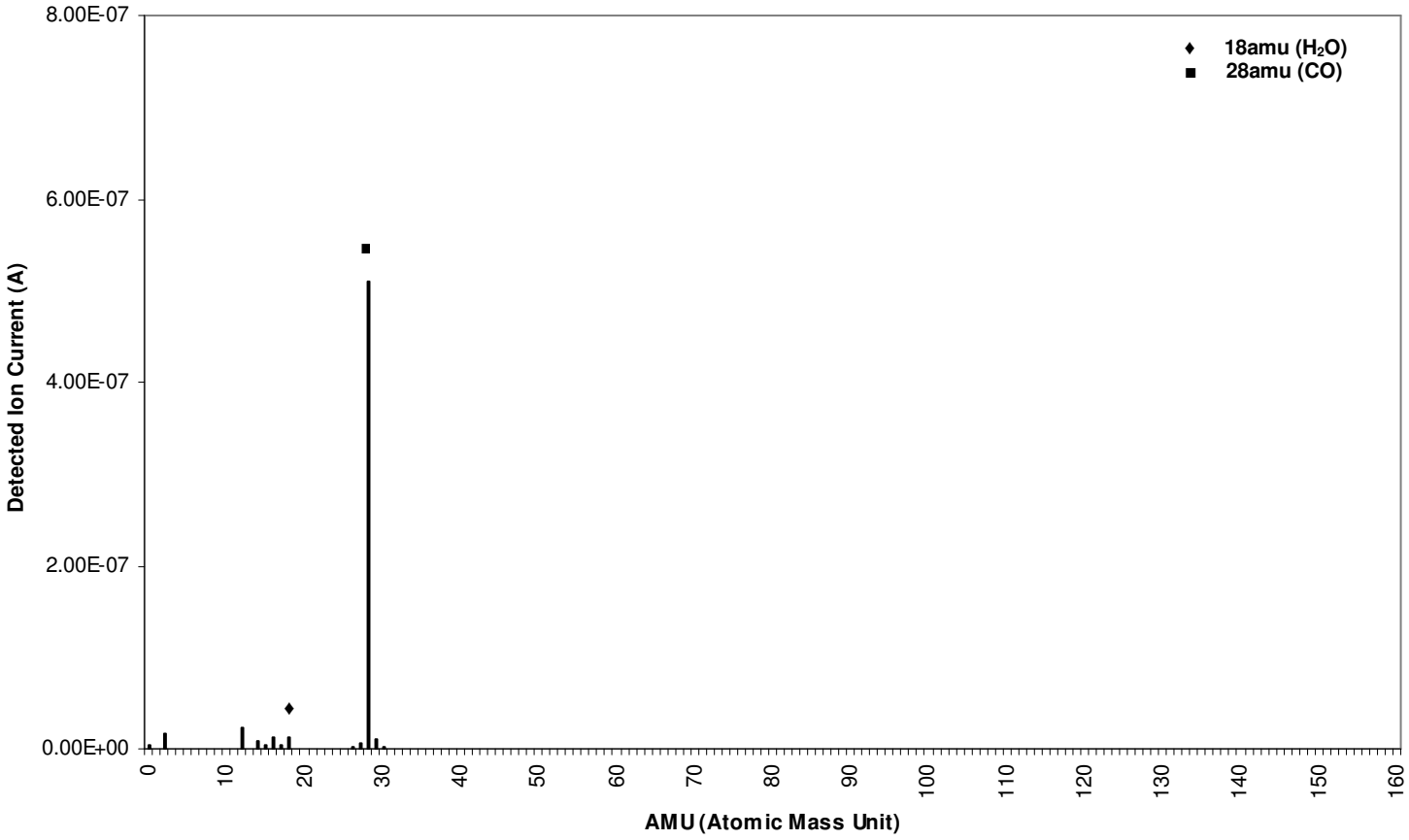

Figure 29 RGA mass spectrum at 1410 ^{o}C

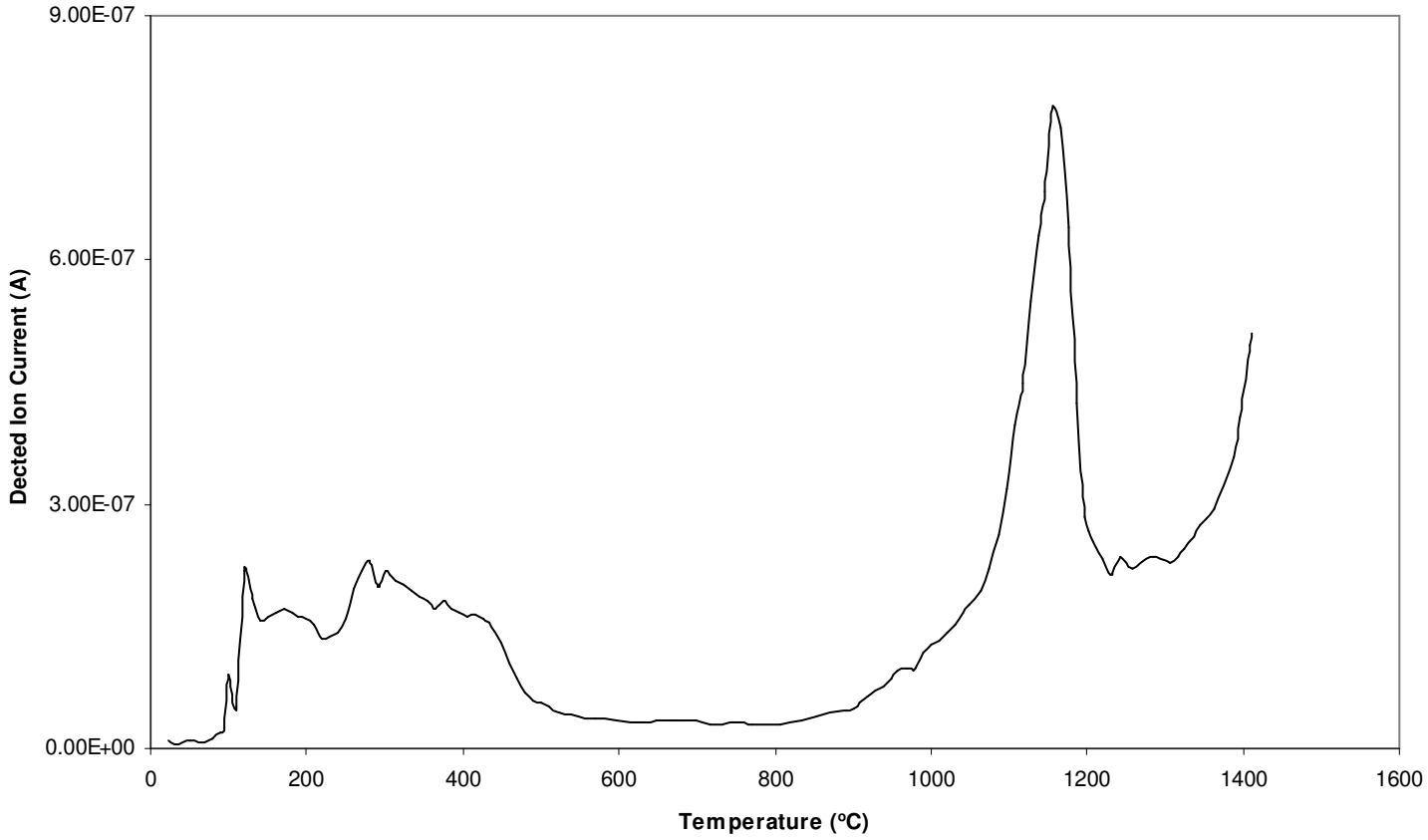

Figure 30 28amu ion concentration profile with increasing temperature

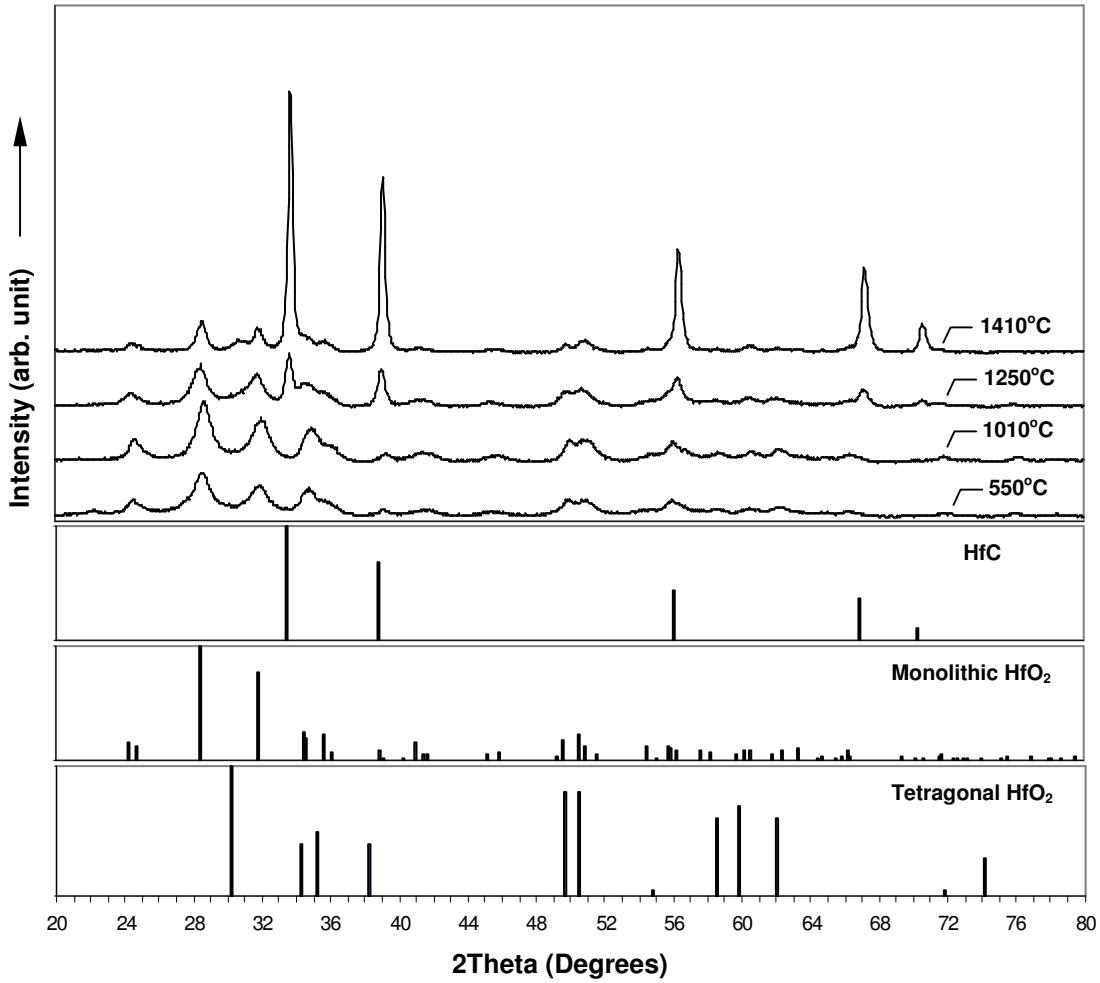

Figure 31 XRD spectra for polymer samples heat treated at different temperatures for 4 hours

5.2 Hand Mixing

Hand Mixing of polymer precursors was performed for a preliminary investigation that provided the basis for later Vacuum Mixing and Polymer Powder Compaction experiments. Several important HfC foaming characteristics were examined, such as polymer mixing ratio effect, the thermolysis parameter effect, and factors affecting the HfC foam structure, to provide guidelines for further experiments.

The polymer precursor hand mixing procedure was described in detail in **4.2.3.1**.

Hand mixing of hafnium trifluoroacetylacetonate with the epoxy mixture was varied in weight ratios from 1:1 to 4:1 (hafnium trifluoroacetylacetonate : epoxy mixture). Increasing the fraction of hafnium trifluoroacetylacetonate was attempted to promote HfC conversion during the subsequent heat treatment process.

The polymer mixture paste was filled into a casting mold and cured at 50 ºC in an open air box furnace. When fully cured, these cylinder-shaped samples were ejected from the mold. One typical cured sample was machined to shape using a lathe and a photograph of the fully cured preform is shown in **Figure 32**. As the picture illustrates, the sample was characterized by numerous white color inclusions in a yellowish polymer matrix. Since hafnium trifluoroacetylacetonate is a white powder, these white inclusions indicate the presence of unmixed Hf containing agglomerated particles.

The cured preforms were then subjected to low temperature themolysis followed by high temperature pyrolysis to complete the HfC conversion and create HfC foams. **Figure 13** shows the typical temperature profile used for the heat treatment.

During the low temperature thermolysis, the furnace vacuum dropped to approximately 10^{-3} Torr, then steadily improved to better than 10^{-6} Torr as the processing continued. This was due to the large amount of gases generated at the thermolysis temperatures as the polymer decomposition reactions occurred. As the furnace temperature increased, the organic vapors were continually removed by the vacuum system, and vacuum was recovered to the initial stage (5×10^{-5} Torr) or even reached 10^{-6} Torr at temperatures over 1000°C.

A photograph of a converted HfC foam sample is shown in **Figure 33**. The HfC foam sample had a significant shrinkage, both in height and girth, compared to the polymer preform samples. The outer surface of the HfC foam was characterized by large, open pockets with sizes up to 1 mm in diameter.

An interesting observation from the collected data was the substantial increase in volume observed after undergoing low temperature thermolysis alone. **Figure 34** shows three different samples, one from each of the three stages of processing (cured preform, after thermolysis, after pyrolysis). The middle specimen was removed from the furnace after thermolysis and showed significant swelling in both its length and girth. Specimens exhibited a substantial increase in their bulk size following thermolysis, but then shrank to their final dimensions during pyrolysis.

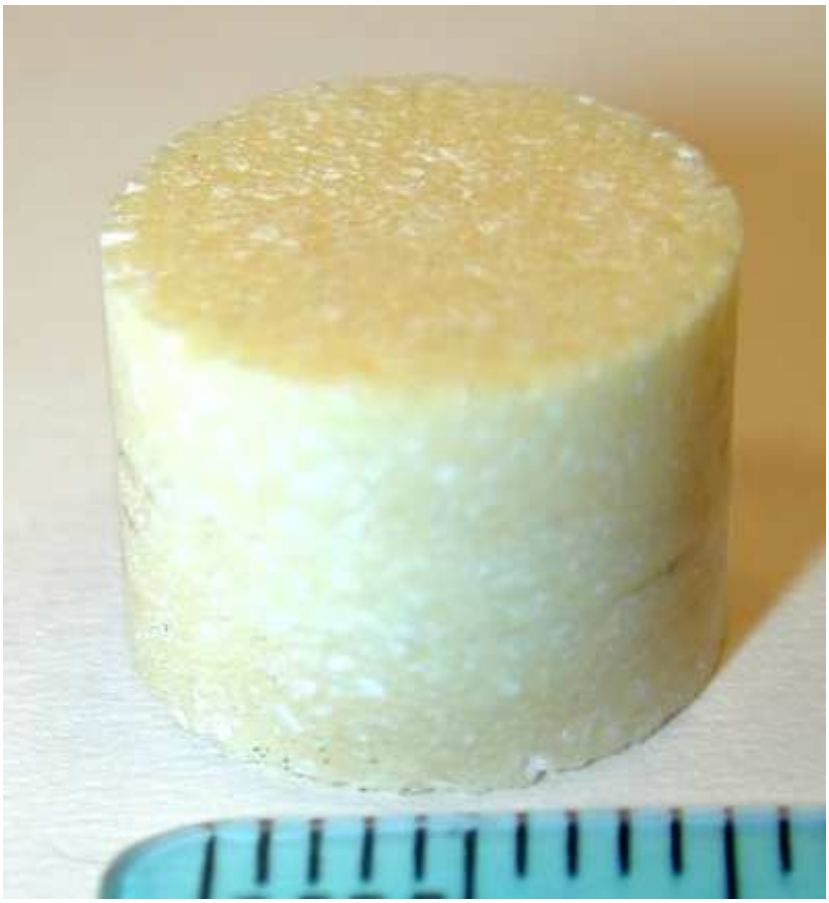

Figure 32 Photograph of preform (mixing ratio: 2:1) before heat treatment

Figure 33 HfC foam (mixing ratio: 3:1) after processing

Figure 34 Three different specimens after halting processing at each of the three major steps (from left to right: preform, after thermolysis, after pyrolysis).

5.2.1 Effect of Mixing Ratio on HfC Foam Density

Mass and geometric volume measurements were made before and after high temperature pyrolysis. To determine the bulk density, simple geometric measurements using calipers combined with weighing by digital scale, were conducted.

Two specimens with a 3:1 mixing ratio were sent to an outside laboratory (Micromeritics Instrument Corporation) for further density measurements. For these two specimens, the measured skeletal density was 2.46 g/cm^3 and the bulk density was 0.62 g/cm^3.

5 polymer preform samples for each ratio from 1:1 to 4:1, a total of 20 samples, were prepared to investigate the mixing ratio effect on the final HfC foam density.

Table 5 shows the measured change in density of the initial polymer preforms, polymer preforms after thermolysis, and the final HfC foam specimens with different mixing ratios.

Table 5 Densities of the polymer preforms and HfC foam specimens.

Mixing Ratios	**Density** (g/cm^3)		
	Polymer State	**After Thermolysis**	**After Pyrolysis**
1:1	1.16 $\pm$ 0.03	0.63 $\pm$ 0.01	0.58 $\pm$ 0.01
2:1	1.55 $\pm$ 0.01	0.39 $\pm$ 0.03	0.50 $\pm$ 0.05
3:1	1.49 $\pm$ 0.02	0.42 $\pm$ 0.04	0.27 $\pm$ 0.03
4:1	1.30 $\pm$ 0.05	0.36 $\pm$ 0.03	0.52 $\pm$ 0.05

Figure 35, which was calculated from **Table 5,** illustrates further the trend of changes in the HfC foam densities produced with different mixing ratios. It seems that

the ratio 3:1 yielded the lowest HfC foam density among the four ratios. All the other three ratios, 1:1, 2:1, and 4:1, have HfC foam densities of about 0.5 g/cm^3, which are almost double that of the ratio 3:1.

As discussed in **Figure 34**, during heat treatment the polymer samples initially showed a substantial increase in volume after thermolysis, but then shrank significantly in volume to their final dimensions. It was observed during experiments that samples with a ratio of 3:1 showed the volume increase after thermolysis, but the samples' volume shrinkage after pyrolysis was considerably less than that for those with ratios of 1:1, 2:1, and 4:1. This difference was the major reason for the lower density of 3:1 ratio foams. This probably arose because the 3:1 ratio samples experienced polymeric reactions which created a "stiffer" foam structure after thermolysis, and the foam did not shrink as markedly during pyrolysis as the foams of other ratios.

Figure 35 further shows the mixing effect ratio on polymer preform density changes. Increasing the weight ratio of the hafnium containing MMC did not result in an increase of density in either HfC foams, or foams after thermolysis.

The HfC foam total porosity for different mixing ratios was calculated and is shown in **Figure 36.** The total porosity was calculated to have a value between 0.954 ~ 0.978 for all four ratios

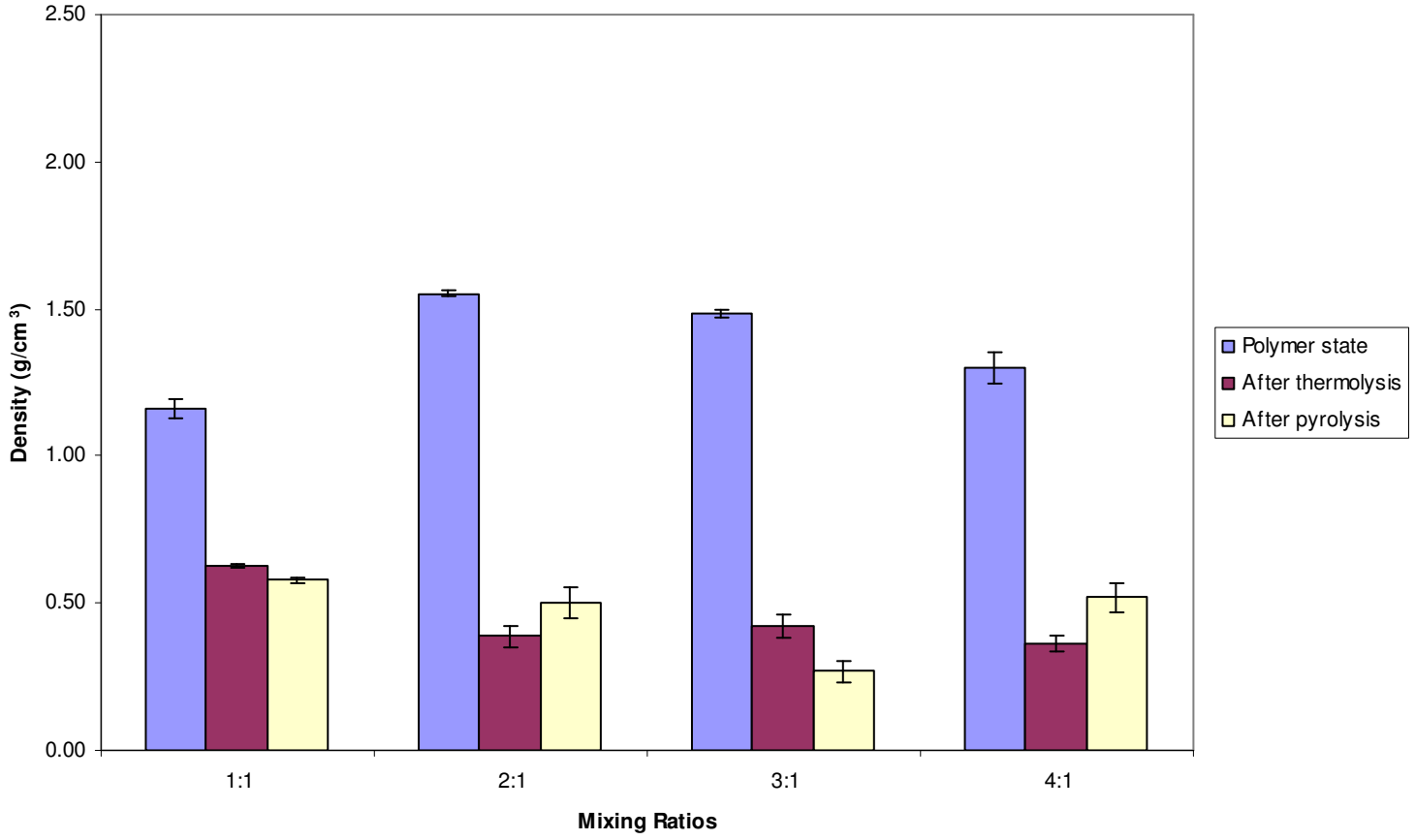

Figure 35 Effect of mixing ratio on HfC foam density

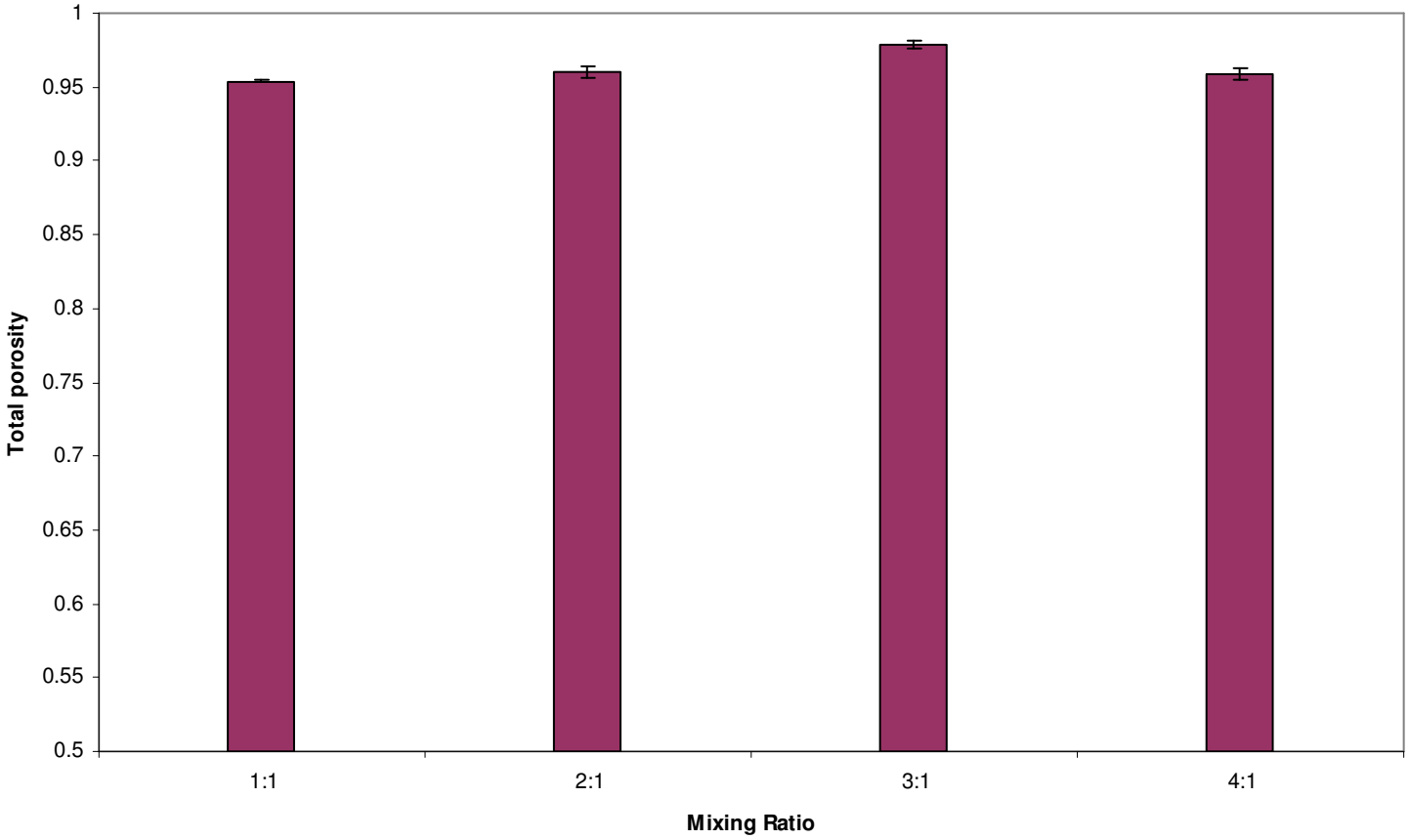

Figure 36 Effect of mixing ratio on HfC foam total porosity

5.2.2 Mixture Ratio Extremes

For comparison with mixing ratios 1:1 through 4:1, two additional specimens were prepared and exposed to the process heat treatment (thermolysis & pyrolysis). One specimen was composed entirely of epoxy (resin and hardener), with none of the hafnium trifluoroacetylacetonate powder present. The second specimen was composed entirely of the Hf containing compound, with no epoxy present. The hafnium containing MMC completely vaporized during the heat treatment, leaving behind only a few specks of char. The epoxy decomposed into an ash-like char, as shown in **Figure 37**. Note that the specimen boat was completely filled with hardened epoxy before the heat treatment. These experiments conclusively proved that the formation of foam structure was not possible by processing the Hf containing MMC or the epoxy alone.

5.2.3 Effect of Thermolysis Parameters on HfC Foam Density

Thermolysis temperature and dwell time at the thermolysis stage were varied and their effects upon foam density evaluated. Three temperatures (175°C, 200°C, 225°C) and two dwell times (30 minutes and 60 minutes) were used. Five polymer preform samples for each thermolysis temperature & time combination were processed, and densities were measured for each of the three major processing steps: polymer preform, after low temperature thermolysis, and after high temperature pyrolysis. All the preform samples were made with 1:1 mixing ratio.

The foam densities obtained are compared in **Figure 38**. When comparing foam densities with different dwell times at the same thermolysis temperatures, it can be seen that only the 200°C (30min), and 200°C (60min) group showed a significantly different

density. Longer thermolysis time of 60 minutes generally yielded a lower foam density than for 30 minutes. For the other processing temperatures, 175°C, and 225°C, different thermolysis processing times did not make statistically differences in the density.

In **Figure 38**, when comparing foam densities at 30 minutes thermolysis time at different thermolysis temperatures [175°C (30min), 200°C (30min), 225°C (30min)], the 200°C (30min) group yielded the largest foam density after pyrolysis. When comparing foam densities at 60 minutes thermolysis time with different thermolysis temperatures [175°C (60min), 200°C (60min), 225°C (60min)], no statistically significant foam density differences after pyrolysis were found among the three conditions.

When comparing foam densities after pyrolysis for all six groups of samples in **Figure 39**, 200°C (30min) had the highest density, while the rest of the groups exhibited no difference in density statistically. Specific polymeric reactions at this thermolysis condition can be attributed to the higher HfC foam density of 200°C (30min).

5.2.4 HfC Foam Characterization

5.2.4.1 XRD Spectrum

X-ray diffraction was performed to confirm the conversion of the polymer preform to HfC and to identify any of oxides or other phases present. Comparison of the XRD spectrum with the JCPDS Powder Diffraction File (PDF) database, as in **Figure 38**, indicates that the foam material was composed primarily of HfC. No residual graphite peak was found. Small amounts of HfO_2 are evident in the diffraction spectrum.

Figure 37 Remains of an epoxy-only specimen exposed to the HfC foam process heat treatment. (Note that the specimen boat was completely filled with hardened epoxy before the heat treatment.)

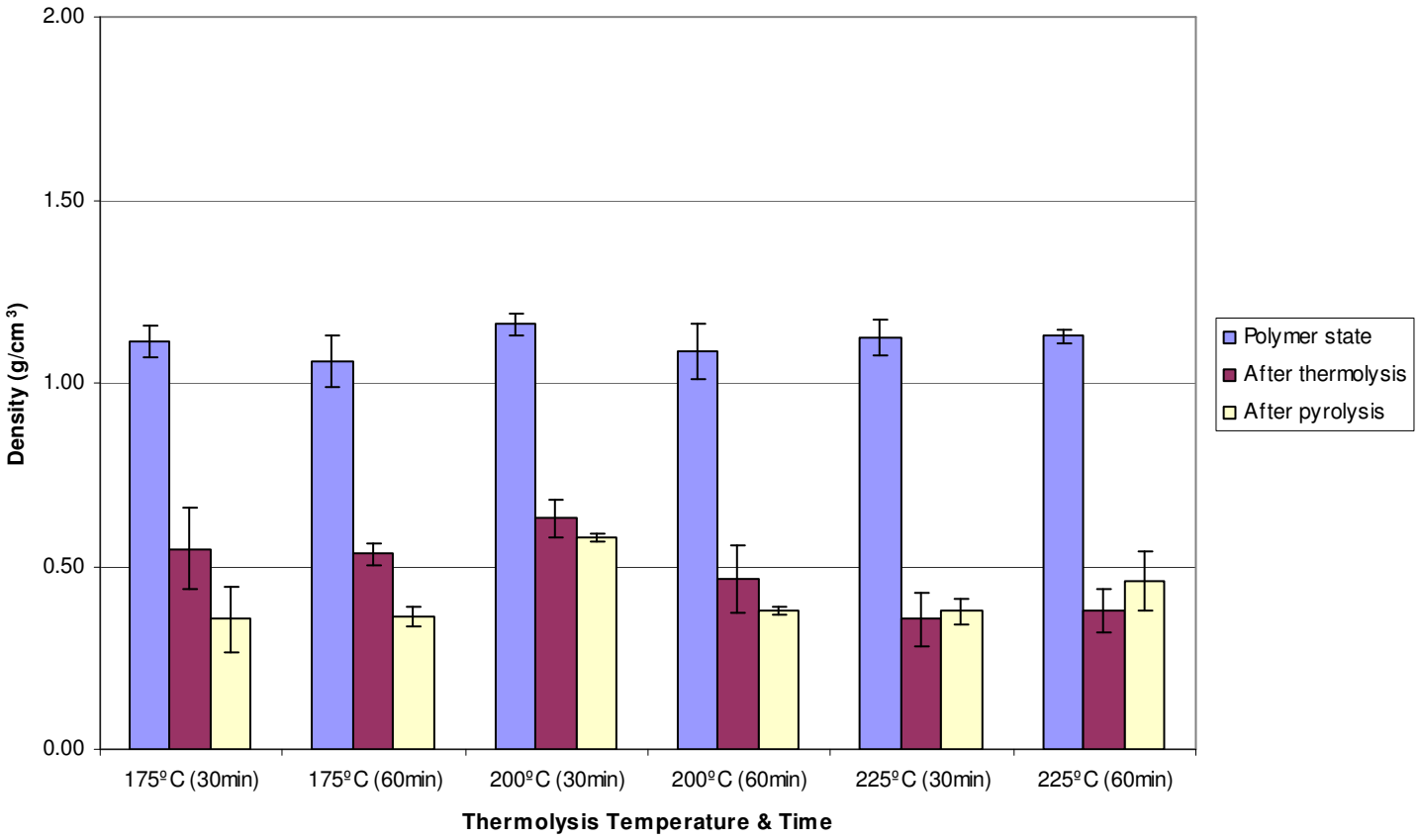

Figure 38 Density of foams produced at different thermolysis times and temperatures

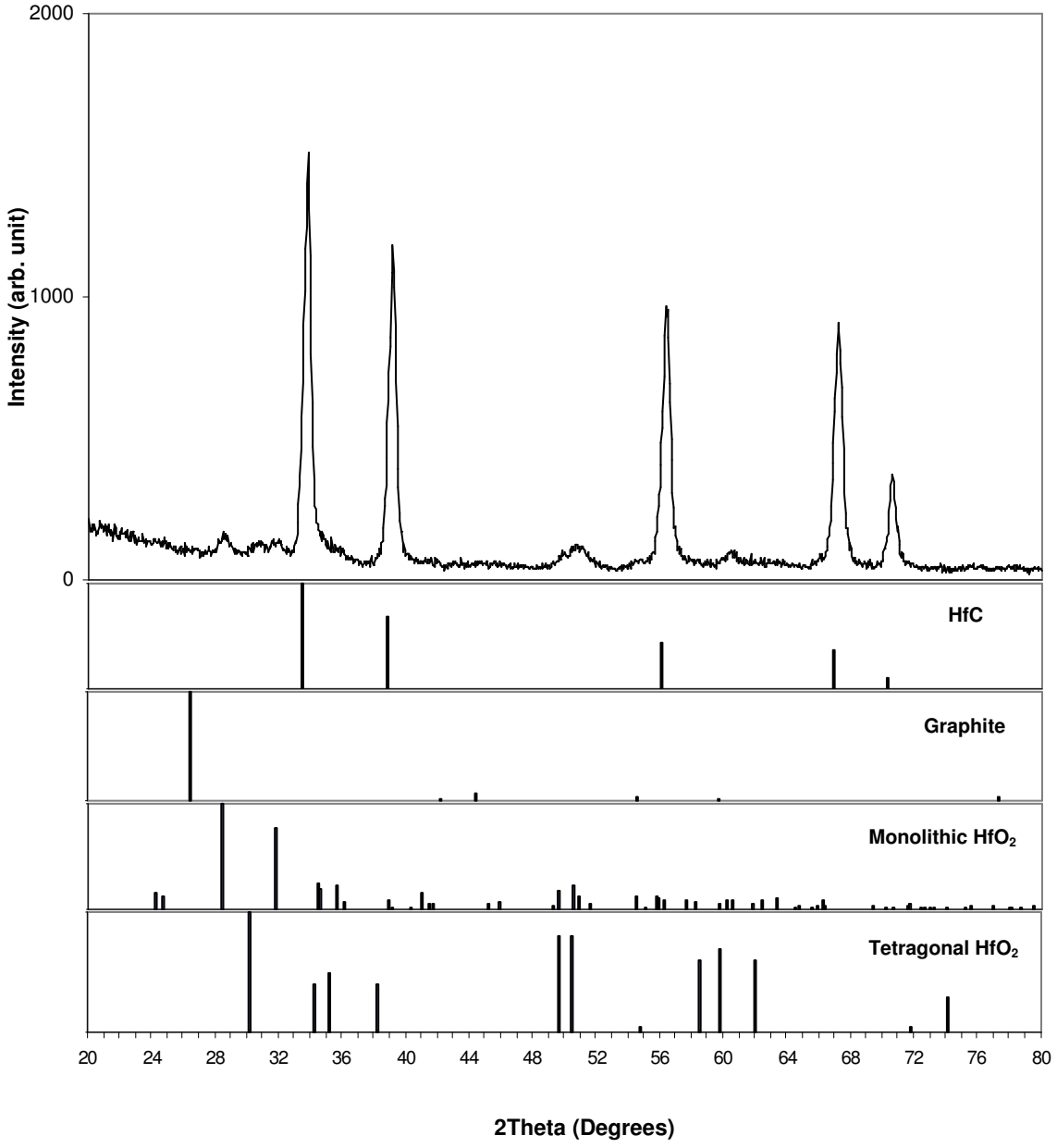

Figure 39 X-Ray diffraction spectrum for an HfC foam (hand mixed with a 3:1 ratio).

5.2.4.2 Estimation of the Amount of HfO_2 in HfC Foam Material

To estimate the amount of HfO_2 in the HfC foam material, pure HfC powder was mixed with HfO_2 powder in different weight percentages (10%. 30% and 50%) and the mixture was analyzed using XRD. The HfO_2/(HfC +HfO_2) XRD peak height ratios were calculated for each weight ratio. A linear relationship between HfO_2 weight percentages and HfO_2/(HfC +HfO_2) XRD peak height ratio was established from the XRD analyses. **Figure 40** shows the XRD spectra of the HfC-HfO_2 powder mixtures. Here, theta angles of #1 and #2 were indicated in the JCPDS spectra of HfC and monolithic HfO_2. HfO_2/(HfC +HfO_2) XRD peak height ratios at these theta angles were calculated using the following equations:

$$\frac{HfO_2 \text{ Peak Height \#1}}{\text{HfC Peak Height \#1} + HfO_2 \text{ Peak Height \#1}}$$

and:

$$\frac{HfO_2 \text{ Peak Height \#2}}{\text{HfC Peak Height \#2} + HfO_2 \text{ Peak Height \#2}}$$

These XRD peak height ratios were plotted vs. respective HfO_2 weight percentages and the results shown in **Figure 41.** A linear relationship was established: the solid trend line was derived from the XRD peak height ratios at theta angle #1; and the dotted trend line was derived from the XRD peak height ratio at theta angle #2. Linear equations are also shown in **Figure 41** that can be used as references to estimate the amount of HfO_2 in HfC foam samples.

Based upon the linear equations shown in **Figure 41,** the HfO_2 weight percentage of hand mixed HfC foam material was estimated to be 23% from peak height ratio at theta angle #1, and 24% from peak height ratio at theta angle #2.

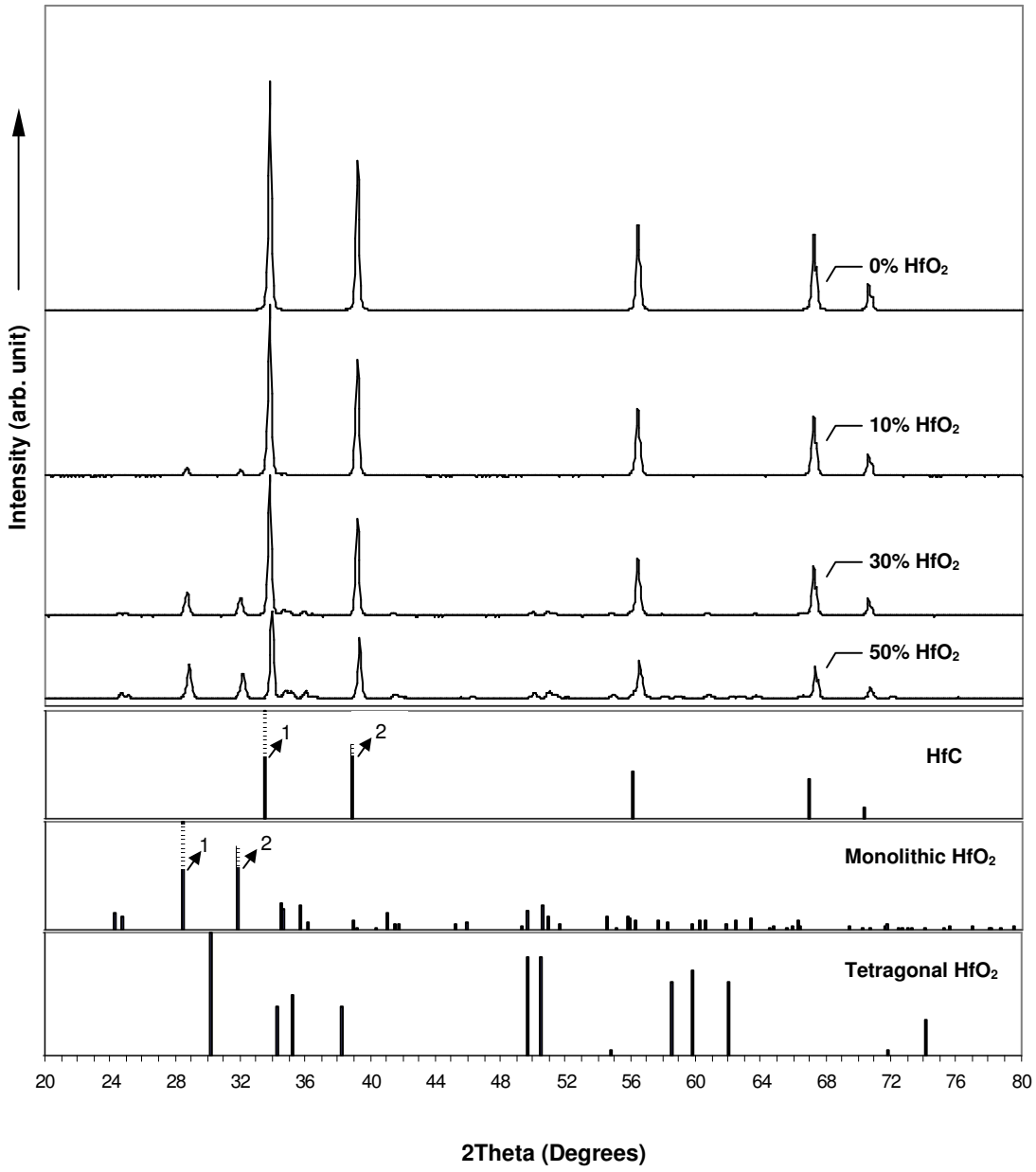

Figure 40 XRD Spectra of HfC-HfO_2 powder mixtures with different HfO_2 weight percentages

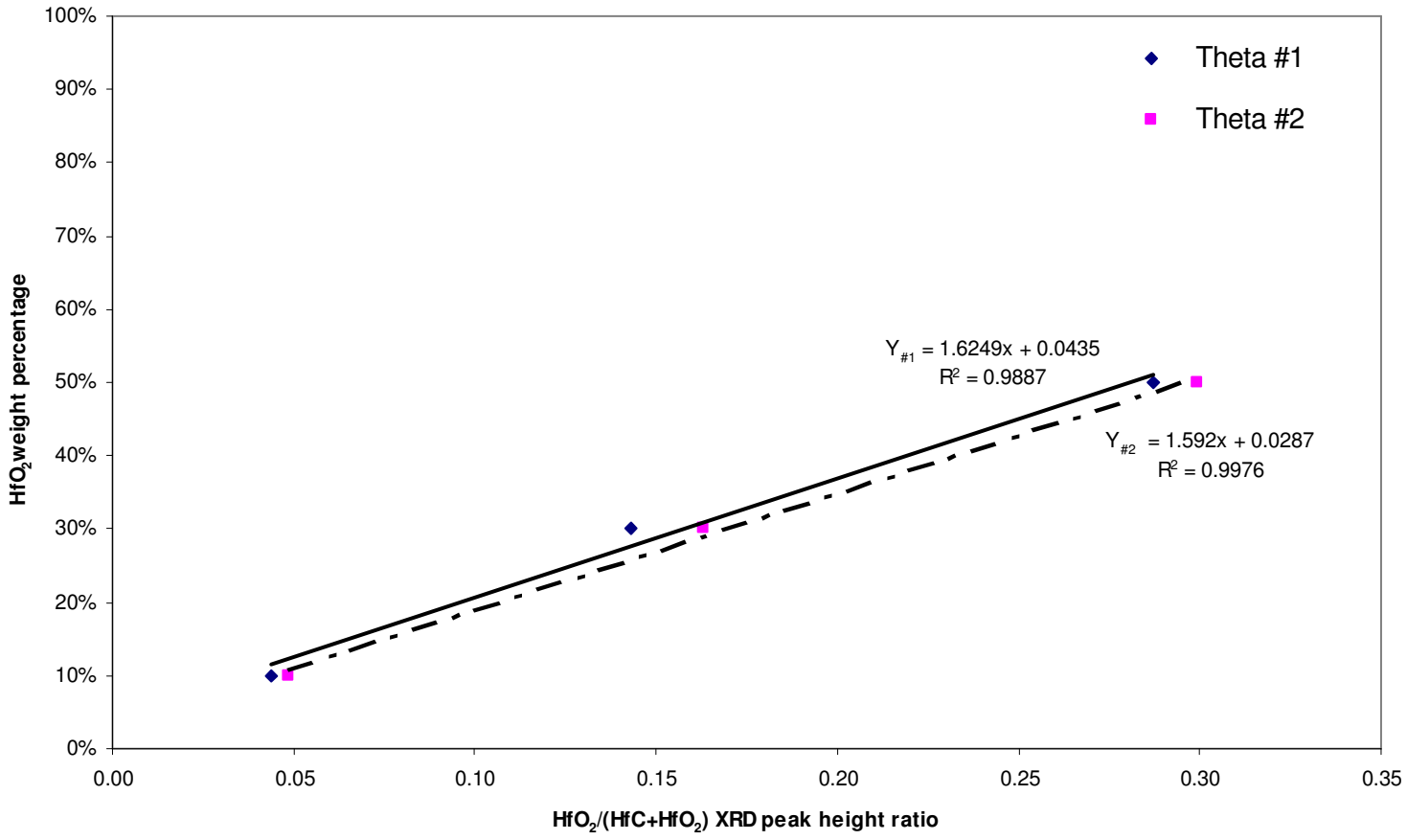

Figure 41 HfO_2 weight percentage vs. $HfO_2/(HfC+HfO_2)$ XRD peak height ratio relationship

5.2.4.3 HfC Lattice Parameter

The lattice parameter (a_0) of the HfC foam material was measured and compared to published values in the open literature. The lattice parameter was measured by plotting the peak positions, as shown in **Figure 42**. Initially, low angle peaks from the XRD spectra, obtained for phase identification, were used for calculating a_0. To improve the accuracy of the a_0 calculation, XRD data spanning the high angle reflection peaks was obtained and analyzed. By plotting a linearized form of the calculated lattice spacing vs. peak position as shown in **Figure 42**, the lattice parameter a_0 for a 1:1 mix ratio specimen was determined by extrapolation to $\theta = 90°$of the least square fit of linearized XRD peak position. **Table 6** contains the measured lattice parameters for 8 of the specimens analyzed. Due to the slow scan rate and small scan interval used to obtain accurate peak positions, only 2 of the samples were analyzed using high angle $K\alpha_1$ X-ray diffraction.

From **Table 6**, a wide range of values were observed, which is in accordance with the wide range of experimental values reported in the literature. The theoretical lattice parameter for HfC is 4.636 Å. Variations in the quantity of vacancies for carbon in the Hf lattice as well as variations in the amount of dissolved oxygen, are the most likely reasons for such a wide range of HfC lattice parameter reported. The behavior of HfC lattice parameter with changing carbon-to-metal ratio is uncertain, due to the variations among reports. Dissolved oxygen has been reported to lower the lattice parameter in hafnium carbide. [11]

Table 6 Lattice parameter measurements for HfC foam specimens.

Sample	Mix Ratio	Lattice Parameter (Å)	
		Low Angle Kα	High Angle Kα
1	1:1	4.644	4.627
2	1:1	4.630	
3	1:2	4.646	
4	1:2	4.643	
5	1:3	4.647	
6	1:3	4.637	
7	1:4	4.650	4.654
8	1:4	4.613	

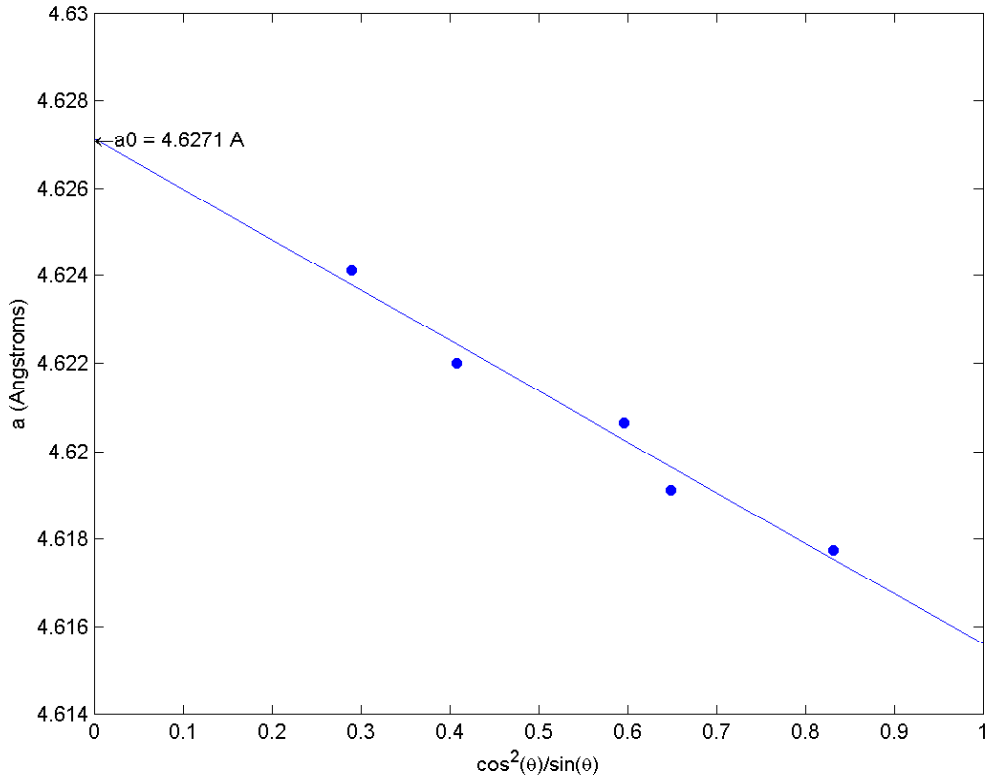

Figure 42 Lattice parameter a_0 determination approach for a specimen mixed with 1:1 ratio.

5.2.4.4 Foam Microstructure

Scanning electron microscopy (SEM) was used to examine the microstructure of the HfC foam. The two SEM micrographs shown in **Figure 43** reveal a window and strut morphology, with open cells interconnected by pores within the windows. Qualitatively, this is in agreement with the porosity measurements described in previous sections. Cell sizes of the sample reached millimeter scale in diameter and had a very wide distribution range.

Several factors could attribute to the wide range of cell dimensions observed:

1. Entrained air pockets during hand mixing: these pockets will expand dramatically under vacuum during heat treatment and create large cells.
2. Inadequate hand mixing uniformity: Hf containing agglomerated particles produced larger cells during heat treatment.
3. Difficulty of gas removal from samples during thermolysis: big cells tend to appear at the center of the foam sample due to longer gas travel path to the outer surface.

In support of the above hypotheses, a preform sample was broken to reveal the polymer preform inner structure. Visual inspection of the preform sample, shown in the lower picture of **Figure 44,** indicates white inclusions which are unmixed Hf containing agglomerated particles. The upper picture in **Figure 44** shows entrained air pockets from hand mixing of the sample. Both of these features are believed to contribute to the creation of the large cells in the final HfC foam structure.

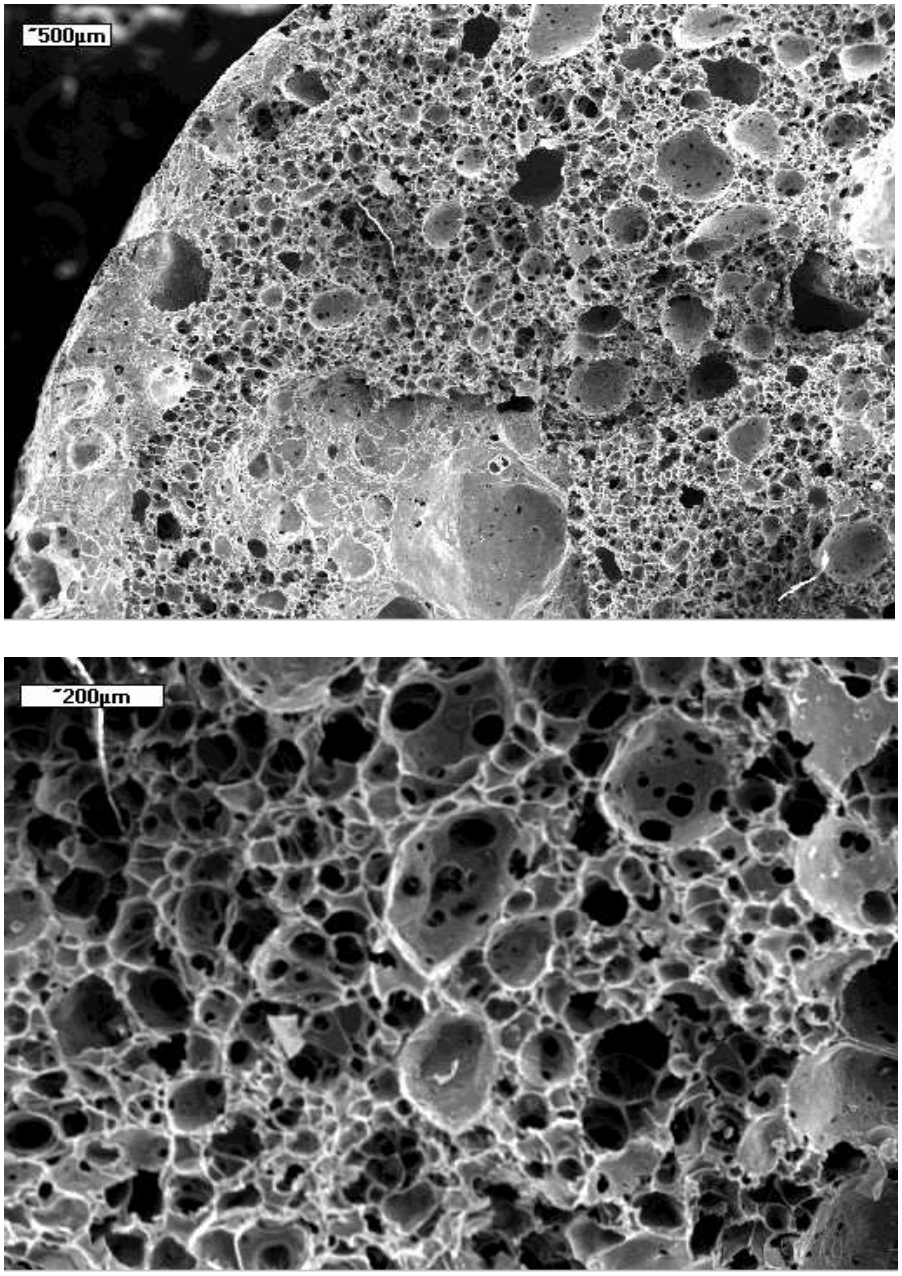

Figure 43 SEM micrographs of a 4:1 ratio HfC foam at 20X (upper) and 80X (lower) magnification

Figure 44 Hand mixed preform sample broken surface (1:1 Mixing ratio). Upper Figure shows entrained air pockets. Lower Figure shows Hf containing agglomerated particles.

5.2.4.5 Foam Compression Strength

Five HfC foam samples produced by hand mixing were machined into cylinders for compression tests. A compression strength of 3.89 ±1.78 MPa was observed. **Table 7** shows the compressive test foam sample dimensions and test results.

Table 7 Compression strength of Hand Mixed HfC foam samples

Sample ID	Sample Dimensions		Compression Strength (MPa)	Average Compression Strength □MPa)	Standard Deviation □MPa)
	Diameter (mm)	Height (mm)			
#1	10.92	10.58	1.02	3.89	1.78
#2	8.95	9.10	3.61		
#3	9.10	8.96	5.32		
#4	8.83	9.04	3.35		
#5	9.38	8.55	6.15		

5.3 Vacuum Mixing

To optimize the microstructure and improve the mechanical properties of HfC foams, vacuum mixing of polymers was also investigated. The equipment and procedures used for vacuum mixing of the polymer precursors were discussed in section **4.2.3.2**.

Vacuum mixing was designed to eliminate the first and second factors affecting the final foam structure discussed in section **5.2.4.4**. Mixing under vacuum should remove or reduce the air pockets trapped inside the polymer paste during the hand mixing process. The limited mixing time due to polymer curing made it hard for hand mixing to remove the Hf containing agglomerated particles and yield a uniform mixture. Vacuum mixing used a motor-driven mixing propeller to provide more thorough stirring during a short mixing duration, thus reducing the amount of Hf containing agglomerated particles.

As described in section **4.2.3.2,** for all the vacuum mixing experiments only a 1:1 mixing ratio was used because higher ratios increased mixing difficulties and did not achieve a uniform mixture.

5.3.1 Polymer Preform Sample

Figure 45 shows a typical polymer preform sample made by vacuum mixing. The sample was ejected from a disposable syringe, and sectioned across the middle of the sample. The sectioned surface was polished with 1000 grit sandpaper before the picture was taken.

Compared to the hand mixed preform sample in **Figure 44**, the size of the white inclusions in these samples was a lot smaller, although tiny white particles were still present. Air pockets which appeared in the hand mixing sample were not observed in **Figure 45.** These observations indicate that the vacuum mixing yielded a more uniform preform than the hand mixing method.

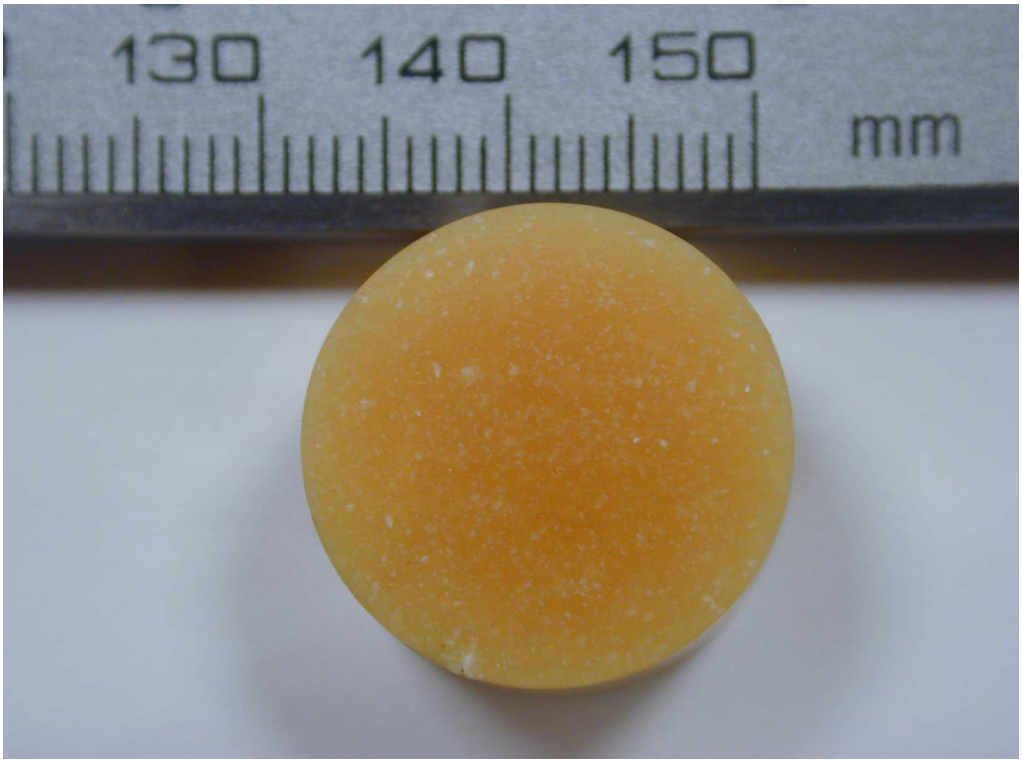

Figure 45 Cross-sectional surface of a vacuum mixed polymer preform sample.

5.3.2 HfC Foam Characterization

5.3.2.1 Density and Microstructure

Vacuum mixed perform samples were then heat treated using the thermolysis and pyrolysis procedure. The temperature profile in **Figure 13** was used.

The HfC foam density measured from 5 samples showed a value of 0.33 ± 0.09g/cm^3, which was lower than the value of 0.58 ± 0.01g/cm^3 obtained for the hand mixed samples with a 1:1 ratio.

The improvement in the HfC foam microstructure compared to that obtained using the hand mixed method had been observed in several samples made with vacuum mixing method. **Figure 46** shows a vacuum mixed sample with good foam microstructure after heat treatment. The sample in **Figure 46** has a smoother outer surface than the hand mixed HfC foam sample in **Figure 33**, and no external open cells were visible. **Figure 47** shows SEM photograph of the broken surface of an HfC foam sample. The lower picture is a magnified view of a small area of the upper picture**.** Compared to the structure of the hand mixed sample in **Figure 43**, the cell sizes were a lot more uniform. In **Figure 47,** the vacuum mixed sample exhibited uniform cell sizes in the range of 20 ~ 200μm, while cell sizes in the hand mixed samples could reach the millimeter scale in diameter and had a much larger range in cell diameter distribution.

Although improvements in the HfC foam microstructure compared to the hand mixed samples were observed, the vacuum mixing method was unable to consistently achieve a uniform HfC foam structure as shown in **Figure 47**.

Figure 46 Vacuum mixed HfC foam sample after heat treatment

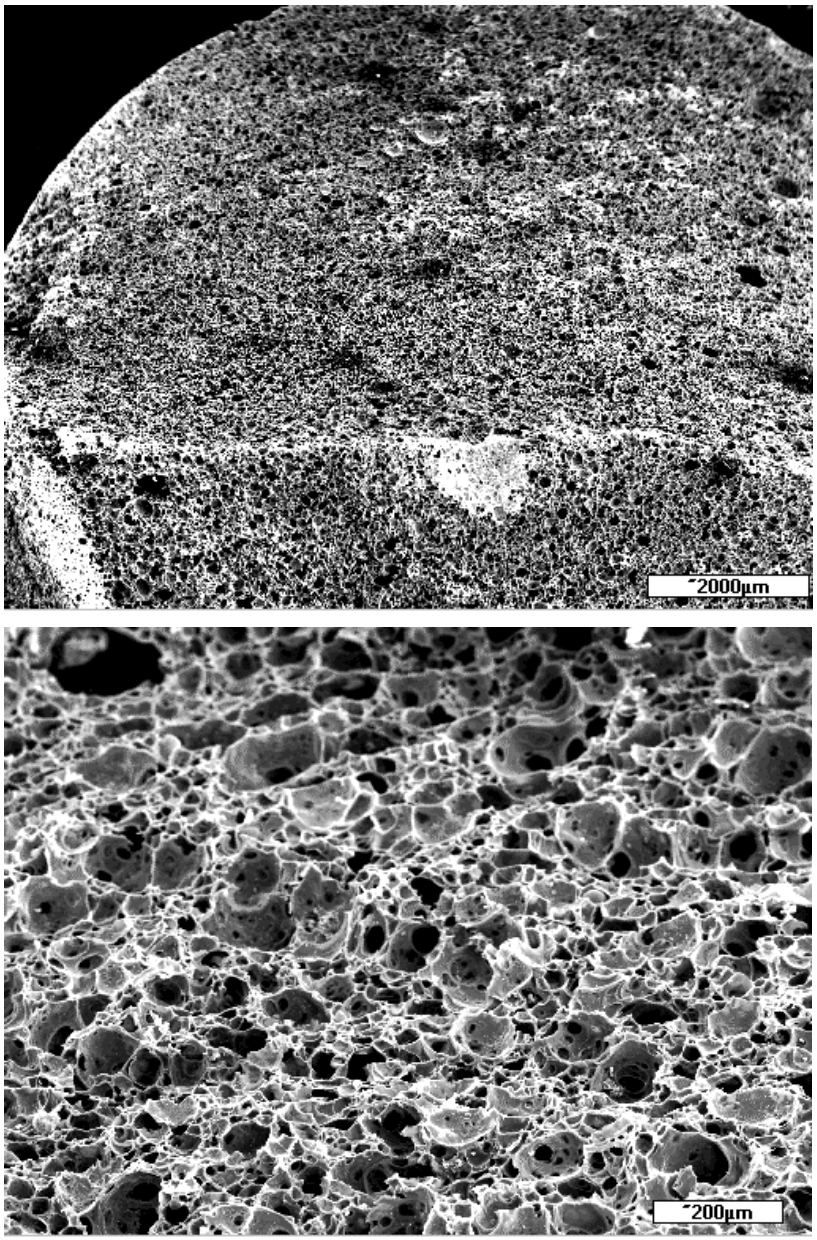

Figure 47 SEM photos of the broken surface of a vacuum mixed HfC foam sample. Upper picture is a general view and lower picture is a magnified view, which show uniform cell sizes in the range of 20 ~ 200µm.

The reason for this inconsistency could be the third factor affecting the final foam structure discussed in section **5.2.4.4.** During thermolysis, large amounts of gas may be generated through polymer decomposition in very short periods of time. These gases are removed by the vacuum system once they travel through the sample and reach the sample outer surface. However when the speed of gas evolution to the outer surface is slow, gases tend to accumulate in the sample and inflate big cells, creating a similar foam structure to that shown in **Figure 43.**

Two methods were investigated to address this problem. The thermolysis heating rate was reduced in order to decrease the gas generation rate, and an easier pathway for faster gas travel was created by using the polymer powder compaction method, which is further discussed in section **5.4**.

5.3.2.2 XRD Spectrum

HfC foam samples made by vacuum mixing were pulverized and inspected with X-ray diffraction (XRD) to confirm the conversion of the polymer preform to HfC. **Figure 48** shows a typical XRD spectrum of vacuum mixed HfC foam samples. Comparison of the sample XRD spectrum with the JCPDS Powder Diffraction File (PDF) database, as shown in **Figure 48**, indicates that the foam material was composed primarily of HfC. No residual graphite peak was found. Small amounts of HfO_2 were evident in the diffraction spectrum.

The XRD spectra of hand mixed (**Figure 38**) and vacuum mixed samples (**Figure 48**) reveal that these samples were similar in their compositions; in both samples, the predominant component was HfC with a small amount of HfO_2.

Based upon the linear equations in **Figure 41,** the estimated HfO_2 weight percentage in **Figure 48** of vacuum mixed HfC foam material was 20% from the peak height ratio at both theta angle #1 and #2.

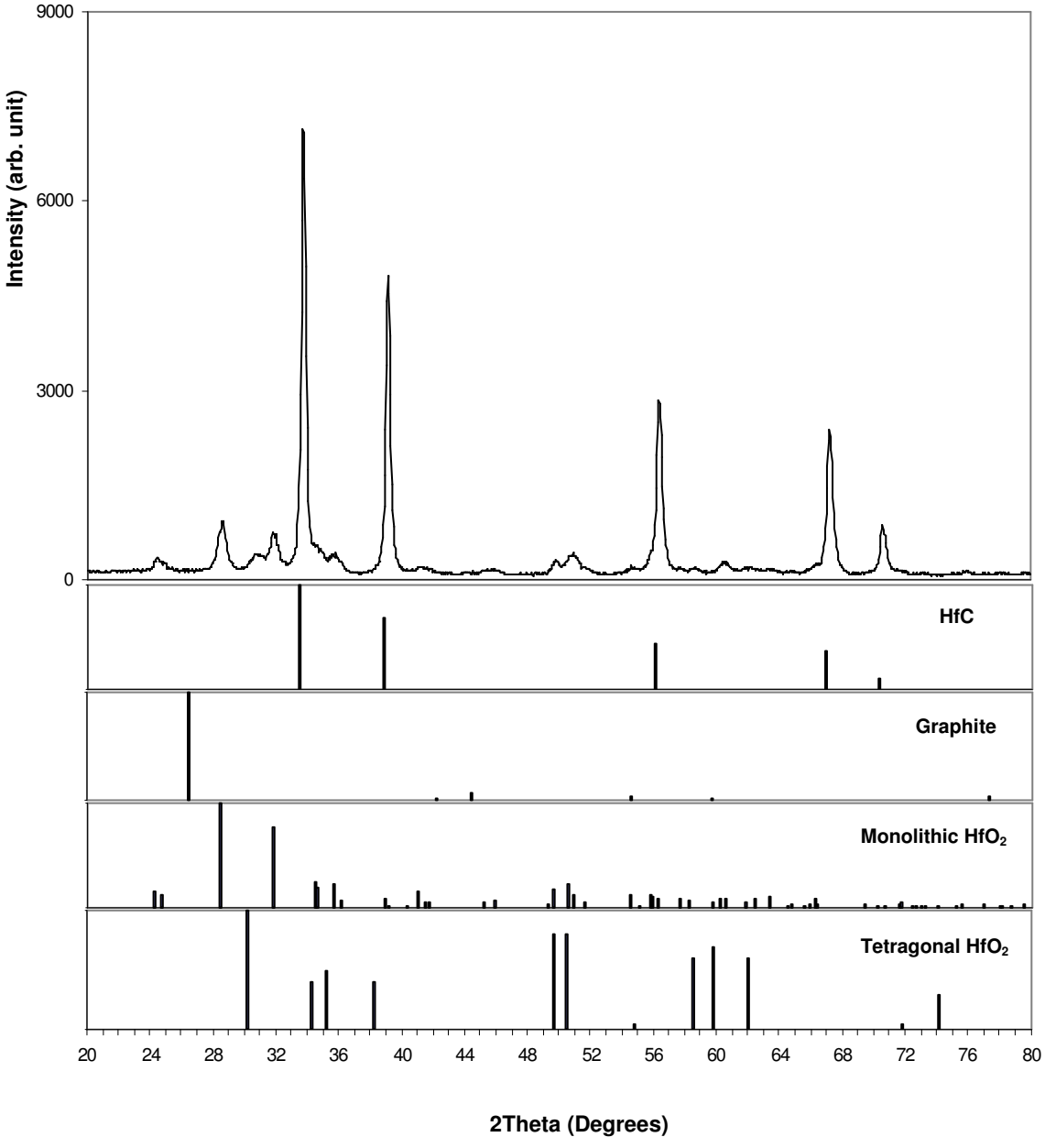

Figure 48 XRD spectrum for a vacuum mixed HfC foam sample

5.3.2.3 Foam Compression Strength

HfC foam samples produced by the vacuum mixing method were machined into cylinders and compression tests were conducted. A compression strength of 1.48 ± 0.21 MPa was measured for five samples with foam structures similar to those of hand mixed samples (**Figure 43**). Due to the difficulty in achieving a good foam structure shown in **Figure 47,** only one sample with good foam structure was tested, which yielded a compressive strength of 6.34 MPa. **Table 8** shows the compressive test foam sample dimensions and test results.

The lower compressive strength (1.48 ± 0.21 MPa) of vacuum mixed samples compared to the compressive strength of hand mixed samples (3.89 ± 1.78 MPa) can be attributed to the lower density and larger size of the vacuum mixed samples, which tended to suffer from deteriorating foam structures due to gas accumulation in the samples during thermolysis, as discussed in **5.2.4.4.**

Table 8 Compression strength of Vacuum Mixed HfC foam samples

Sample ID	Sample Dimensions		Compression Strength (MPa)	Average Compression Strength □MPa)
	Diameter (mm)	Height (mm)		
#1	15.82	16.76	1.23	1.48 ± 0.21
#2	15.29	14.72	1.76	
#3	14.32	17.55	1.55	
#4	17.52	16.89	1.24	
#5	19.94	13.25	1.64	
#6 (good structure)	14.32	7.51	6.34	6.34

5.4 Polymer Powder Compaction

The Polymer Powder Compaction method was employed in an attempt to further optimize the HfC foam microstructure and mechanical properties. As mentioned earlier, the vacuum mixing method was not able to consistently achieve a uniform HfC foam structure.

This lack of uniformity is likely to arise because the cell forming process for vacuum mixed samples was an uncontrolled, natural growth process. During thermolysis, large amount of gases are generated in vacuum mixed samples within a very short period of time. Gases generated close to the outer surface of the sample have a relative shorter travel distance to reach the vacuum atmosphere. Thus, these gases can travel through the sample more easily and be removed by the vacuum system. However gases generated close to the center of the sample have a longer distance to travel to reach the vacuum atmosphere. These gases have more difficulty traveling through the sample, and they tend to accumulate and form bigger bubbles, and thus bigger cells, inside the sample, which causes the inconsistencies in the HfC foam structure for different vacuum mixed samples.

To address this problem, measures were taken to either reduce the gas generation speed during thermolysis, or reduce the gas accumulation by creating easier pathways for gases traveling through the sample to reach the vacuum atmosphere.

The thermolysis heating rate was reduced in an attempt to decrease the gas generation rate, but was proved to be ineffective. It was found that once the polymer decomposition temperature was reached, polymer decomposition reactions were very fast and intense, and large amounts of gases were produced quickly in spite of the very slow heating rate.

Polymer Powder Compaction method was then used in order to create easier pathways for gas release. The method proved to be capable to producing a foam structure that allow faster gas escape, and was thus able to produce a uniform cell size and mechanically stronger foam structure.

The method started with cured hand-mixed or vacuum-mixed polymer preform samples. These samples were first heat treated using low temperature thermolysis, and then the heat treatment was stopped and the polymer preform samples removed from the furnace. The samples were pulverized, sieved, and cold pressed into polymer cylinders. These polymer cylinders were then heat treated with a second thermolysis and the final pyrolysis to produce HfC foam. Details of the procedure for Polymer Powder Compaction are described in section **4.4**.

The key step for the procedure was to pulverize the polymer sample after the initial thermolysis and then compress the resulting powder into polymer cylinders. This step created a structure that allowed for easy gas escape.

5.4.1 Polymer Powder and Polymer Cylinders

As described in section **4.4,** polymer performs were removed from the vacuum furnace after the initial thermolysis and pulverized with a mortar and pestle. These particles were analyzed using an SEM.

To prepare the powder sample for SEM, a thin layer of polymer powder was sprinkled onto a piece of copper tape which had conductive adhesive on both sides. The copper tape was then attached to an aluminum stud sample holder. A Pelco SC-6 Sputter Coater was used to coat a layer of gold with a thickness of 60nm on polymer particles on

the copper tape. In this way, an electrical conductive path was created from the polymer particles to the aluminum stud sample holder, which is required for SEM operation.

Figure 49 and **Figure 50** show SEM pictures of polymer particles on the copper tape. **Figure 49** is a general view of the particles, while **Figure 50** shows a magnified view of a corner in **Figure 49**. There was a large span in polymer particle sizes; particles ranged from small particles of 3µm up to large particles of about 85µm.

Particle size measurement was conducted using a particle size analyzer. **Figure 51** shows the particle size distribution diagram generated by the Microtrac S3500 for polymer powder produced with mortar and pestle. In **Figure 51**, the bar graph uses the secondary Y axis (%Channel), and each bar height indicates the population of particular particle size group as a percentage of the total particle population. The curve in **Figure 51** uses the major Y axis (%Passing), and is known as a "cumulative percent smaller curve"; for instance, the point (84.35um, 80%) on the curve, should be read as "80% percent of the particles are smaller than 84.35 um." The bar graph was employed to show the particle size distribution characteristics (wide, narrow, bimodal, etc); while the "cumulative percent smaller curve" was used to extract the volume median diameter, namely the particle size corresponding to 50% of the particle population.

The particle size distribution shown in the bar graph of **Figure 51** had a near symmetric distribution. The measured particle volume mean diameter was 56.44 µm.

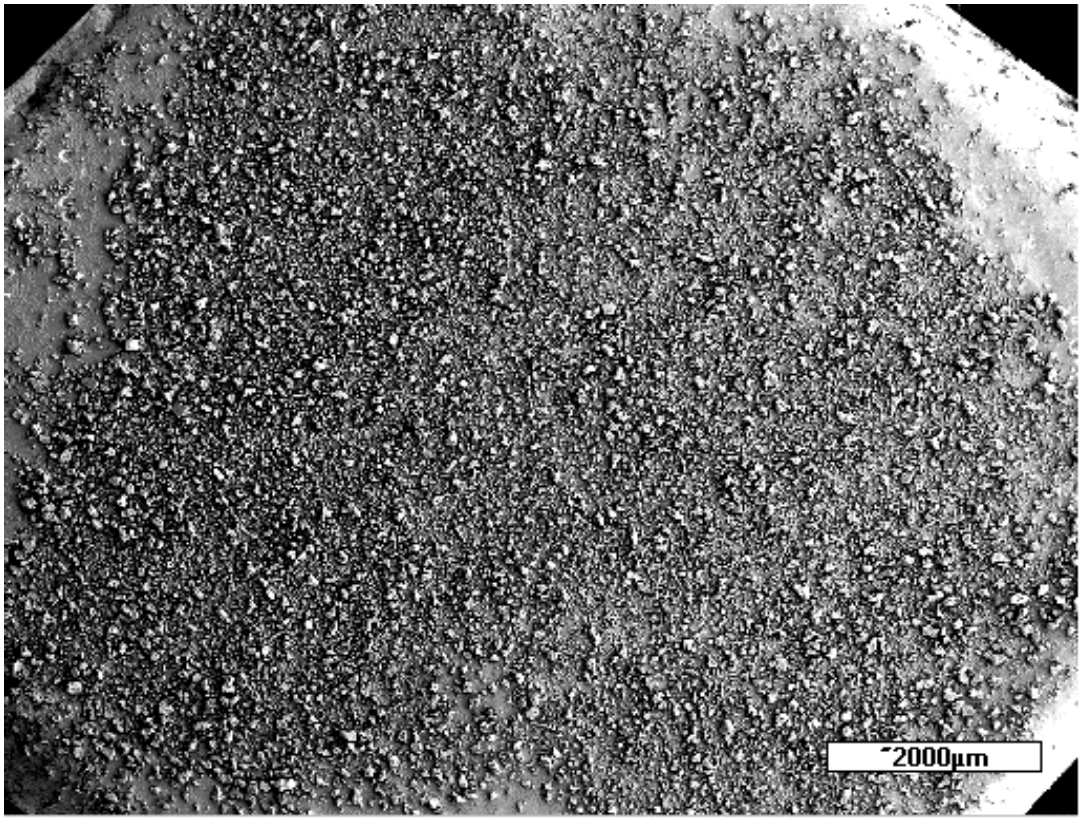

Figure 49 Polymer particles on a copper tape

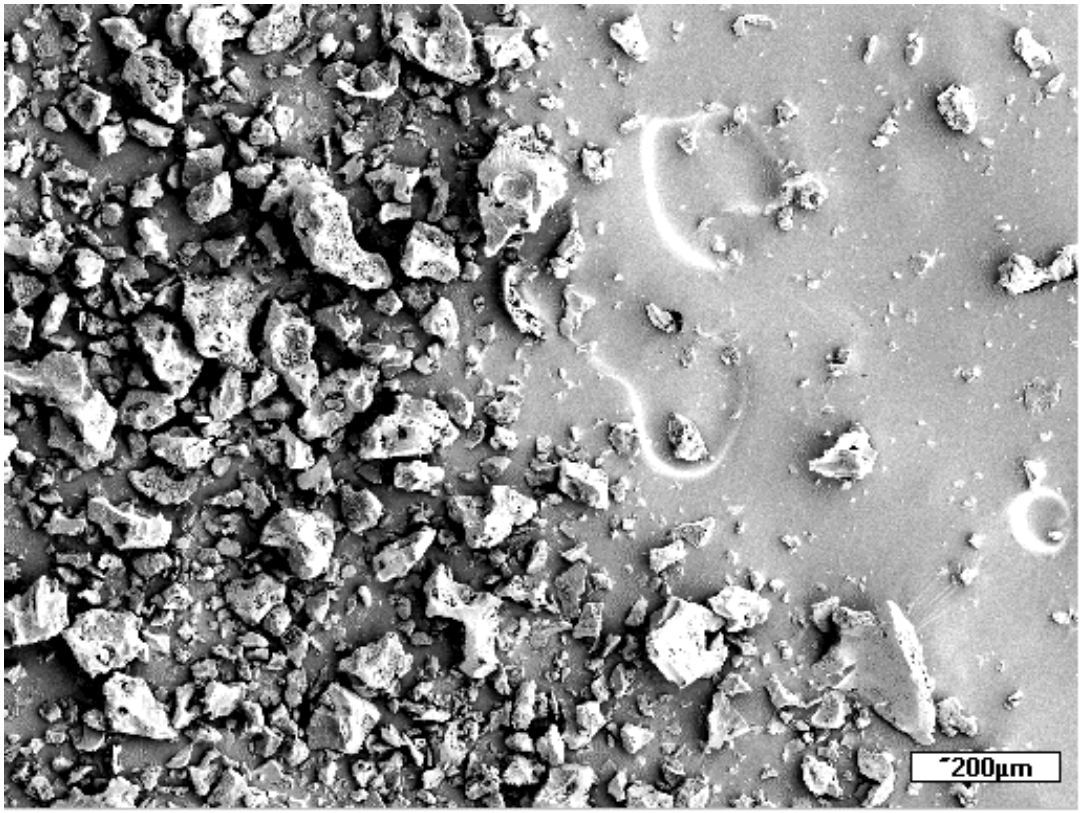

Figure 50 Magnified view of polymer particles

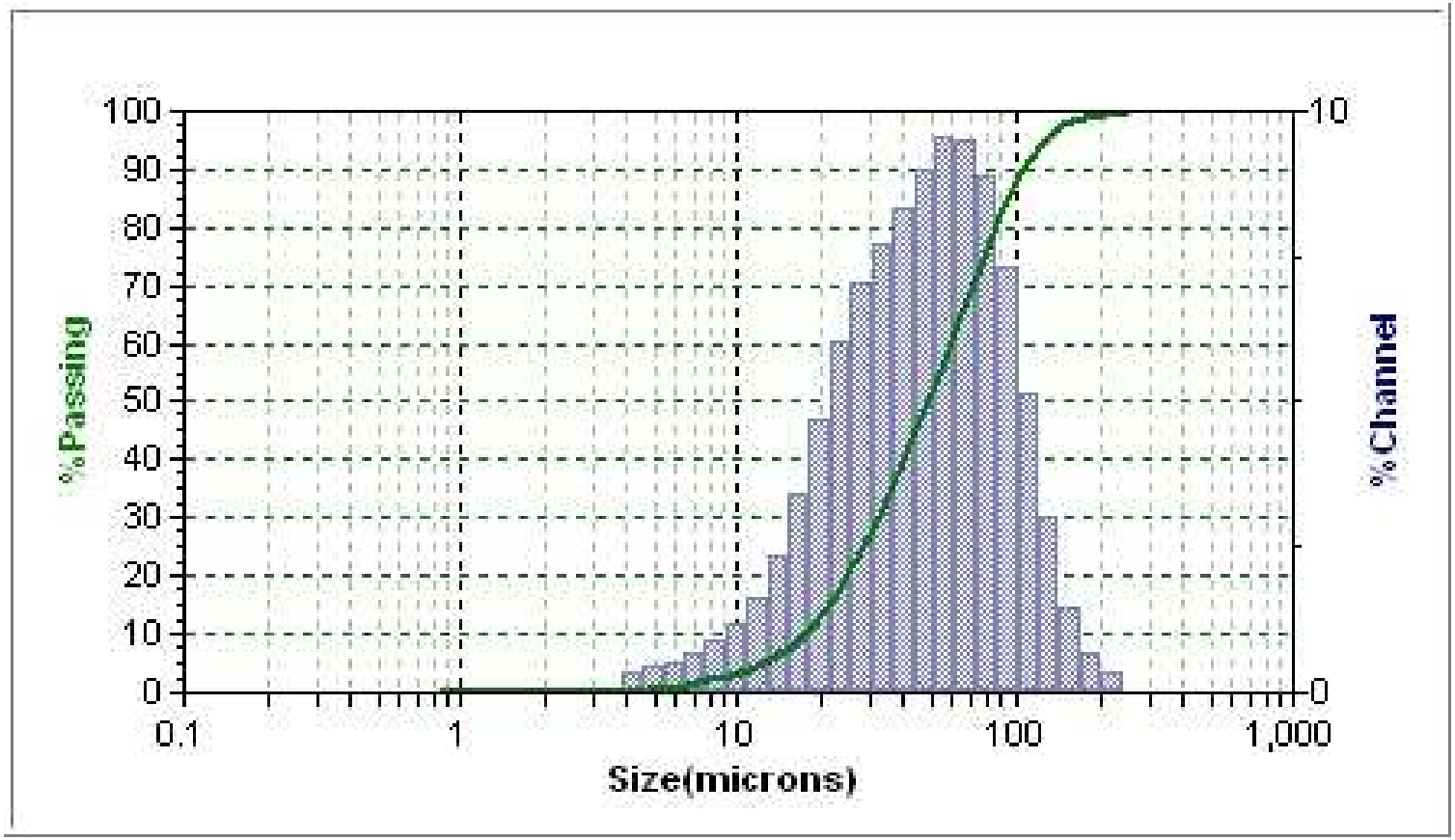

Figure 51 Particle size distribution of powder made by mortar & pestle

Figure 52 is a picture of a polymer pellet that has been cold pressed from polymer powder. The pellet was brown in color and had a dimension of 13 mm in diameter, and 2-3 mm in thickness. As shown in **Figure 52**, the outer surface of the cylinder was smooth; the pellet maintained a correct cylinder shape and the pellet edges were sharp and clean.

Simple geometric measurement using calipers combined with weighing by digital scale was conducted to determine the polymer cyclinder bulk density. The average bulk density from the 5 polymer cylinders was measured to be 1.13 ± 0.02 g/cm^3.

Figure 53 and **Figure 54** are SEM pictures of the broken surface of a polymer cylinder sample. **Figure 53** shows a general profile of the polymer cylinder inner structure: large and small particles were compressed together tightly; gaps between particles, although small, were still evident. **Figure 54** shows a magnified view of **Figure 53**. In **Figure 54**, particles conformed to each other very well after plastic deformation. Gaps between particles were about 1-5 μm. Merging between particles was not observed.

Figure 52 Polymer pellet (cylinder) made from cold pressing of polymer powder

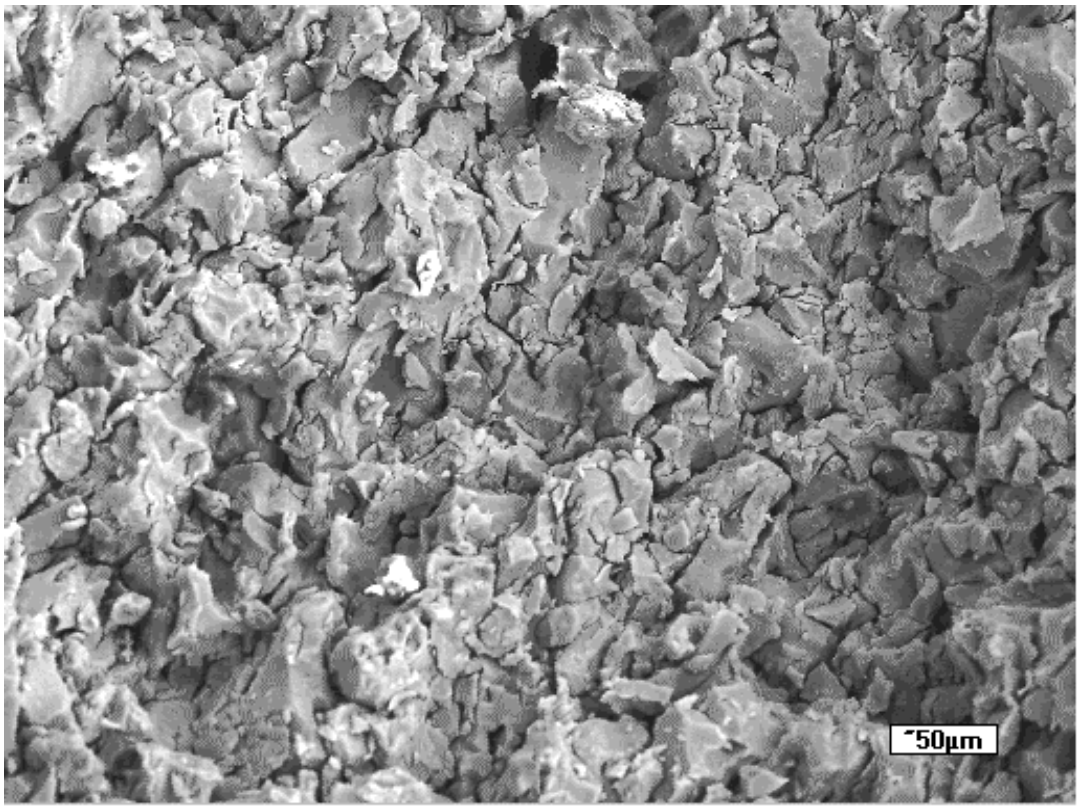

Figure 53 Broken surface of the sample in Figure 52

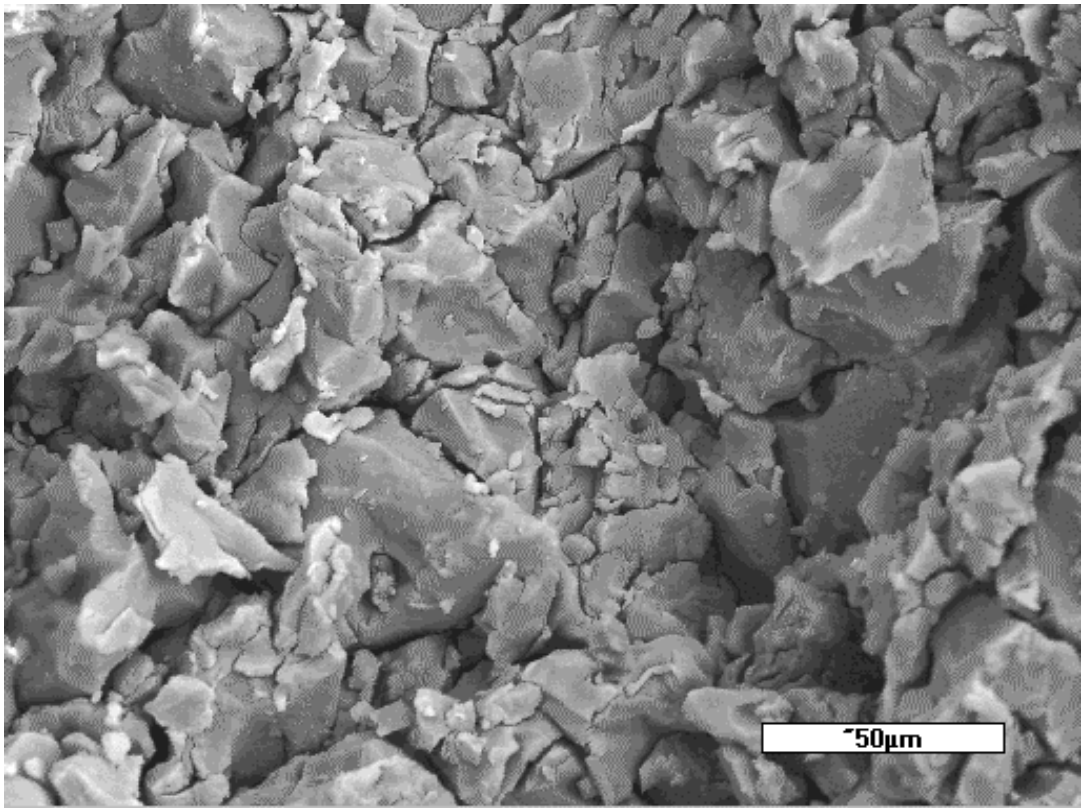

Figure 54 Magnified view of Figure 53

5.4.2 HfC Foam Sample Characterization

5.4.2.1 Density and Microstructure

The polymer cylinders were subjected to a second thermolysis and final pyrolysis heat treatment to create HfC foams. **Figure 55** is a picture of an HfC foam sample after the heat treatment. The HfC sample maintained the polymer state exact cylinder shape. The sample was strong and solid and free from shape distortion compared to the hand mixed and vacuum mixed HfC foam samples.

Geometric measurements using calipers combined with weighing by digital scale was conducted to determine the sample's physical changes after the heat treatment. It was found that the HfC samples had a significant shrinkage of 75.8% in volume, and a mass loss of 73% from the polymer cylinder state. The average HfC foam density measured from 5 samples was 1.25 ± 0.05 g/cm^3 and the calculated total porosity was about 90%. The HfC foam density for the polymer powder compaction method doubled the density of the hand mixed samples.

Figure 56, **Figure 57** and **Figure 58** are SEM images of the broken surface of the typical HfC foam sample shown in **Figure 55**. **Figure 56** is a general view, which shows a uniform structure throughout the broken surface. Variation between cell sizes is small, indicating significant improvement from the hand mixed samples. **Figure 57**, which is a closer view of **Figure 56**, shows evenly distributed, equiaxed half cells as well as connected particles in the HfC foam structure.

The major structural element of these HfC foams was the connected HfC particles. Gaps between particles provided easy pathways for gas release during

thermolysis. The equiaxed half cells shown in **Figure 58** could be formed from large particles that accumulated gases and expanded during heat treatment. However, due to the presence of easy gas release pathways around these large particles, these bubbles did not expand further or connect to adjacent bubbles to form larger cells, as was the case in hand mixed samples.

Compared to the vacuum mixing method, foam microstructure inconsistencies were not observed with the polymer powder compaction method. All the samples produced with this method have similar foam structures to that shown in **Figure 56**.

5.4.2.2 XRD spectrum

X-ray diffraction (XRD) was used to confirm the conversion of HfC for samples made using the Polymer Powder Compaction method. Comparison of the XRD spectrum with the JCPDS Powder Diffraction File (PDF) database, **Figure 59**, indicates that the material is composed primarily of HfC. No residual graphite peak was found. Small amounts of HfO_2 were evident in the diffraction spectrum.

It can be seen that the XRD spectrum is similar in composition to the hand mixed and vacuum mixed samples. As before, the predominant component is HfC together with small amounts of HfO_2. However the peak height for HfO_2 is considerably lower in **Figure 59** compared to hand mixed and vacuum mixed samples, indicating a smaller concentration of HfO_2. The reason could be that the presence of easy gas release pathways results in a more complete polymeric decomposition during thermolysis, and thus a reduction in the amount of trapped oxygen in the HfC lattice compared to hand mixed and vacuum mixed samples.

Based upon the linear equations in **Figure 41,** the estimated HfO_2 weight percentage in **Figure 59** was 9% from peak height ratio at theta angle #1 and 10% from peak height ratio at theta angle #2.

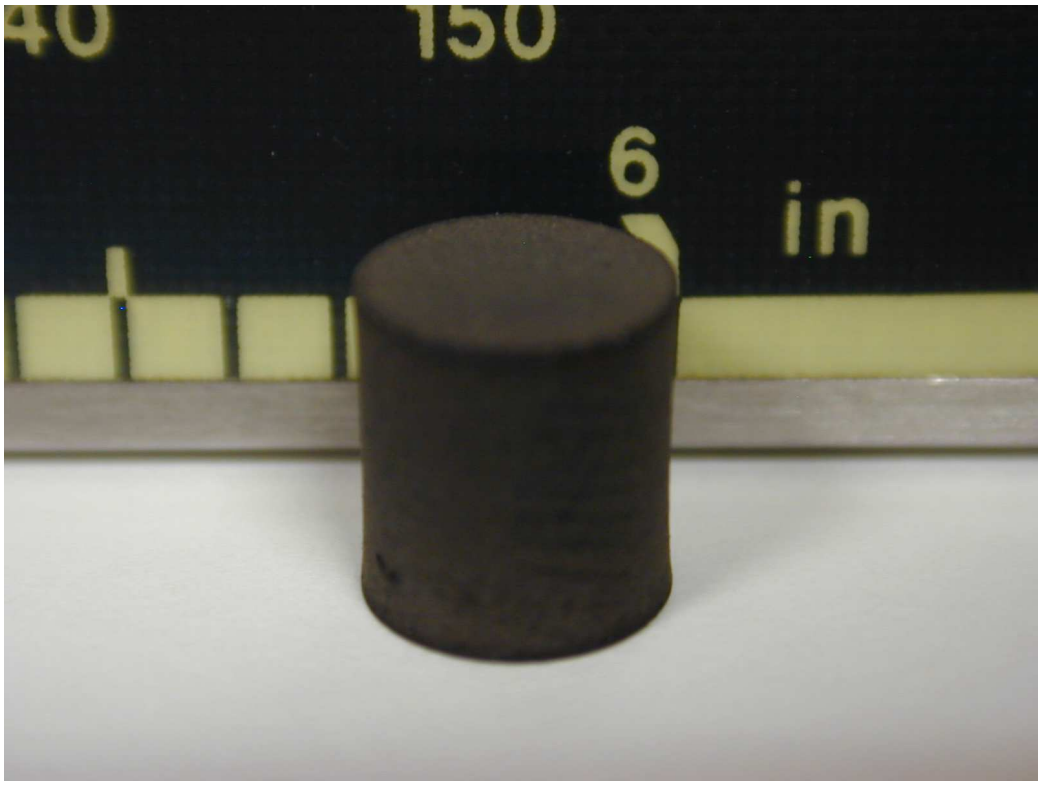

Figure 55 HfC foam created from polymer cylinders

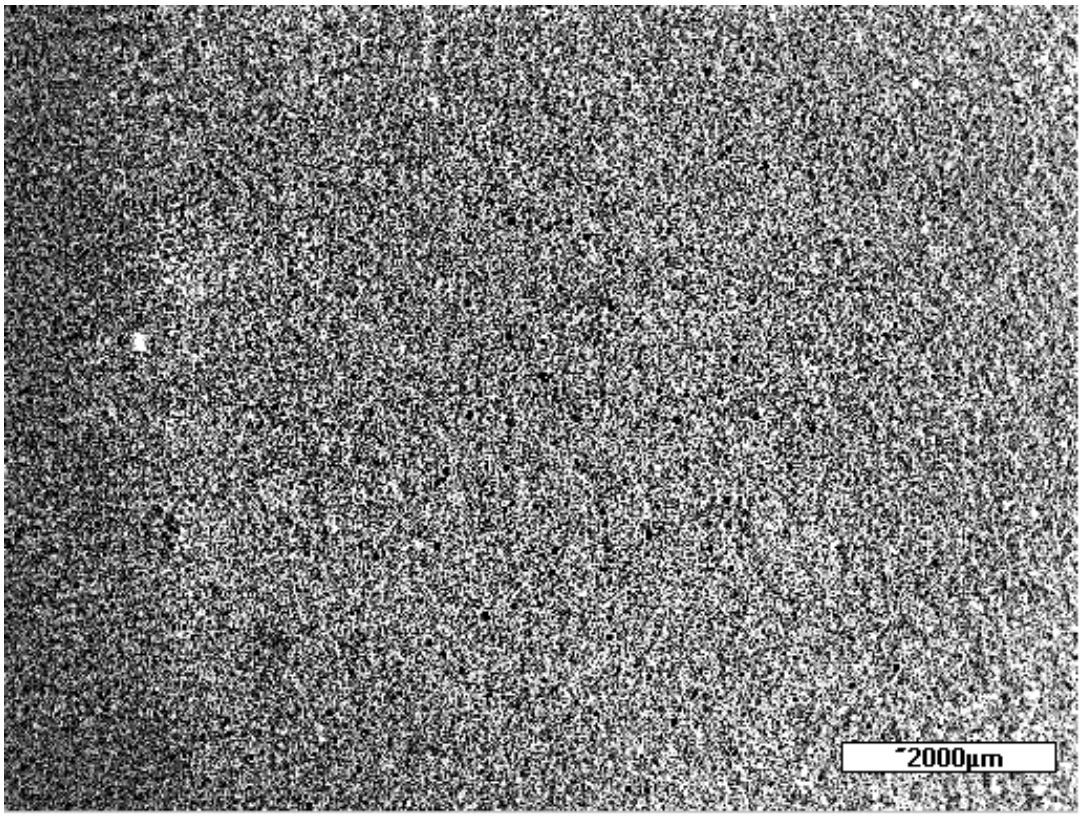

Figure 56 Broken surface of HfC foam sample made from Polymer Powder Compaction

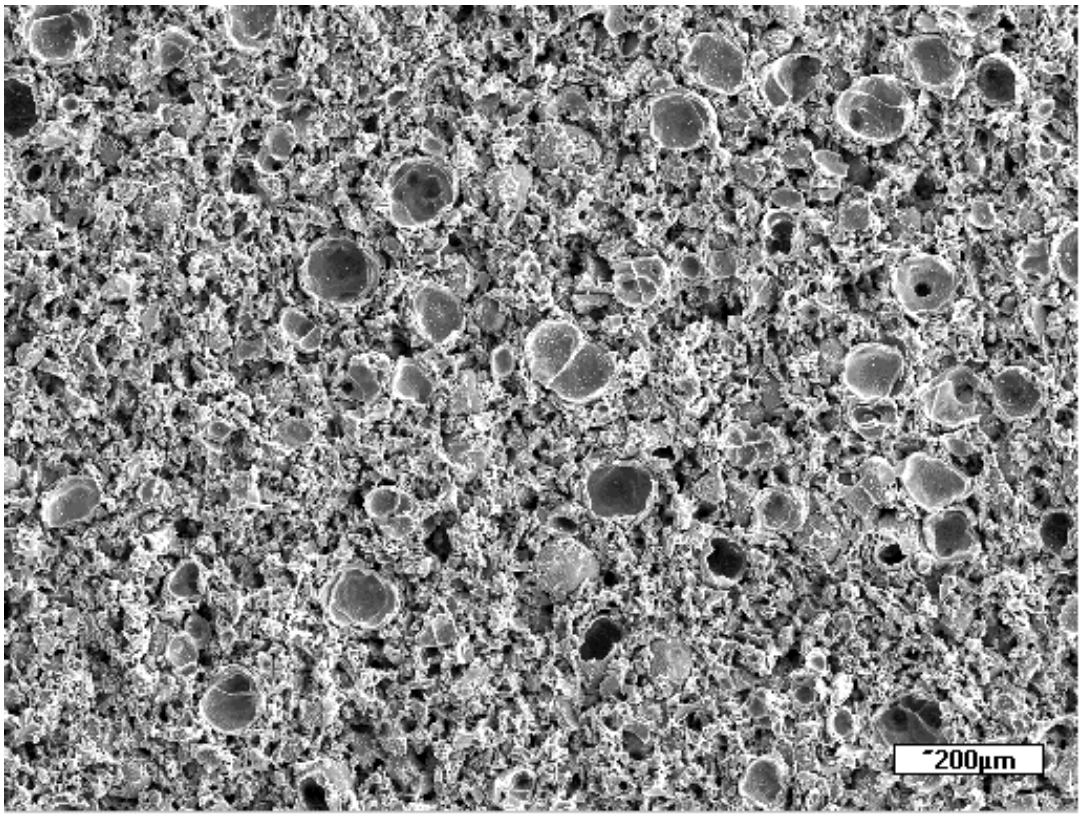

Figure 57 Cell structure of HfC foam sample in Figure 56

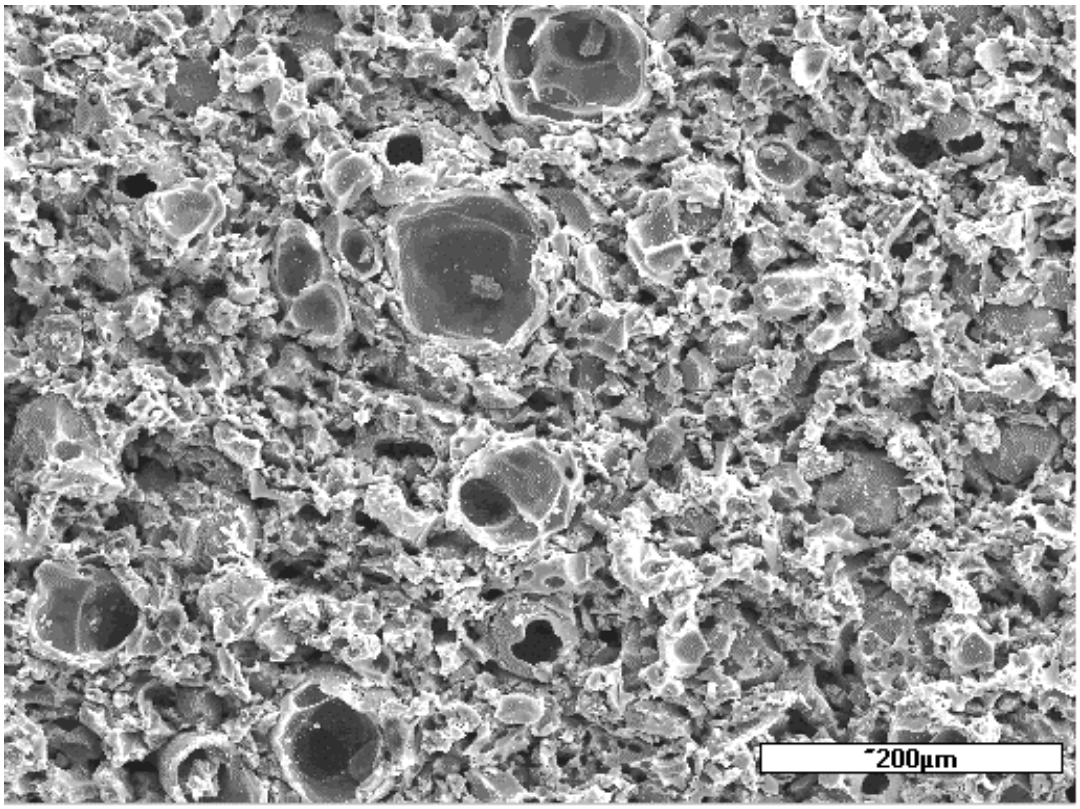

Figure 58 Connected particles and cells of HfC foam sample in Figure 56

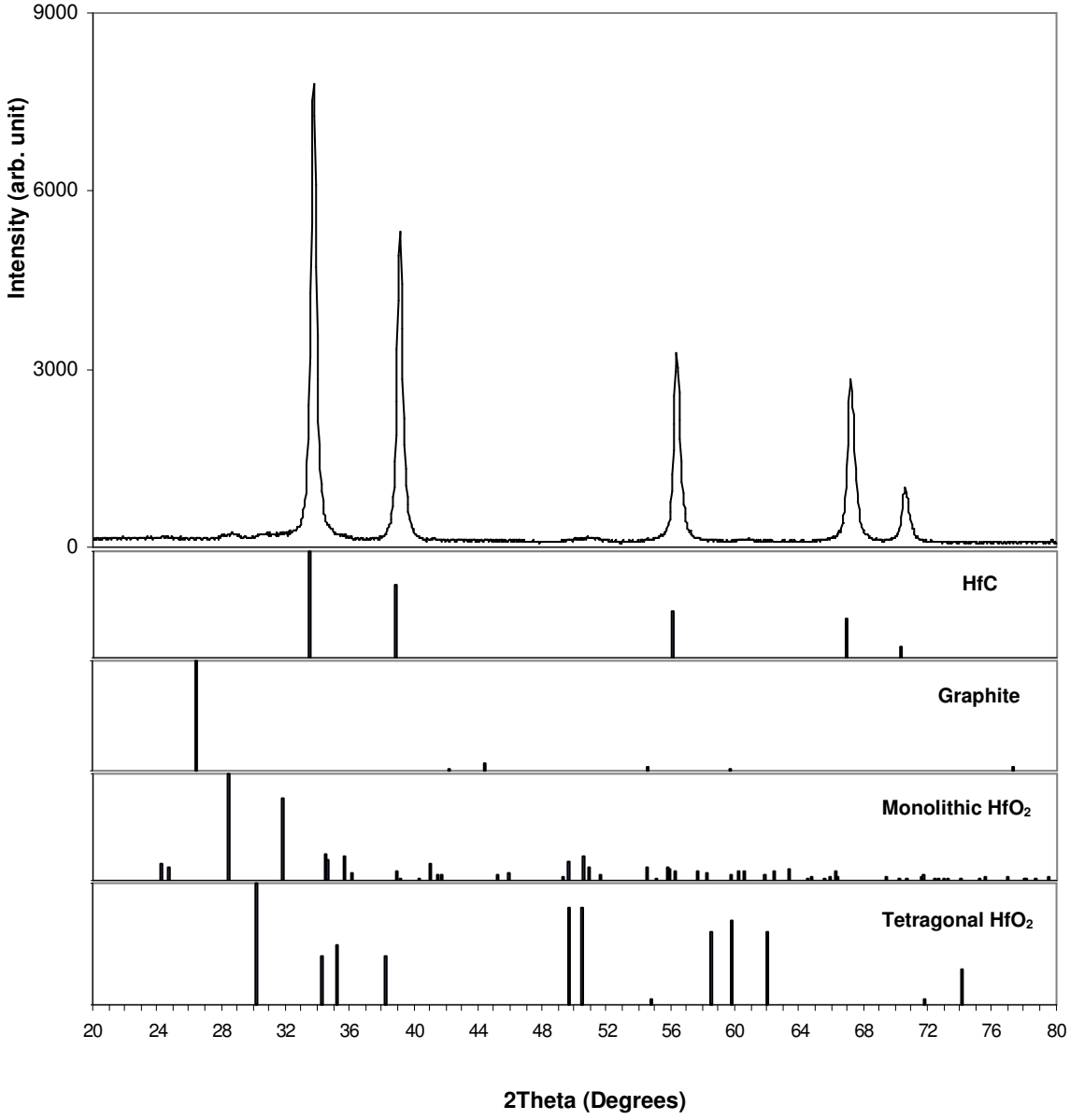

Figure 59 XRD spectrum for HfC foam sample made using Polymer Powder Compaction

5.4.2.3 Foam Compression Tests

The HfC foam samples produced using the Polymer Powder Compaction method from mortar and pestle, as shown in **Figure 55,** had a regular, exact cylinder shape. In accordance with *ASTM Standard C1424-04*, these samples were directly compression tested without machining.

Table 9 shows the foam sample dimensions for compressive tests and the test results. Five samples were tested, which yielded compression strength of 15.16 ± 4.66 MPa. The compression strength value showed significant increases compared to both hand mixed and vacuum mixed samples. The phenomenon can be explained by the improved quality of the HfC foam microstructure; and by an increase in HfC foam density compared to previous foam samples. HfC foam density for Polymer Powder Compaction samples was double that of samples made using the other two methods.

Table 9 Compression strength of HfC foam samples made using Polymer Powder Compaction (mortar and pestle)

Sample ID	Sample Dimensions		Compression Strength (MPa)	Average Compression Strength MPa)
	Diameter (mm)	Height (mm)		
#1	7.55	6.05	11.18	15.16 ± 4.66
#2	6.97	7.00	18.90	
#3	7.57	6.13	11.75	
#4	7.56	6.50	11.48	
#5	7.45	6.67	22.47	

5.4.2.4 Effects of Polymer Powder Processing Effects on Compression Strength

Polymer particles were produced by grinding of polymer preform samples using a pestle and mortar during an initial study. Although this method is adequate for initial HfC foam fabrication, the method's consistency in achieving the same particle size distribution between powder batches could be affected by the researcher. To address this issue, Polymer sample pulverization using an auto-pulverizer, the Labtechnics dish and puck crusher, was investigated to obtain consistent particle size distributions and smaller particle sizes. Three pulverizing times was used, 5 minutes, 15 minutes and 30 minutes, to obtain different particle sizes and size distributions. Particle size measurements were made using a Microtrac S3500 particle size analyzer. The compression strengths of HfC foams made from powders produced with different powder processing methods and processing parameters were measured.

Figure 51, **Figure 60**, **Figure 61**, and **Figure 62** show the particle size distribution diagrams for polymer powder produced with different processing methods or processing times. As discussed in **5.4.1,** the bar graph in these figures uses the secondary Y axis (%Channel), and each bar height indicates the percentage of the population of a particular particle size group compared to the total particle population. The curve in these figures uses the major Y axis (%Passing), and is named the "cumulative percent smaller curve", which can be used to extract the volume median diameter, namely the particle size corresponding to 50% of the particle population.

A comparison of **Figure 51**, **Figure 60**, **Figure 61,** and **Figure 62** revealed that particle size distribution was more symmetric for powder made by mortar & pestle (**Figure 51**), and powder made by auto-pulverizing for 5 minutes (**Figure 60**) than

powder made by auto-pulverizing for 15 minutes and 30 minutes (**Figure 61, Figure 62).** The powder made by auto-pulverizing the polymer for 15 minutes and 30 minutes (**Figure 61, Figure 62)** showed bimodal distributions and a larger particle size than the powder made by auto-pulverizing for 5 minutes (**Figure 60**), which could be the result of powder agglomeration due to the longer pulverizing period and the temperature rise of the pulverizer bowl from room temperature to 50~80°C.

Table 10 summarizes the particle size measurements of powders made with different methods and processing times.

Table 10 Summary of particles size analysis for polymer powder made with different methods and processing times.

	Mortar & pestle powder	Pulverizer powder (5min)	Pulverizer powder (15min)	Pulverizer powder (30min)
Volume mean diameter (um)	56.44	28.91	31.42	70.55

Figure 63 shows the effects of different powder processing methods on HfC foam density and compression strength. For each group in **Figure 63**, the density and compression strength results were measured for 5 to10 samples.

Figure 63 reveals that powder made by auto-pulverizing for 5 minutes (**Figure 60**) yielded foams with higher density and higher compression strength than powder made by mortar & pestle (**Figure 51**). Comparison of **Figure 60** and **Figure 51** shows that both powders had a near symmetric size distribution, but the average particle size of

the powder made by auto-pulverizing for 5 minutes was smaller than powder made by mortar & pestle (**Table 10**). Since a smaller powder particle size favors a higher packing density, this could explain the higher final HfC foam density for powder made by auto-pulverizing for 5 minutes. The increased foam density also led to a higher foam compression strength.

Figure 63 also shows that different pulverizing times introduced significant differences in the foam density and compression strength. When pulverizing time increased from 5 minutes to 15 min or 30 min, the foam density increased from 1.35g/cm^3 to 1.8~1.9g/cm^3, and the foam compression strength was improved from 25MPa to about 200MPa. This could be explained by the particle size distribution difference between powder pulverized for 5 min, and powders pulverized for 15 min or 30 min. Powders pulverized for 15 min or 30 min had a non-uniform bimodal distribution, which enabled the finer particles to fill the holes between the larger particles during cold pressing and created a higher packing density and higher foam density. An increased foam density led to higher compression strength foams made from powder that was auto-pulverized for 15 and 30 min than foams made from powder that was auto-pulverized for 5 min.

Powder pulverized for 30 min yielded higher density (1.9g/cm^3) foams than foams made from powder pulverized for 15 min (1.8g/cm^3). This could be explained by the more specific characteristics of powder particle non-uniform distribution, such as size ratio and population ratio for fine/coarse particles.

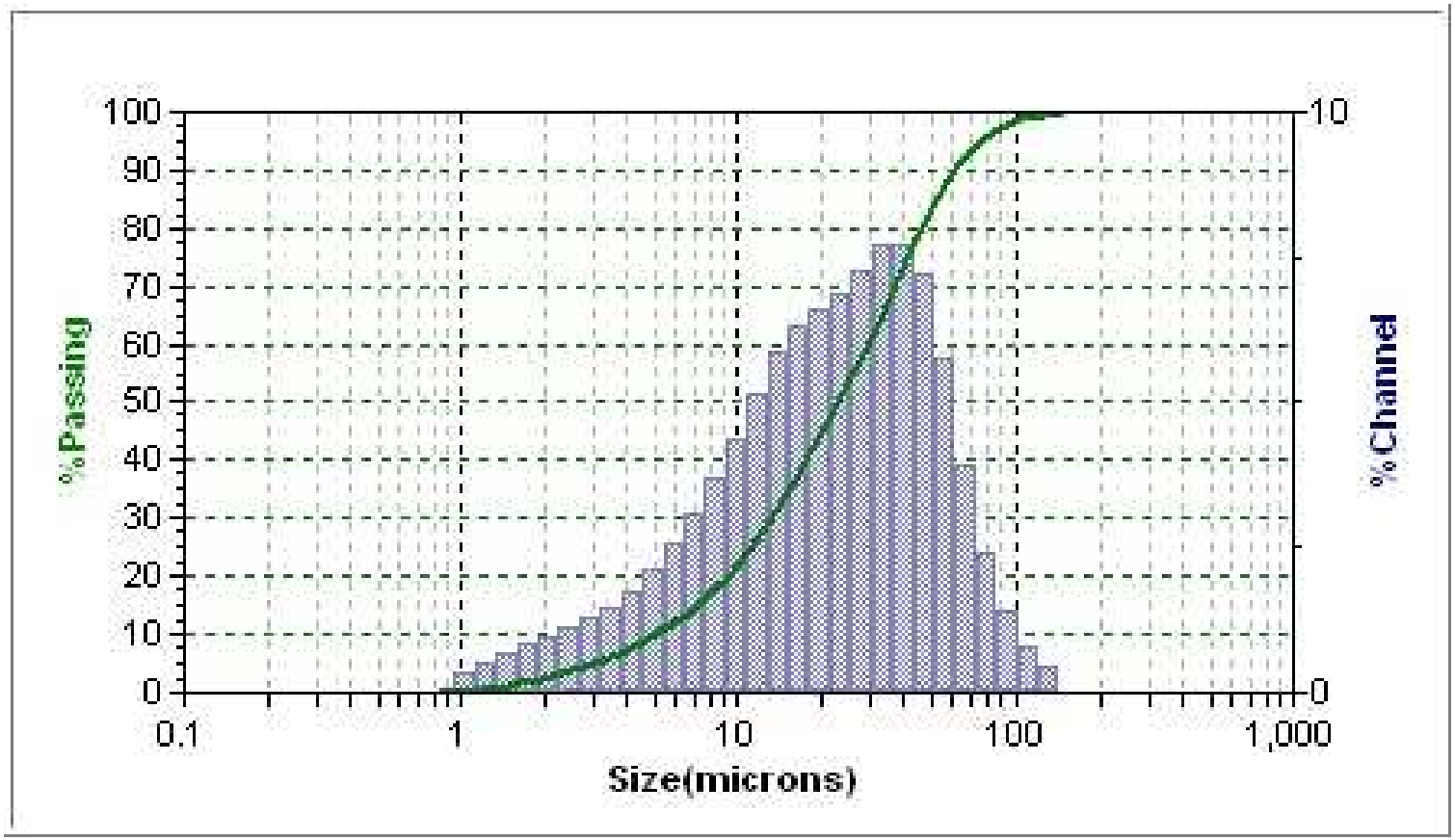

Figure 60 Particle size distribution of powder pulverized for 5min using Labtechnics pulverizer

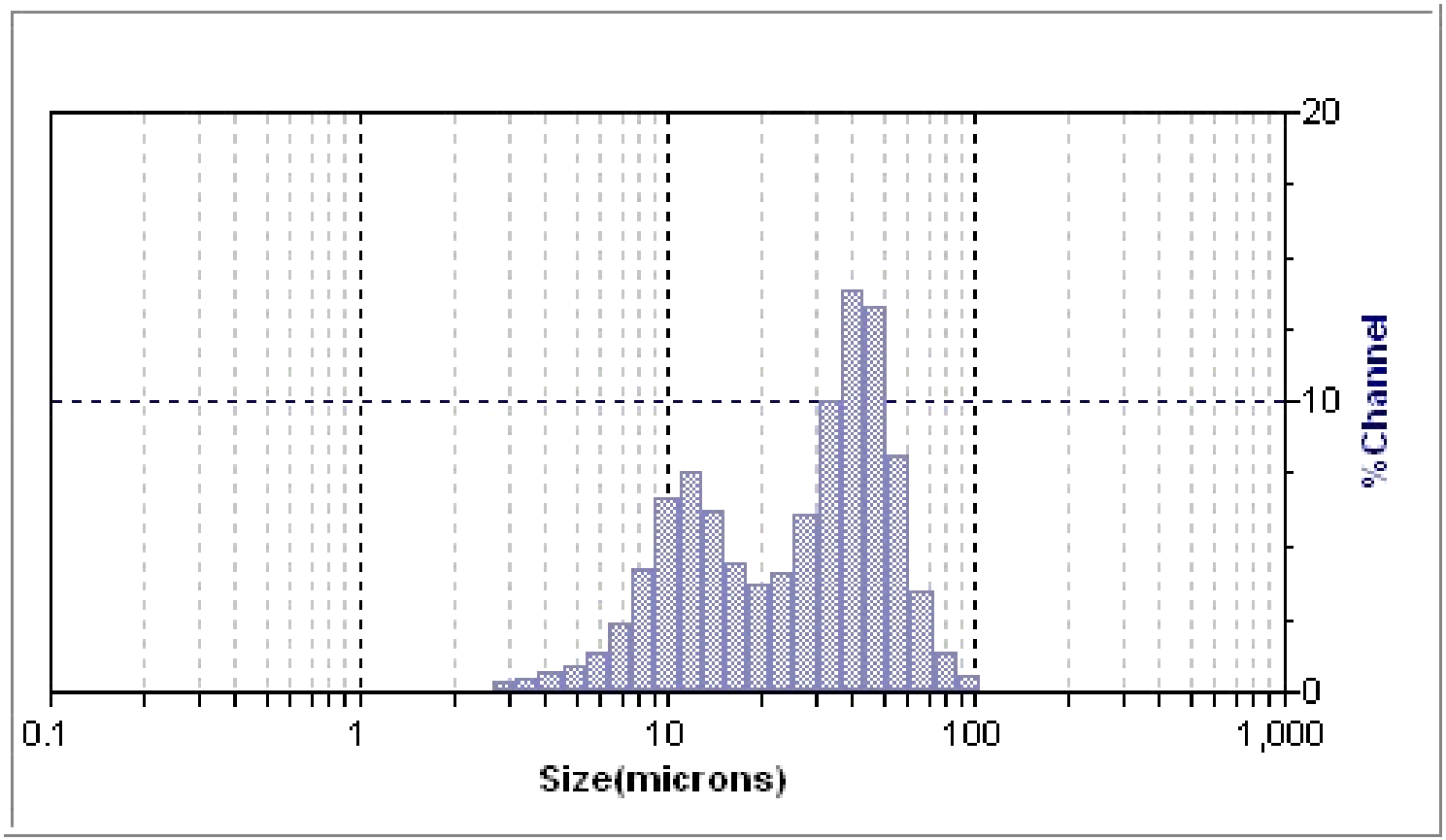

Figure 61 Particle size distribution of powder pulverized for 15 min using Labtechnics pulverizer

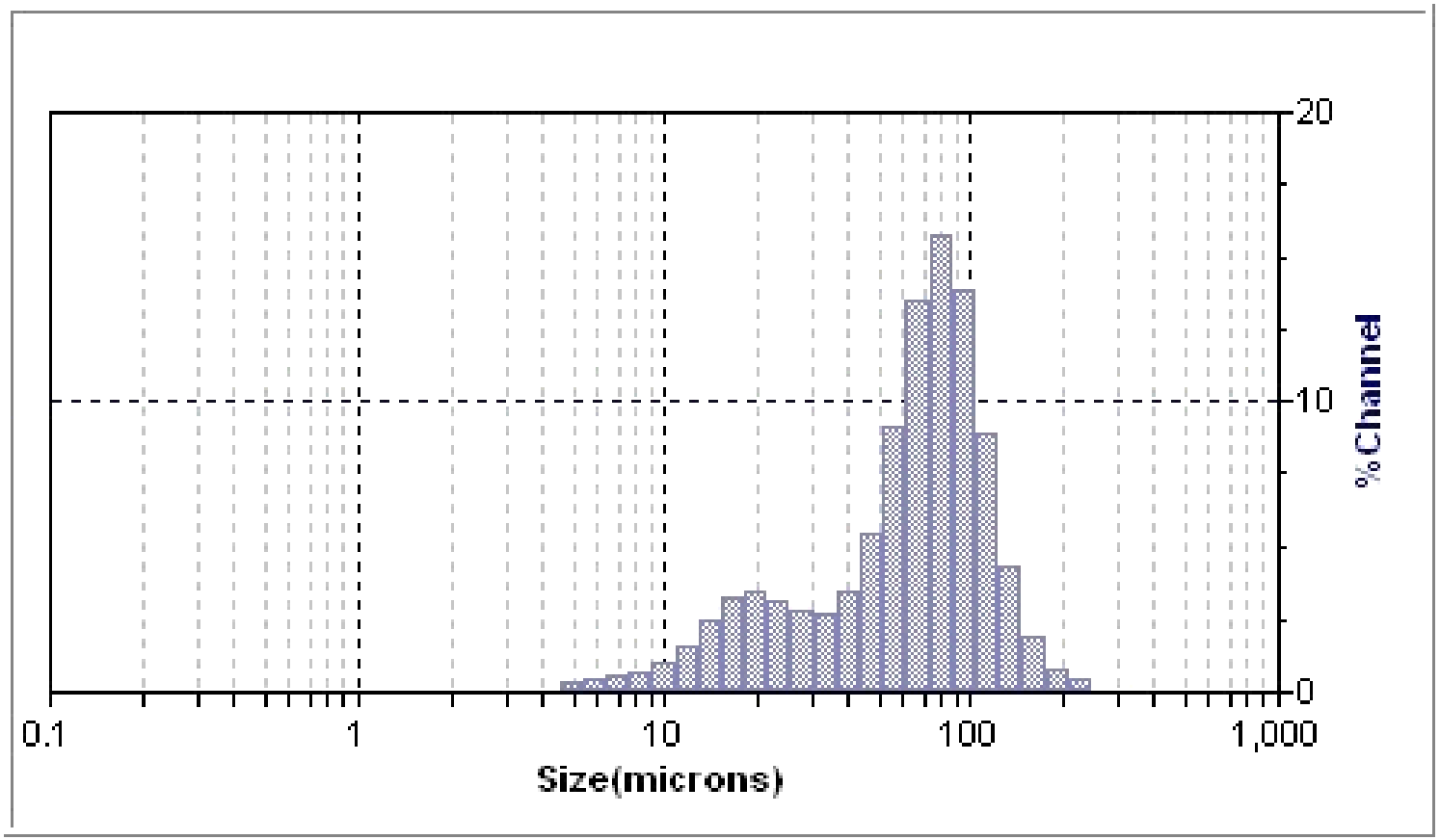

Figure 62 Particle size distribution of powder pulverized for 30 min using Labtechnics pulverizer

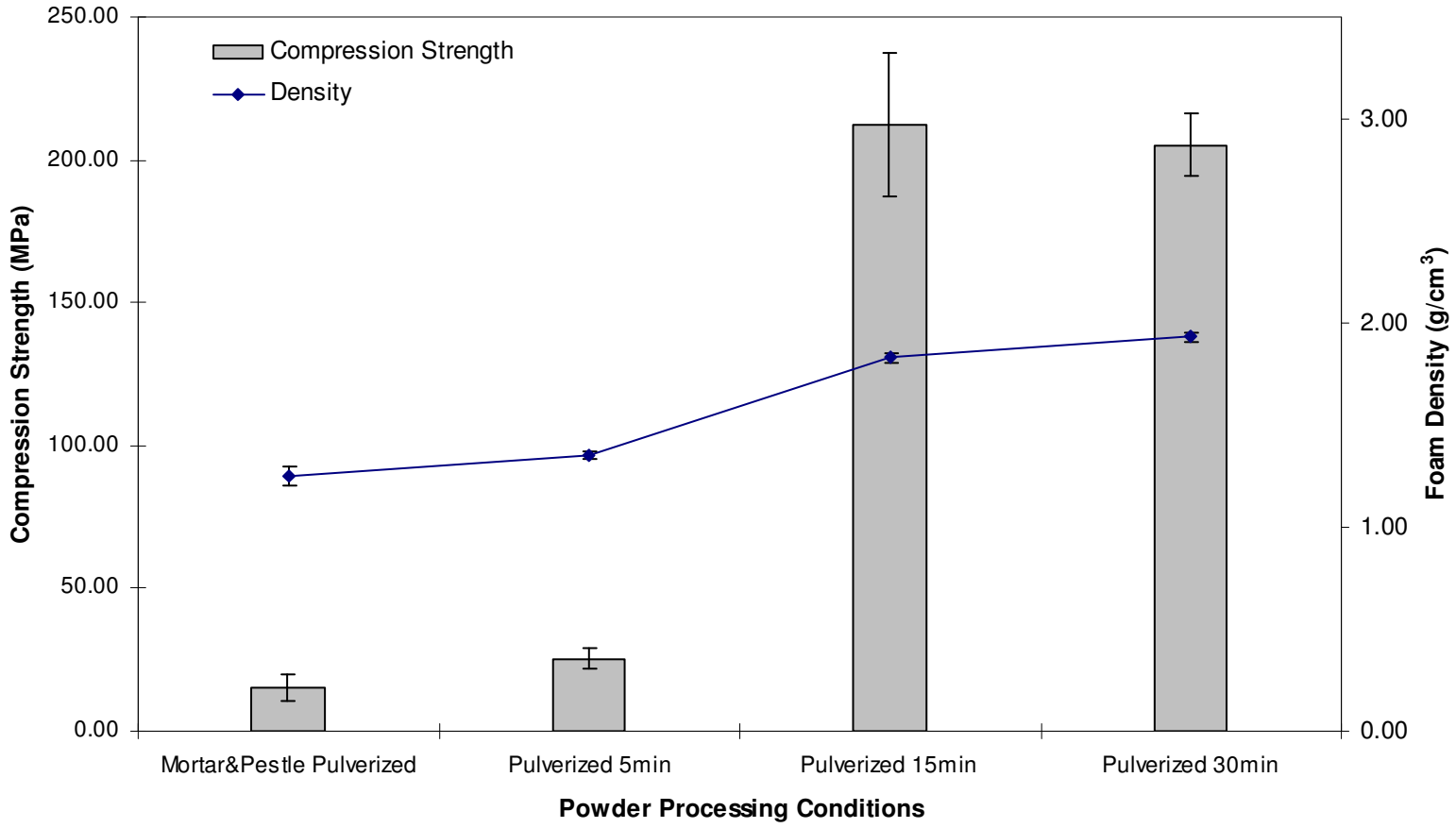

Figure 63 Effect of powder processing methods on foam density and compression strength

6 CONCLUSIONS

The present research investigated a simple, low cost method to produce HfC foam from polymer precursors. The method involved mixing hafnium containing MMC and epoxy, followed by heat treatment of the polymer mixture at 1410°C under vacuum to produce HfC foams. Other HfC foam manufacturing methods, such as CVD, VPS and Reaction Foaming, are either slow or require expensive and complicated set-up, or involve very high operating temperatures.

The following conclusions can be drawn from the experimental results:

1. HfC foam can be produced through the thermolysis and pyrolysis of Hf containing and epoxy polymer mixtures under vacuum. The XRD spectra of the HfC foam samples showed that the foam material was composed primarily of HfC. Small amounts of HfO_2 were evident in the diffraction spectra.
2. Several polymer mixing weight ratios (1:1 ~ 4:1), were tested to investigate their effect on foam properties. 1:1 ratio foams had the highest density, $0.58 \pm 0.01 g/cm^3$, and 3:1 ratio yielded the lowest HfC foam density, $0.27 \pm 0.03 g/cm^3$. The lower HfC foam density at 3:1 ratio may be used in the future to tailor the HfC foam properties. The polymer mixture extremes experiment proved that the formation of the foam structure could not be obtained by processing the Hf containing MMC or the epoxy alone.

3. Different thermolysis temperatures and times (175°C, 200°C, 225°C and 30 minutes, 60 minutes) were used to determine their effect on foam densities. It was seen that 200°C (30min) produced the highest density, of about 0.58g/cm^3, while the rest of the sample groups showed no difference in density statistically and had a lower density of about 0.4g/cm^3.
4. Mechanisms of thermolysis and pyrolysis chemistry were investigated. According to RGA, XRD and vacuum pressure measurements, polymer decomposition of the preform samples occurred from 80°C to 550°C and HfC conversion reactions occurred from 1010°C ~ 1410°C. Chemical reactions for HfC conversion were proposed.
5. Three HfC foam preparation techniques were investigated. Hand Mixing and Vacuum Mixing methods were both used to produce HfC foam, but not able to repeatedly produce a uniform cell size. The Polymer Powder Compaction method yielded consistently a uniform cell structure, higher density, and higher compression strength. Factors affecting HfC foam structure during thermolysis were discussed.
6. The HfC foam mechanical properties and microstructure were improved by optimizing the Polymer Powder Compaction method and processing parameters. The initial research yielded HfC foams with a compression strength of about 15.16MPa, a density of about 1.25g/cm^3 (total porosity 90.2%), and evenly distributed foam cells with diameter sizes up to 50μm. Continued research showed that HfC foams with a density of 1.8~1.9g/cm^3 (total porosity about 85%), and a foam compression strength about 200MPa were achievable. Polymer particle size and size distribution changes, introduced by different powder processing methods and parameters, were believed to be the reason for these density and compression strength changes. A smaller polymer

particle size and a non-uniform bimodal size distribution seemed to increase foam density and compression strength.

7 FUTURE WORK

7.1 Thermolysis and Pyrolysis Chemistry

Although the present investigation provides some insight about the temperature ranges involved in polymer decomposition and HfC conversion reactions, detailed polymer decomposition reactions were not identified.

There are numerous unknown factors concerning the thermolysis reactions that may be highly relevant for further optimizing the initial foam producing process. Chemical analysis techniques such as GC/MS and NMR are recommended for identifying the gaseous and solid state products during thermolysis reactions.

8 REFERENCES

[1.] Leverenz, R.V., Bost, J. & Oakes, J.J., "Wear-resistant multilayer ceramic coatings for cemented carbide cutting tools," Us Patent # 6447890 (2002).

[2.] Ueda, H. & Ishii, T., "Coated cemented carbide cutting tool with high wear and chipping resistance," Jp Patent # 2002239813 (2002).

[3.] Nagao, M. et al. "Fabrication of polycrystalline silicon field emitter arrays with hafnium carbide coating for thin-film-transistor controlled field emission displays," *Japanese Journal of Applied Physics, Part 1: Regular Papers, Short Notes & Review Papers* **43**, 3919-3922 (2004).

[4.] Sato, T. et al. "Fabrication and characterization of HfC coated Si field emitter arrays," *Journal of Vacuum Science & Technology, B: Microelectronics and Nanometer Structures--Processing, Measurement, and Phenomena* **21**, 1589-1593 (2003).

[5.] Mackie, W.A. et al. "Emission fluctuation and slope-intercept plot characterization of Pt and transition metal carbide field-emission cathodes in limited current regimes," *Journal of Vacuum Science & Technology, B: Microelectronics and Nanometer Structures--Processing, Measurement, and Phenomena* **21**, 1574-1580 (2003).

[6.] Wei, Y. et al. "Fabrication of molybdenum carbide and hafnium carbide field emitter arrays," *Journal of Vacuum Science & Technology, B: Microelectronics and Nanometer Structures* **19**, 42-46 (2001).

[7.] Rakhshandehroo, M.R. & Pang, S.W. "High-current Si field emission devices with plasma passivation and HfC coating," *International Vacuum Microelectronics Conference, 11th, Asheville, N. C., July 19-24, 1998*, 291-292 (1998).

[8.] Lu, M.L., Hussey, B.W., Kratschmer, E., Chang, T.H.P. & Mackie, W.A. "Improved emission stability of carburized HfC{100} and ultrasharp tungsten field emitters," *Journal of Vacuum Science & Technology, B: Microelectronics and Nanometer Structures* **13**, 2436-40 (1995).

[9.] Lengauer, W. et al. "Solid state properties of group IVb carbonitrides," *Journal of Alloys and Compounds* **217**, 137-147 (1995).

[10.] Opeka, M.M., Talmy, I.G., Wuchina, E.J., Zaykoski, J.A. & Causey, S.J. "Mechanical, thermal, and oxidation properties of refractory hafnium and zirconium compounds," *Journal of the European Ceramic Society* **19**, 2405-2414 (1999).

[11.] Pell, J.W. "Liquid Precursors to Hafnium and Tantalum Carbides," in *Inorganic Chemistry* (Massachusetts Institute of Technology, 1999).

[12.] Moffatt, W.G. "*Handbook of Binary Phase Diagrams*," (Genium Publishing, Co, 1984).

[13.] Divakar, R. "Silicon carbide," in *Kirk-Othmer Encyclopedia of Chemical Technology* (John Wiley & Sons, New York, 1991).

[14.] Sayir, A. "Carbon fiber reinforced hafnium carbide composite," *Journal of Materials Science* **39**, 5995-6003 (2004).

[15.] Hinze, J.W., Tripp, W.C. & Graham, H.C. "High-temperature oxidation behavior of a hafnium boride + silicon carbide composite," *Journal of the Electrochemical Society* **122**, 1249-54 (1975).

[16.] Tripp, W.C., Davis, H.H. & Graham, H.C. "Effect of a silicon carbide addition on the oxidation of zirconium diboride," *American Ceramic Society Bulletin* **52**, 612-16 (1973).

[17.] Bargeron, C.B. & Benson, R.C. "X-ray microanalysis of a hafnium carbide film oxidized at high temperature," *Surface and Coatings Technology* **36**, 111-5 (1988).

[18.] Bargeron, C.B., Benson, R.C., Jette, A.N. & Phillips, T.E. "Oxidation of hafnium carbide in the temperature range 1400 Deg to 2060 DegC," *Journal of the American Ceramic Society* **76**, 1040-6 (1993).

[19.] Wuchina, E.J. & Opeka, M.M. "The oxidation behavior of HfC, HfN, and HfB2," *Proceedings - Electrochemical Society* **2001-12**, 136-143 (2001).

[20.] Wuchina, E.J. & Opeka, M.M. "Oxidation of Hf-based ceramics," *Proceedings - Electrochemical Society* **99-38**, 477-488 (2000).

[21.] Shimada, S., Nakajima, K. & Inagaki, M. "Oxidation of single crystals of hafnium carbide in a temperature range of 600 degrees to 900 degrees C," *Journal of the American Ceramic Society* **80**, 1749-56 (1997).

[22.] Shimada, S. "Formation and mechanism of carbon-containing oxide scale by high temperature oxidation of carbides," *Proc. - Electrochem. Soc.* **98-9**, 334-348 (1998).

[23.] Shimada, S., Yoshimatsu, M., Yunazar, F. & Otani, S. "Deposition and characterization of carbon at the interface by oxidation of single crystals of carbides (HfC, ZrC, TiC)," *Tanso* **190**, 223-228 (1999).

[24.] Shimada, S., Yunazar, F. & Otani, S. "Oxidation of hafnium carbide and titanium carbide single crystals with the formation of carbon at high temperatures and low oxygen pressures," *Journal of the American Ceramic Society* **83**, 721-728 (2000).

[25.] Shimada, S. "Interfacial reaction on oxidation of carbides with formation of carbon," *Solid State Ionics* **141-142**, 99-104 (2001).

[26.] Shimada, S. "Formation and mechanism of carbon-containing oxide scales by oxidation of carbides (ZrC, HfC, TiC)," *Materials Science Forum* **369-372**, 377-384 (2001).

[27.] Shimada, S. "A thermoanalytical study on the oxidation of ZrC and HfC powders with formation of carbon," *Solid State Ionics* **149**, 319-326 (2002).

[28.] Eckel, T.P.H.A.A.J. "Ceramic Composites for Rocket Engine Turbines," *Society of Automotive Engineers* (Apr 1991).

[29.] Palmisiano, M.N., Jakubenas, K.J. & Baranwal, R., "Reaction-forming method for producing near net-shape refractory metal carbides," Us Patent # 6764620 (2004).

[30.] Gibson LJ, A.M. "*Cellular solids, structure and properties, 2nd edn.*," (Cambridge University Press, UK, 1999).

[31.] Schwartzwalder, K. & Somers, A.V., "Porous ceramic bodies," Us Patent # 3090094 (1963).

[32.] Emig, G., Schoch, G. & Wormer, O. "Chemical vapor deposition of hafnium carbide and hafnium nitride," *Journal de Physique IV: Proceedings* **3**, 535-40 (1993).

[33.] Ache, H.F. et al. "Chemical vapor deposition of hafnium carbide and characterization of the deposited layers by secondary-neutral mass spectrometry," *Thin Solid Films* **241**, 356-60 (1994).

[34.] Sourdiaucourt, P., Derre, A., David, P. & Delhaes, P. "Thermodynamic study of the hafnium-carbon system for hafnium carbide chemical vapor deposition," *Proceedings - Electrochemical Society* **97-25**, 31-39 (1997).

[35.] Sourdiaucourt, P., Derre, A., Delhaes, P. & David, P. "Thermodynamical and experimental conditions of hafnium carbide chemical vapour deposition," *Journal de Physique IV: Proceedings* **9**, 373-380 (1999).

[36.] Sourdiaucourt, P., Derre, A., Delhaes, P. & David, P. "Mechanical reinforcement of carbon foam by hafnium carbide deposit," *Journal de Physique IV: Proceedings* **9**, 1187-1194 (1999).

[37.] Sourdiaucourt, P., Derre, A., Delhaes, P. & David, P. "Hafnium carbide deposit on a carbon foam," *Chocs* **24**, 51-61 (2001).

[38.] Wunder, V., Popovska, N. & Emig, G. "Chemical vapor deposition of hafnium carbide on carbon substrate," *Proceedings - Electrochemical Society* **97-25**, 608-615 (1997).

[39.] Wunder, V., Popovska, N., Wegner, A., Emig, G. & Arnold, W. "Multilayer coatings on CFC composites for high-temperature applications," *Surface and Coatings Technology* **100-101**, 329-332 (1998).

[40.] Wunder, V.K., Popovska, N. & Emig, G. "Study of hafnium carbide growth by CVD from in situ chlorinated hafnium," *Proceedings - Electrochemical Society* **98-23**, 264-267 (1999).

[41.] Wunder, V.K., Popovska, N. & Emig, G. "Hafnium carbide as a barrier in multilayer coatings by chemical vapor deposition (CVD)," *Journal de Physique IV: Proceedings* **9**, 509-516 (1999).

[42.] Popovska, N., Held, D., Wunder, V., Gerhard, H. & Emig, G. "Chemical vapour deposition of pyrolytical carbon and graded C/SiC/Si-films at atmospheric pressure," *Proceedings - Electrochemical Society* **98-23**, 407-412 (1999).

[43.] Healy, M.D., Smith, D.C., Rubiano, R.R., Springer, R.W. & Parmeter, J.E. "The organometallic chemical vapor deposition of transition metal carbides: the use of

homoleptic alkyls," *Materials Research Society Symposium Proceedings* **327**, 127-32 (1994).

[44.] Spatenka, P., Suhr, H., Erker, G. & Rump, M. "Formation of hafnium carbide thin films by plasma enhanced chemical vapor deposition from bis(h-cyclopentadienyl)dimethylhafnium as precursor," *Applied Physics A: Materials Science & Processing* **A60**, 285-8 (1995).

[45.] Agarwal, A., McKechnie, T., Starett, S. & Opeka, M.M. "Near net shape forming of hafnium-based ceramic components: synthesis and characterization," *Elevated Temperature Coatings: Science and Technology IV,* [Papers presented at a Symposium held during the TMS Annual Meeting], New Orleans, LA, United States, Feb. 11-15, 2001, 302-315 (2001).

[46.] Grant, N.J. & Robinson, R.K., "High hafnium carbide-containing alloys," Us Patent # 4481034 (1984).

[47.] Grant, N.J. & Robinson, R.K., "High hafnium carbide-containing alloys," Us Patent # 4084964 (1978).

[48.] Panasyuk, A.D. "The activated sintering process of tantalum and hafnium carbides," *Izvestiya Akademii Nauk SSSR, Neorganicheskie Materialy* **1**, 1065-70 (1965).

[49.] Ordan'yan, S.S., Zaitsev, G.P., Khokhlov, A.M. & Sokhor, M.I. "Sintering and homogenization in the hafnium carbide-tantalum carbide system," *Zhurnal Prikladnoi Khimii (Sankt-Peterburg, Russian Federation)* **50**, 1440-5 (1977).

[50.] Suganuma, M. & Kitagawa, Y. "Pulsed electric current sintering of carbides with high melting temperature," *Aichi-ken Kogyo Gijutsu Senta Kenkyu Hokoku* **36**, 6-8 (2000).

[51.] Kecskes, L.J., Benck, R.F. & Netherwood, P.H., Jr. "Dynamic compaction of combustion-synthesized hafnium carbide," *Journal of the American Ceramic Society* **73**, 383-7 (1990).

[52.] A.D.Pomogailo, V.S.S.Y. "Synthesis and Polymerization of Metal-Containing Monomers.," *CRC Press, Boca Raton*, 164 p. (1994).

[53.] A.D.Pomogailo, D.W. *Macromolecule-Metal Complexes (Eds. F.Ciardelli, E.Tsuchida, D.Woehrle)*, p.11-129 (1996).